Durham E-Theses

Special wave finite and infinite elements for the solution of the Helmholtz equation

Rie Sugimoto

How to cite:

Sugimoto, Rie (2003) Special wave finite and infinite elements for the solution of the Helmholtz equation. Doctoral thesis, Durham University.

Use policy

Special Wave Finite and Infinite Elements

for the Solution of the Helmholtz Equation

by

Rie Sugimoto

A thesis submitted for the degree of

Doctor of Philosophy

School of Engineering

The University of Durham

2003

Special Wave Finite and Infinite Elements
for the Solution of the Helmholtz Equation

by

Rie Sugimoto

A thesis submitted for the degree of Doctor of Philosophy

School of Engineering, The University of Durham

2003

Abstract

The theory and the formulation of the special wave finite elements are discussed, and the special integration schemes for the elements are developed. Then the special wave infinite elements, a new concept of the mapped wave infinite elements with multiple wave directions, are developed. Computational models using these elements coupled together are tested by the applications of wave problems.

In the special wave finite elements, the potential at each node is expanded in a discrete series of approximating plane waves propagating in different directions. Because of this a single element can contain many wavelengths, unlike the standard finite elements. This is a great advantage in the reduction of the degree of freedom of the problem, however the computational cost of the numerical integration over an element becomes high due to the oscillatory shape functions. Therefore the special semi-analytical integration schemes for the special wave finite elements are developed. The schemes are independent of wavenumber and efficient for short waves problems.

In many cases of wave problems, it is practical to consider the domain as being infinite. However the finite element method can not deal with infinite domains. Infinite elements are an extension of the concept of finite elements in which the element has an infinite extent in one or more directions to address this limitation. In the special wave infinite element developed in this study multiple waves propagating in different directions are considered, in contrast to conventional infinite elements in which only a single wave propagating in the radial direction is considered. The shape functions of the special wave infinite elements contain trigonometric functions to describe multiple waves, and the amplitude decay factor to satisfy the radiation condition. The special wave infinite elements become a straightforward extension to the special wave finite elements for wave problems in an unbounded domain.

Declaration

This thesis is dedicated

to

my parents

Acknowledgements

First of all, I would like to express my most sincere gratitude to my supervisor, Professor Peter Bettess, for his guidance, valuable advice and enthusiastic supervision throughout my research at the University of Durham. He employed me as a Research Associate, which gave me the opportunity to work and study for PhD simultaneously in Durham.

I am very grateful to my colleague, Dr Omar Laghrouche, for his continuous encouragements and support. His help with research on special wave finite elements and living in Durham was invaluable. I would like to express my warm appreciation to Dr Jon Trevelyan and Dr Emmanuel Perrey-Debain, for useful discussions and constructive comments, which were always stimulating.

I am thankful to Professor R. Jeremy Astley, Institute of Sound and Vibration Research, University of Southampton, for useful suggestions and discussions at his stay in Durham in 2000.

I would like to thank Professor Zun-iti Maekawa, Professor Masayuki Morimoto and Dr Kimihiro Sakagami, my supervisors when I was a student at Kobe University, Japan. Their sincere attitude towards research had a great influence on me. I also would like thank my former colleagues at Kobe Steel Ltd., Japan. I enjoyed working with them for nearly nine years until I moved to Durham. Even after I left the company, our friendship continues and it encourages me all the time.

Finally, I would like to express my deepest gratitude to my parents for their understanding and support.

Contents

List of Tables

List of Figures

List of Symbols

A	Double of distance from the pole to the inner edge of infinite elements
A_i	$A(\eta)$ at the i-th node on the inner edge of infinite element
$\bar{A}$	Area of an triangular element
$\bar{A}_1, \bar{A}_2, \bar{A}_3$	Partial areas for area co-ordinates of an triangular element
$\{\mathcal{A}\}$	Amplitude vector
$\hat{A}$	Area of the standard finite element $\hat{E}$
A_t	Area of finite element E_t
A_j^l	Amplitude of the l-th plane wave at node j in special wave finite element
$\mathcal{A}_j$	Amplitude vector at node j in special wave finite element
a	Distance from the 'pole' to the inner edge of the infinite element
$\bar{a}$	Radius of cylinder
$\mathbf{a_t}, \mathbf{b_t}, \mathbf{c_t}$	Vectors in two dimensions
B_j^l	Amplitude of the l-th wave at node j in special wave infinite element
$\mathcal{B}_j$	Amplitude vector at node j in special wave infinite element
b_x, b_y	Dimensions of rectangular element in the x and y directions
$[\mathbf{C}]$	Damping matrix
C_1, C_2	Constants depending on the order of the finite element
C_{ij}	Damping matrix component
C_t, F_t, G_t, H_t	Real coefficients in integral
$\mathcal{C}_j$	Extra term to ensure continuity on the finite/infinite element interface
c	Speed of wave
e	Error
$\hat{\mathbf{e}}_j^l$	Unit vector in the direction of angle θ_j^l
$\mathbf{e_x}$	Unit vector in the x direction
$\mathbf{e_y}$	Unit vector in the y direction
F, G, H	Coefficients to ξ, η and $\xi\eta$ in integral

$\{\mathbf{F}\}$	Forcing vector
F_i	Forcing vector component
$f(\xi)$	Function
f_1	Function for the first term of d'Alembert solution
f_1'	Time derivative of function f_1
$f_{pqi\ j}^{t\ m\ l}$	Coefficients to the interpolating polynomials $\mathcal{L}_{pq}$ and the oscillating functions $\exp(ik\hat{\mathbf{e}}_{\mathbf{j}}^{\mathbf{l}} \cdot \mathbf{r})\exp(ik\hat{\mathbf{e}}_{\mathbf{i}}^{\mathbf{m}} \cdot \mathbf{r})$
g	Parameter for Robin boundary condition
g_1	Function for the second term of d'Alembert solution
h	Length of the element (stepsize of the mesh)
h'	Half length of the element
$H_m^{(i)}$	Hankel function of the i-th kind of the m-th order
$H'^{(i)}_m$	Derivative of Hankel function of the i-th kind of the m-th order
I	Integral
i	The imaginary number, the square root of -1
J	Jacobian matrix
$\bar{J}$	Jacobian matrix for subelement of infinite element
J_m	Bessel function of the first kind of the m-th order
J'_m	Derivative of Bessel function of the first kind of the m-th order
K_{ij}	Stiffness matrix component
$\mathcal{K}_{ij}^{IE}$	Element matrix component of an infinite element
$\mathcal{K}_{ij}^{gl}$	Element matrix component by Gauss-Legendre integration
$\mathcal{K}_{ij}^{sa}$	Element matrix component by semi-analytical integration
$\mathcal{K}_{ij}^{sp}$	Element matrix component by Zienkiewicz integration
$[\mathbf{K}]$	Stiffness matrix
k	Wavenumber
k_r	Wavenumber in the radial direction
k_z	Wavenumber in the z direction
$\mathbf{k}_\theta$	Wavenumber vector in angle θ
$\mathbf{k}_{\mathbf{j}}^{\mathbf{l}}$	Wave number of the l-th plane wave associated with node j
$(\bar{L}_1, \bar{L}_2, \bar{L}_3)$	Area co-ordinates of an triangular element
$L_p(\xi), L_q(\eta)$	Lagrange polynomials

$L_i^n(\eta)$	Lagrange polynomials of order n
$\mathcal{L}_{pq}(\xi,\eta)$	Interpolating polynomial, $= L_p(\xi)L_q(\eta)$
l	Regularity of the exact solution
$[\mathbf{M}]$	Mass matrix
M_j	Mapping functions
$\mathcal{M}_l$	Element mapping function in two dimensions
$\mathcal{M}_l^n$	Element mapping function in two dimensions for n-node element
M_{ij}	Mass matrix component
m	Wavenumber along the circumference of cylindrical wave
m_j	Number of approximating wave associated with node j
$\bar{m}$	Minimum of the order of the finite element and the regularity of the exact solution -1
N_j	Polynomial shape function associated with node j
$\tilde{N}_0, \tilde{N}_2$	Functions for infinite element defined at the 'pole' and mid-side node
$[N]$	Polynomial shape function vector
n	Number of nodes of an element
n_L	Highest power of ξ and η in Lagrange polynomials
$\mathbf{n}$	Outward normal vector
n_{div}	Number of subelements of infinite element in the infinite direction
n_{max}	order of polynomial of original shape function in the η direction
n_ξ, n_η	Number of integration points of an element in the ξ and η directions
$n_{\bar{\xi}}$	Number of integration points of a subelement of infinite element in the $\bar{\xi}$ directions
n_p	Total degree of freedom of the element
n_x	x component of normal $\mathbf{n}$
n_y	y component of normal $\mathbf{n}$
$[\mathcal{P}]$	Row matrix of special shape functions of a special wave finite element
$\mathcal{P}_j$	Row matrix component of special shape functions of a special wave finite element associated with node j
P_j^l	Special shape functions of a special wave finite element associated with the l-th approximating wave at node j
p	Order of the finite element

$\Re$	Real part of a complex value
r	Global co-ordinate in the radial direction
r_{div}	Length of subelement of infinite element
r_{max}	Number of terms to truncate the infinite series of Taylor's expansion
$r_{s(max)}$	Largest r in the s-th subelement in infinite element
$r_{s(min)}$	Smallest r in the s-th subelement in infinite element
$\mathbf{r}$	Position vector
(r, θ)	Polar co-ordinates in two dimensions
(r, θ, z)	Cylindrical co-ordinates
S_j	Shape functions of a mapped wave infinite element at node j
S_j^l	Special shape functions of a special wave infinite element for the l-th approximating wave at node j
$[\mathcal{S}]$	Row matrix of special shape functions of a special wave infinite element
$\mathcal{S}_j$	Row matrix component of special shape functions of a special wave infinite element associated with node j
T_{gl}	Time taken to integrate the element matrix by Gauss-Legendre integration
T_{sa}	Time taken to integrate the element matrix by semi-analytical integration
t	Time
U_0	Particle velocity on the surface of the cylinder
u	Normal velocity
$\bar{u}$	Given value of u
W	Weighting function
W_j^l	Weighting function corresponding to the l-th plane wave at with node j
$[w]$	Weighting function row matrix
w_j	Weighting functions
w_{pq}	Integral for a special wave finite element
$w_{pq}{}'$	A term in integral w_{pq}
(x, y)	Cartesian global coordinates in two dimensions
(x, y, z)	Cartesian global coordinates in three dimensions
Y_m	Bessel function of the second kind of the m-th order
Y'_m	Derivative Bessel function of the second kind of the m-th order
z	Acoustic impedance

α, β, γ	Real coefficients
α	Angle of the radial direction at a position $\mathbf{r}$
α_j, β_j	Real coefficients ($j = 1, 2, 3, \cdots$)
α_m, β_m	Real coefficient to $\cos m\theta$ of circumferencial wavenumber m
Γ	Boundary of domain
Γ_i	Interior boundary
Γ_o	Exterior boundary
Γ_R	Outer boundary of an infinite element at a finite distance
Γ_∞	Outer boundary of an infinite element at infinity
Γ_1	Interior boundary of finite element domain
Γ_2	Exterior boundary of finite element domain
ϵ_m	Coefficients, $\epsilon_0 = 1$ and $\epsilon_m = 2$ for $m = 1, 2, 3, \cdots$
θ	Azimuthal angle
θ_j^l	Angle of the direction of the l-th wave at node j
λ	Wavelength
ξ_R	Local co-ordinate corresponding to outer boundary Γ_R of an infinite element
$\bar{\xi}$	Local co-ordinate for subelement of infinite element
(ξ, η)	Local co-ordinates
ρ	Fluid dencity
Φ	Potential, variable of interest in the wave equation
ϕ	Potential, variable of interest in the Helmholtz equation
$\bar{\phi}$	Given value of ϕ
ϕ^i	Incident wave
$\{\phi\}$	Nodal potential vector
ϕ^r	Radiated outgoing wave
ϕ^s	Scattered wave
ϕ^{an}	Analytical solution of potential
ϕ^{gl}	Potential obtained using Gauss-Legendre integration
ϕ^{num}	Numerical result of potential
$\phi_r(r)$	Radial component of the factored solution ϕ
$\phi_\theta(\theta)$	Circumferencial component of the factored solution of ϕ

$\phi_z(z)$	Vertical component of the factored solution ϕ
ψ_j^l	l-th plane wave at node j, $e^{i\mathbf{k}_j^l \cdot \mathbf{r}}$
Ω	Domain
Ω_i	Interior domain enclosed by a boundary
Ω_R	Infinite element domain bounded by outer boundary Γ_R
ω	Angular frequency

Chapter 1

Introduction

This thesis is concerned with the development of special wave finite and infinite elements which use special shape functions incorporating trigonometric functions for the solution of wave problems governed by the Helmholtz equation. The aim is to solve short wave problems, where the wavelength is much smaller than any other length dimensions of the problem, in unbounded domain efficiently. In the wave problems where the solution is oscillatory, the usual polynomial spaces cannot resolve the essential features of the solution unless the mesh size is very small or the polynomial degree is very large. In both cases the computational costs become very high. They can also become much higher in the case where the domain considered is very large compared to the wavelength and practically can be treated as unbounded. Especially the computational costs of more realistic three dimensional problems are often prohibitively expensive. Therefore the development of efficient numerical techniques for the solution of such problems is quite important.

In this thesis the theory and the formulation of the special wave finite and infinite elements which contain many wavelengths, new numerical integration procedures which are required to accurately evaluate the integration over these elements, and applications of these elements are presented. Although the real problems are in three dimensions, this thesis is concerned with only two dimensional problems. The same development is expected to be applicable also to the three dimensions.

1.1 Objectives

The objective of this thesis is to develop the special wave infinite elements, for the efficient solution of the Helmholtz equation for the time-harmonic wave problems in homogeneous

medium in unbounded domain in two dimensions. In association with this, the development of the efficient semi-analytical integration scheme for the special wave finite elements is also the objective. Both special wave finite and infinite elements use special shape functions containing discrete set of approximating waves propagating in multiple directions at a node, and can be much larger than the wavelength unlike conventional elements. These elements are intended to be applied to the short wave problems, where the wavelength is much smaller than any other length dimensions of the problem.

1.2 Background

Wave problems governed by the Helmholtz equation are important in many fields, such as surface waves on the sea, acoustics and electromagnetic waves. For example the practical applications include:

- The patterns of waves along coastlines which influence wave forces on harbours, and sediment transport, among other effects.

- The propagation of sound and noise, with a huge range of applications from acoustics of concert halls, to the noise from jet engines, and road noise in vehicles.

- The propagation of elastic waves through the earth, arising from earthquakes and in seismic prospecting for hydrocarbons.

- The radar cross sections of aircraft, and other electro-magnetic effects.

Most of these wave problems are governed by the Helmholtz equation, or an equation with similar properties. The numerical methods dealt with in this thesis are all intended to solve the Helmholtz equation.

In many cases of wave radiation and scattering problems, the domain considered is much larger than the wavelength and the particular area of interest where the problem is to be solved. In that case it is practical to treat the domain as being unbounded. Such exterior wave problems have been solved by a number of numerical analysis methods, such as finite elements, finite differences and boundary integrals. These methods have been developed and applied to many fields in Engineering. However these numerical methods have some limitations.

In this chapter previous works of such numerical methods for wave problems are surveyed.

1.3 Finite Elements

The finite element method is one of the numerical methods which are most widely used in many fields in engineering. There are many textbooks on the method. One well-known book, which provides a comprehensive introduction is by Zienkiewicz and Taylor [99]. It is one of the 'domain-based' methods. Most domain-based methods require the truncation of the computational domain at some boundary at a sufficiently large distance from the radiating or scattering object and the suitable boundary condition applied to approximate the Sommerfeld radiation condition [88].

The first application of finite elements to wave problems in acoustics was by Gladwell [52] in 1965. He formulated finite element 'force' and 'displacement' models for the undamped modes of an acoustic enclosure with a sprung piston at one end, and used one dimensional and two dimensional acoustic finite elements. This formulation was virtually identical to that by Zienkiewicz and Newton [98] in 1969 to model the effects of compressibility of fluid on the added mass of submerged structure. Craggs [38] applied finite elements to various interior problems in acoustics.

The principal limitation of standard finite element formulation for wave problems is the difficulty of resolving spatially oscillating wave-like solutions using node-based interpolation schemes. It has been known for a long time that in order to resolve details of wave problems when using finite elements, it is necessary to use about 10 degrees of freedom per wavelength. It was also well-known that this fineness of meshing must be maintained throughout the entire domain because it is essential to resolve the wave details everywhere.

In recent years, this approximate rule has been sharpened by mathematical analysis by a number of workers. Ihlenburg and Babuška [61] and Babuška *et al.* [15, 16] show from numerical experiments that for a domain of *unit length* the effects, described above can be summarised in two sources of error. One is a *local error* proportional to some power of $kh/2p$, where k is the wavenumber, h is the length of the element, and p is the order of the element. The other is a *pollution error* proportional to k multiplied by some power of $kh/2p$. This means a *pollution error* increases as the wavenumber k increases even though the value of kh is kept constant. Their results indicate how these errors increase due to

3

the combination of the wavenumber and the order of the element.

Another limitation of the finite element formulation for wave problems is the difficulty of dealing with unbounded domains. The finite element method is essentially based on the governing equation and the formulation for a *bounded* domain. To solve the wave field by finite elements, the domain is divided into a finite number of elements of finite sizes, and the integration over the domain is treated as a sum of the contributions of each elements. To deal with the wave field in unbounded domain with a domain-based method, it is necessary to truncate the domain at a finite distance with an artificial outer boundary and to link the finite elements inside to an outer representation which satisfies the Sommerfeld radiation condition at infinity. The condition is often approximated by a local absorbing boundary condition and the locality of the boundary operator and the distance at which it is applied significantly influence the computational efficiency. There is a very extensive literature on radiation conditions. Key developments are reviewed by Givoli [50, 51] and Ihlenburg [59]. The proceedings of the IUTAM conference [47] also gives access the main developments.

The simplest local non-reflecting boundary condition is the 'plane damper' boundary condition, which is also called 'ρc impedance boundary condition' in acoustics. This uses the constant relationship between the field variable such as potential or pressure and its normal derivative. This boundary condition is accurate at large distances from radiating or scattering object. However it gives spurious reflections if the boundary where it is applied is not at a sufficiently large distance. Therefore it is important to choose a sufficiently large distance to approximate the Sommerfeld radiation condition and a suitable numerical boundary condition. The distance between boundaries is crucial for finite element modelling because it determines the enclosed area or volume to be discretized and consequently the size of system matrices to solve. It is also crucial for the accuracy of the approximated boundary condition and for the solution. The finite domain to be treated can be reduced when higher order local non-reflecting boundary condition, such as cylindrical or higher order dampers, are applied.

However, despite these limitations the finite element method is still one of the most widely used numerical methods for wave problems, and it has been getting much more interest in recent years. It has the great advantages of a firm theoretical basis. It also produces a sparse banded system matrix, which may lead to economical matrix solu-

tions. Traditionally the boundary element method, which is introduced in section 1.6, was regarded as being a more effective way than domain-based method. But it has the disadvantage of full complex system matrix which leads to a high computational cost.

In 1981, Bettess [22] showed the comparison of the storage requirements and numbers of operation between boundary element and finite element methods for simple cases of interior problems such as a square domain for two dimensional problem and a cubic domain for three dimensional problem. He also showed the advantage of the finite element method for a problem of a large aspect ratio, and concluded that dimensionality advantage of boundary integral method over the finite element method is more apparent than real. In 1992, Harari and Hughes [54] applied the same approach of operation counts to compare two methods for two-dimensional and three-dimensional, and interior and exterior domain problems using direct and iterative solvers. They also concluded that the finite element method is economically competitive with the boundary element method. Despite the fact that the boundary element method uses fewer equations to discretise the same physical problem, the advantages of the finite element method due to the sparse character of the domain-based matrices may lead to more economical storage requirement and solution. The computational advantage of the finite element method compared to boundary element method was supported by Burnett [29]. He compared elapsed time required to form the matrix and solve the equations by boundary element method and finite element method, which uses infinite elements on the outer boundary, for a large coupled structural acoustic problem. He showed that the elapsed time required by the boundary element method rapidly increases as the number of degrees of freedom of the problem increases, in contrast to the gradual increase of the time required by finite and infinite element combination.

However the situation has been changing both for finite and boundary elements. As a new finite element formulation, the discontinuous Galerkin method has been developed recently and applied to wave problems mostly in the time domain. In this formulation the approximation space may be discontinuous across element interfaces, and the continuity is enforced by constraints at the element interfaces. This method has advantages that it requires relatively few points per wavelength and has low dispersion and dissipation errors [58, 83]. Also it can be easily parallelised. On the other hand the fast multipole approach [85] has been applied to boundary element formulation for wave problems [41]. This method leads a sparse system matrix and is very efficient although it is limited to

homogeneous problems.

A more comprehensive survey of the development of the conventional finite element method for wave problems is given by Astley [5].

1.4   Plane Wave Basis Finite Elements

The principal limitation of standard finite element formulation for wave problems is the difficulty of resolving spatially oscillating wave-like solutions using node-based interpolation schemes. In practice, as discussed in section 1.3, at least 10 degrees of freedom per wavelength are required for reasonable accuracy. Infinite elements have an infinite extent in one or more directions, but the shape function in the direction of finite length is the same as that of standard finite elements. Therefore the requirement for the ratio of element size to the wavelength is the same as in conventional elements.

Thus attempts to include the nature of wave solution in the shape functions have been made to release elements from the limitation of the ratio of element size to wavelength so that they can be larger and that the degrees of freedom of the problem can be reduced. The first attempt was made by Bettess and Zienkiewicz [95, 27] in the form of infinite elements, and that on finite elements was made by Astley *et al.* [10, 1] using wave envelope elements. Both were intended to be applied to unbounded domain problems and the wave envelope element was extended to have infinite extent, which will be discussed in Section 1.5. Following Astley, Chadwick *et al.* [33] attempted to develop wave envelope finite elements in which the wave direction was unknown, *a priori*, and to iterate for the correct wave direction, using some type of residual.

Melenk and Babuška [75, 17] proposed a new finite element method named the partition of unity finite element method (PUFEM). In one variant of this, applied to the Helmholtz equation, finite element shape functions incorporating the wave shape are used, as presented in Bettess and Zienkiewicz infinite elements [95, 27] and the Astley wave envelope elements [10, 1]. But the shape functions of Melenk and Babuška, have the innovation that they include multiple wave directions. They applied this formulation to the Helmholtz equation and demonstrated that the method works for a plane wave propagating through a square mesh of square finite elements, even when the direction of the wave was *not included* in the nodal directions. Subsequently Laghrouche and Bettess extended this approach to various finite element types for the solution of the Helmholtz equation and applied them

6

to solve more realistic wave problems such as diffraction problems [67, 71]. This method overcomes the requirement for the ratio of the element size to the wavelength. The method was also developed independently by Ortiz and Sanchez [78]. They developed a different integration scheme for linear triangle elements and produced excellent results for cylinder diffraction problems. They applied local co-ordinate rotation to the integrand so that the oscillatory component is transformed into the form depending only on one 'effective' direction with an 'equivalent' wavenumber. This simplifies the integration procedure and reduce the number operations. In this approach the potential at each node is expanded in a discrete series of approximating plane waves propagating in different directions so that the nodal shape functions are multiplied by trigonometric functions. Because of this choice of basis function a single finite element can contain many wavelengths, unlike standard elements. In previous years, the same idea has been theoretically investigated by de La Bourdonnaye [43, 44] under the title of 'microlocal discretization' for solving scattering problems with integral equations, but no numerical results were reported. Other authors have experimented with similar, though not identical concepts [45, 74]. And also similar ideas have also been applied to boundary elements with great success [79, 80]. These results demonstrate that the method can solve short wave diffraction problems with a greatly reduced number of active variables.

In the standard n-node finite element formulation, the domain Ω is divided into n-node finite elements. The unknown field variable ϕ within each element is described using polynomial shape functions N_j and the nodal values of the potential ϕ_j. In special wave finite elements based on PUFEM the field variable at each node, ϕ_j, is expanded in a discrete series of approximating plane waves propagating in different directions $\theta_j^l (l = 1, \ldots, m_j)$ with amplitudes $A_j^l (l = 1, \ldots, m_j)$, where m_j is the number of the approximating plane waves for node j. The number of the degrees of freedom of the special wave finite element matrix becomes $\sum_{j=1}^n m_j$ which is larger than the degree of freedom of element matrices in the case of a standard n-node finite element, $n \times n$, unless all $m_j (j = 1, 2, \cdots, n)$ are equal to 1. However this special wave finite element can be larger than the wavelength, unlike the standard finite elements which normally need to satisfy the requirement of using about 10 degrees of freedom per wavelength as mentioned in the previous section. This will lead to a great reduction in the dimensions of the problem, and also have an advantage that the mesh model can remain unchanged even though the wavenumber increases [67, 69, 71].

The special wave finite elements dealt with in this thesis are those of Laghrouche and Bettess [67, 69, 71], which will be discussed more in detail in chapter 3.

1.5 Infinite Elements

The infinite element scheme is also a 'domain-based' method. It is an extension of the concept of finite elements in which the elements have an infinite extent in one or more directions. It does not require the truncation of the computational domain or the boundary condition applied to approximate the Sommerfeld radiation condition. When applied to wave problems the shape functions within such elements include outgoing wave-like factors. It is easily implemented together with finite elements, and an advantage is that the system matrix remains banded and symmetrical, in contrast to full un-symmetric complex system matrix obtained by the boundary element method.

The original concept of infinite elements for wave problems was proposed by Bettess and Zienkiewicz [94], and since then much research on infinite elements have been carried out. Much of the subsequent development of the method is described in Bettess' monograph [24], and more recently, a review of formulations and an assessment of accuracy have been presented by Astley [8] and Gerdes [48, 49].

In this section, the main developments of infinite elements are briefly described.

1.5.1 Exponential Decay Infinite Elements

The first concept of infinite elements was introduced by Zienkiewicz and Bettess [94] in 1975. This was subsequently extended by the same authors [27] in 1977. This first infinite element for wave problems was based on an exponential model of the wave shape. In this paper, a set of shape functions based on Lagrange polynomials multiplied by exponential decay term and a periodic function is used for the infinite direction ξ in the local co-ordinate system, to deal with fluid-structure interaction problem of surface waves in two dimensions. When n points are considered, the first $n-1$ points have finite ξ co-ordinates and the n-th point is infinitely distant. This set of shape functions are chosen to model satisfactorily a wave which is reflected away from the structure and dies away gradually for a fluid-structural interaction problem for surface waves. The functions also satisfy the Sommerfeld radiation condition. The shape functions consists of three terms: the first term represents the spatially periodic nature of the reflected wave, with the wavenumber k, the

second term is introduced to force the wave to decay as ξ becomes large with the measure of the severity of the decay called 'decay length', and the last term is a conventional Lagrange polynomial. This infinite element was presented in variational terms, which is identical to the use of the Bubnov-Galerkin weighted residual method. Integration over elements was performed numerically, using either Gauss-Laguerre quadrature or a novel Newton Cotes type formula.

Although these elements do not behave correctly in the far field, they can be tuned to give accurate solutions within the inner region. A suitable value for the decay length must be selected, although the solutions are in general not too sensitive to the exact value. This set of shape functions can be applied to two or three dimensional cases, in combination with conventional Lagrange polynomials in the other finite direction or infinite shape functions in the other infinite directions. This element was effective in representing the effect of the exterior region on the interior region of interest, but it was unable to represent the correct asymptotic decay for the two-dimensional case in the far field.

1.5.2   Mapped Infinite Element

The first mapped infinite elements for static elastic problem were introduced by Beer and Meek [20]. A different mapping for such problems was introduced by Zienkiewicz [96, 97], which was later applied to periodic wave problems with the addition of the appropriate wave components, by Bettess *et al.* [25] and Zienkiewicz *et al.* [93]. It can model very closely the appropriate decay of the wave amplitude with distance, and was thus an improvement over the exponential decay element. This mapped infinite element for waves was also presented in variational terms. In the original expressions of infinite element formulation by Bettess and Zienkiewicz, mapping from a local finite co-ordinate to a global infinite co-ordinate is written in terms of functions defined at x_0, the 'pole' of the infinite element and x_2, the node which is at twice the distance between the 'pole' and the inner edge of the infinite element. Marques and Owen [73] dealt with the same mapping with slightly different expressions. They achieved the mapping functions defined at x_1, the node at the inner edge of the infinite element and x_2 explained above. These infinite mapping are essentially based on the same concept, but the Marques and Owen expression clearly show the similarity between finite and infinite element mappings and makes mapped infinite elements easier to understand. A similar procedure was also suggested by

Kumar [62].

The essential effect of using a mapped infinite element is that the finite domain $-1 \leq \xi \leq 1$ in the local co-ordinates is mapped onto an unbounded domain $a \leq r \leq \infty$ in the global co-ordinates, where r is the distance from the 'pole' of the infinite element and a is a distance from the 'pole' to the inner edge of the infinite element. For the two dimensional case in which an infinite element extends to infinity in the radial direction and is finite in the angular direction, the infinite geometry mapping in the radial direction is combined with a usual finite mapping in the angular finite direction. The mapping in the radial direction from ξ to r is given by $r = 2a/(1 - \xi) = A/(1 - \xi)$ where $A = 2a$. In the formulation of this first type of mapped infinite elements, A was a constant. This means that infinite elements had a common 'pole' and they had to be placed on a circular mesh in the two dimensional case and a spherical mesh in the three dimensional case.

The field variable ϕ is interpolated using polynomial shape functions P_j and the nodal values ϕ_j in the local co-ordinates. The expression for ϕ takes the form of a polynomial in powers of ξ. Substituting the mapping between ξ and r into the polynomial form yields a polynomial in inverse powers of r. This shape function in the global co-ordinates contains a decay term of the form $1/r$, which is suitable to describe the decay of the outgoing wave in three dimensional exterior wave problems. In two dimensional exterior wave problems, however, the asymptotic solution to the Helmholtz equation can be described by a series of combined Hankel and trigonometric functions, the simplest solution to the Helmholtz equation being the zeroth-order Hankel function of the ℓ-th kind $H_0^{(\ell)}(kr)$ where ℓ equals to 1 or 2. For large r, $H_0^{(\ell)}(kr)$ oscillates roughly like $\cos(kr) \pm i \sin(kr)$ while decaying in magnitude as $r^{-1/2}$. Therefore, in order to describe the wave behaviour of decay and wave-like oscillation in two dimensional domain, the shape function needs to be multiplied by $r^{1/2}$ and the periodic component $\exp(\pm ikr)$.

The original mapped wave infinite element theory concentrated on circular problems. Although some elliptical diffraction problems were solved, the outer ring of infinite elements were placed in a circular mesh. The theory as originally presented does not allow for the infinite elements to be non-circular. In particular, the mapping terms are taken to be constant, which implies circularity of the mesh of infinite elements. For problems which are not approximately circular, the requirement of a circular outer ring of infinite elements can lead to excessively large meshes of finite elements, with associated computa-

tional cost. The extension of the mapping so as to allow infinite elements to have arbitrary pole locations so that they can be placed on arbitrary boundary was first applied to wave envelope elements using conjugate weighting functions, which is introduced later in 1.5.4, by Astley *et al.* [14], Cremers *et al.* [40] and Cremers and Fyfe [39]. Bettess and Bettess [21] followed their mapping, but used the Bubnov-Galerkin or unconjugated method and the original shape functions of the Bettess and Zienkiewicz papers [25, 93]. They demonstrated that a relatively simple extension of the original mapped wave element theory enables the method to be used for wave diffraction problems of large aspect ratio, and that the results are accurate.

1.5.3 Spheroidal and Ellipsoidal Infinite Element

Burnett and Holford [29, 31] proposed the formulation of unconjugated prolate and oblate spheroidal infinite elements to address the defect that mapped infinite elements must be placed in a circular or spherical mesh. They developed 'prolate and oblate spheroidal infinite elements' for three dimensional problems. These elements are based on trial and test functions which closely resemble those of the mapped infinite element by Bettess. However in their elements a spheroidal co-ordinate system is used rather than a spherical one. The shape functions are expressed as products of shape functions of radial and angular directions and the radial shape function is a truncated form of the radial part of multipole expansion of a radiation function in the region exterior to the ellipsoid, which is in a power series in $1/r$ where r is an ellipsoidal radius, for radiated or scattered fields. The radiating or scattering object can be enclosed in a spheroidal inner mesh. Burnett and Holford prove that the solution will converge as the element order is increased. This is a key strength of their method. It provides a much more economical solution for problems of large aspect ratio than using a spherical mesh.

By using separable shape functions in each directions, element contributions to the system matrix can be formed as products of separable integrals in radial and angular directions. In particular the radial integrals are common to all elements and can be evaluated analytically, which leads to the big reduction of the computational cost for forming matrices. Subsequently Burnett and Holford [30] extended their infinite element to ellipsoidal co-ordinates as a generalised formulation including their former elements as limiting cases.

11

1.5.4 Wave Envelope Element

The 'wave envelope' elements presented by Astley in a series of papers with co-workers [1, 2, 10, 11, 12, 13] were based on Petrov-Galerkin approach in which complex conjugates of wave-like shape functions were used as weighting functions. This made the resulting element matrix Hermitian, i.e. a matrix whose transpose is equal to the matrix of the complex conjugate of its entries, but simplified the element integrations considerably since the oscillatory components in the basis and test functions cancelled identically within the integrands. These 'wave envelope' elements incorporated the correct, asymptotic behaviour in the far field.

In references [1, 2, 12], Astley proposed a wave envelope element for aeroacoustic applications, in which the lack of symmetry is of little concern since 'mean flow' terms generate a non-symmetric coefficient matrix irrespective of the residual formulation. The wave envelope element included the asymptotic decay and the harmonic behaviour of the solution within the shape functions for a large but finite outer domain, so that wave envelope elements are required to resolve only the discrepancy between the actual solution and the implied harmonic and amplitude variations incorporated in the discretization instead of the solution itself. Therefore it was possible for an element to extend over many wavelengths and for the dimension of the whole problem to be reduced.

The formulation of the wave envelope element is similar to that of the infinite element. The weighting and shape functions are identified with the global shape functions within the inner region. In the near field to the radiating or scattering objects standard finite elements were applied and in the exterior region extending to the far field wave envelope elements were applied. The shape functions of a wave envelope element were defined so that the basis functions incorporate reciprocal decay and a wave-like variation corresponding to a locally outward travelling wave. The weighting functions are chosen to be the complex conjugates of the basis functions.

These original wave envelope elements were finite rather than infinite, being truncated at a finite distant far enough from the spherical surface. Integrals evaluated over this surface contributed to the resulting coefficient matrix but approached a finite limit for large radii.

1.5.5 Mapped Wave Envelope Element

The wave envelope element was extended to the mapped wave envelope element which has infinite extent for a one dimensional problem by Bettess [23]. However Bettess solved an artificial problem, which did not display all the subtleties of true wave behaviour and thus a key feature was glossed over. The first application of mapped wave envelope element to real two and three dimensional problems was by Astley [14], Cremers et al. [40] and Cremers and Fyfe [39]. In the formulation of the mapped wave envelope element, the shape functions are derived from mapping the finite element on to an infinite domain, which is essentially the same as the mapped infinite elements by Bettess *et al.* [25] and Zienkiewicz *et al.* [93] except that the requirement for mapped infinite elements that they must conform to the exterior of a circle or sphere was removed. The weighting functions are based on the complex conjugates of the shape functions as in the wave envelope finite elements by Astley [1]. The weighting functions are products of the complex conjugate of the shape function and the factor $(a/r)^2$ to ensure finiteness of the integrals involved in the evaluation of the system matrices and the elimination of integrals at infinity.

In the mapped wave envelope element by Astley *et al.* [14], the mapping can vary from one element to the next and the elements can be placed on the boundary of arbitrary shape, although explicit expressions for the derivatives of the shape functions with respect to the non-radial local co-ordinates are not presented. Astley also presented several oblate and prolate spheroidal mapped wave envelope elements for axisymmetric problems in reference [6]. This formulation is in terms of spheroidal co-ordinates so that numerical representation for wave fields in the vicinity of objects of large aspect ratio are improved.

Cremers *et al.* [40] gave the explicit expressions for the derivatives of the shape functions in the local co-ordinates for mapped wave envelope elements of the same type as Astley *et al.* [14], which permit variations in the mapping parameter. Their elements for two dimensional problems used linear mapping in the angular direction and variable order of infinite mapping in the radial direction, and were applied to a range of problems in acoustics. Cremers and Fyfe [39] also presented three dimensional wave envelope elements using linear or quadratic mapping in the angular directions and a variable order of infinite mapping in the radial direction.

1.5.6 Conjugated Infinite Element

A conjugated infinite element formulation based on Burnett [29] was implemented by Shirron and Babuška [87]. It was similar to the wave envelope elements by Astley in that both preserve the correct asymptotic behaviour in the trial solution - as $(1/r)\exp(-ikr)$ in three dimensions - and both use complex conjugates of the trial functions as test or weighting functions. The finite contributions from the spherical boundary at 'infinity' are however dealt with differently in each case. In the wave envelope approach, as originally formulated, these contributions were evaluated numerically on a distant boundary, whereas in the more recent conjugated formulations they are evaluated analytically as the radius of this surface becomes infinite.

1.5.7 Review and Assessment of Infinite Element Formulations

As many types of infinite elements have been developed, there are a number of studies which review infinite element schemes and evaluate the performance by comparison.

Gerdes [48] compared the formulations of infinite elements on the same benchmark problem of the scattering of a plane wave on the surface of the unit sphere and analysed the convergence properties. His conclusion was that the unconjugated formulations converges on the boundary of the scatterer and in the near field more rapidly than the conjugated formulations however that the latter converges in the entire exterior domain. The unconjugated Burnett scheme was the most efficient to get the accurate solution in the near-field and the conjugated Astley-Leis formulation is efficient when the solution in the whole exterior is needed.

Astley [6, 7] presented some comparisons of accuracy of conjugated spherical and spheroidal infinite elements (mapped wave envelope element). He also derived the transient formulation by taking an inverse Fourier transform of the discrete infinite element equations in the frequency domain using spherical and spheroidal co-ordinate system [3, 4, 6, 7]. This is practicable in the case of conjugated infinite element formulations since the coefficient matrix can be written in terms of frequency-independent (acoustics) 'mass', 'stiffness' and 'damping' matrices. Cipolla [34] and Cipolla and Butler [35] demonstrated that this procedure of applying an inverse Fourier transform is not practical for unconjugated infinite elements because convolution integrals arise due to the exponential integral function in the frequency domain. Thus they used the Burnett formulation using spheroidal co-

14

ordinate system with conjugated weighting functions as the basis for a transient scheme and which was implemented for first-order elements.

Shirron and Babuška [87] compared conjugated and unconjugated infinite elements based on the Burnett spheroidal formulation [29] with various approximate boundary conditions for unbounded problems. Their comparison used simple examples of the scattering of a plane wave by a rigid circle in two dimensions and that by a rigid sphere in three dimensions. The conclusion is that the unconjugated elements serve a highly accurate boundary condition on the inner boundary of infinite elements but fail to provide an accurate approximation of the solution in the exterior domain, i.e., inside infinite elements. On the other hand, conjugated elements closely approximate the exact solution in the exterior domain while the approximation diverges in the unconjugated elements in the far field. This conclusion agrees with that by Gerdes [48] introduced above. Shirron and Babuška [87] also simulated a spherical monopole solution generated by a cylinder of the aspect ratio 10 : 1 with hemispherical caps on both ends. The results indicate that very high radial orders are required in the conjugated formulation. Unconjugated models gave good results but become ill-conditioned at very low radial orders.

Recently Astley reviewed these infinite element schemes and comparisons, and presented a procedure for assessing their performance [8]. The orthogonal transverse basis was used for the trial solutions for the comparison of conjugated and unconjugated Burnett formulations and conjugated Astley-Leis formulations. Infinite elements were directly attached to a spherical radiator. He concluded that the conjugated element, especially the conjugated Burnett formulation, is more effective in the near-field computation and that the conjugated Astley-Leis formulation is the most effective in the far-field, which is in agreement with the conclusions by Gerdes [48] and Shirron and Babuška [87]. Astley also indicated that all of the infinite element schemes become ill-conditioned for sufficiently large radial orders.

Gerdes [49] also reviewed various infinite element formulations and addressed in particular the choice of shape functions and the variational formulation by using a unified notation throughout.

1.6 Boundary Elements

The boundary element method is also one of the numerical techniques which are widely applied to wave problems [36]. In this method the differential operator and the boundary conditions in the domain are replaced by an equivalent boundary integral equation on the boundary. Through the use of the free-space Green's function satisfying the Helmholtz equation and Green's theorem, the problem can be reduced to solving a boundary integral equation, and the dimension of the problem is reduced by one. For instance, the volume integration for the three dimensional problem is transformed into the surface integration over the boundary which encloses the domain. With this method the boundary rather than the domain is divided into elements, so that the dimension of the elements is smaller by one than that of finite elements. The values on the boundary are obtained as the solution of the problem and values inside the domain will be calculated afterwards by summing up the contributions of the values on the whole boundary.

One of the advantages of the boundary element method over domain-based methods is the simpler modelling due to the reduced dimension of the problem. Discretization over the boundary is generally easier to handle than that over the domain, and the number of elements is normally much smaller. Another advantage of the boundary element method is that it can deal with unbounded domain problems without truncation because the Green's function automatically satisfies the Sommerfeld radiation condition. The external domain of the radiating or scattering objects can be enclosed by the inner boundary consisting of the surface of the objects and the outer boundary at a large distance. The outer boundary can be a sphere in three dimensions or a circle in two dimensions. As the distance to the outer boundary extends to infinity, the contribution of the outer boundary tends to zero because of the Sommerfeld radiation condition. Consequently the integration over the outer boundary disappears from the integral equation. This enables the method to deal with an unbounded domain without truncation or approximated boundary condition.

However the conventional boundary element method also has disadvantages. The reduction of the number of elements does not simply mean the reduction of the computational cost, as demonstrated in studies introduced in section 1.3. Due to the non local operator leading to full complex system matrix, the computational cost of forming and solving the matrices and the memory demand become large very quickly as the number of degrees of freedom of the problem increases. These costs can be prohibitive and may

indeed prevent the computation of a reliable numerical solution. Also, the non-uniqueness problem is a crucial problem of the boundary element method [32, 86]. The boundary integral equation formulation for exterior problems does not yield a unique solution at certain characteristic frequencies, so-called 'irregular frequencies'. This problem is caused by the fictitious resonance of the internal domain of the radiating or scattering objects, i.e. the domain enclosed by the boundary Γ_i, although they have no physical significance for exterior boundary value problem being solved. They are a consequence of the boundary function, not the particular numerical implementation of the method.

As already mentioned in Section 1.3, however, the situation has been changing. The fast multipole approach, which was first introduced by Rokhlin [85] has been applied to boundary element formulation for wave problems [41]. This method provides an efficient mechanism for computation in large scale systems and drastically reduces computational cost although it involves some highly complex programming. Applying this approach at multi-levels leads a sparse system matrix and great efficiency for unbounded problems although it is limited to homogeneous problems from the nature of boundary element formulation.

1.7 Outline of the Thesis

In this thesis, the theory and the formulation of the special wave finite elements are discussed, and the special integration schemes for the elements are developed. Then the special wave infinite elements, a new concept of the mapped wave infinite elements with multiple wave directions, are developed. The coupling of the special wave finite elements to the mapped wave infinite elements and the special wave infinite elements are also discussed.

In Chapter 2, some basics about wave problems in unbounded domain are introduced. The Helmholtz equation, which governs the time-harmonic wave problems discussed throughout in this work, and the Sommerfeld radiation condition for the waves propagating to infinity are shown, and then the general solutions and the analytical solution of typical examples of radiation and scattering problems are shown. In Chapter 3, theory and the formulation of discrete equations for special wave finite elements, developed by Laghrouche and Bettess [67, 69, 71], are presented. Also some numerical results obtained by them [67] are presented to demonstrate the basic features of the elements. In Chapters 4 and 5, semi-analytical integration schemes specially developed for the special

wave finite elements are presented. Chapter 4 is concentrated on the rectangular and triangular element that are relatively simple. These integration schemes were developed by Bettess *et al.* [26] including the author. Then Chapter 5 deals with the more complicated case of quadrilateral elements. The development of the integration scheme in this chapter was conducted by the author [92]. In Chapter 6, the theory and the formulation of discrete equations for the mapped wave infinite elements are presented. The infinite elements used in this chapter, and the coupling of the elements with the standard finite elements are based on the Bettess formulation [21]. Then the coupling of the elements with the special wave finite elements are also discussed, which was developed by the author [89]. In Chapter 7, the new formulation of special wave infinite elements, the expansion of mapped wave infinite elements to include multiple wave directions instead of using a single single radial direction, is described. The application of a conventional numerical integration scheme to the mapped wave infinite elements is also presented. This enables the inclusion of multiple wave directions into the mapped wave infinite element scheme. The special wave infinite element is a novel element developed by the author, which forms the core of the work. Finally a summary of this thesis is given in Chapter 8.

Chapter 2

Wave Problems in Unbounded Domains

In many cases of wave radiation and scattering problems, the domain considered is much larger than the wavelength and the particular area of interest where the problem is to be solved. In that case it is practical to treat the domain as being unbounded.

In this chapter, the basics of the wave problem governed by the Helmholtz equation in unbounded domain, which is the target of this research, are discussed. The Helmholtz equation dealt with in this paper governs various wave problems such as acoustic wave fields and shallow water problems in certain conditions.

2.1 Wave Problems in Unbounded Domains

The simplest type of unbounded wave problem is the radiation problem, where a wave is generated by a object in the medium. Another type is the scattering problem, where there is an incoming wave, which encounters an object, is modified and then is radiated away. This is more complicated than radiation problems. For the case of surface wave on the sea, an example for the former case can be a floating object in the middle of the sea generating surface waves and an example of the latter case can be an incident surface wave on the sea hitting an offshore structure. For the case of acoustic waves, the former can be the radiated sound from a loudspeaker or a vibrating machine and the latter can be the scattering of sound waves by noise barriers.

The fundamental domain problem is illustrated in Figure 2.1. A domain Ω_i is enclosed with boundary Γ_i and Γ_o. The interior boundary Γ_i is the surface of a radiating or
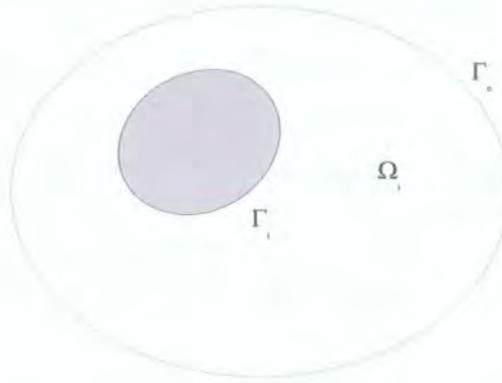
Figure 2.1: Unbounded problem.

scattering object, and the exterior boundary Γ_o is at a certain finite distance for a bounded domain problem, or at infinity for an unbounded problem. Because domain-based methods normally can not deal with the infinite extent of a domain, Γ_o can be an artificial boundary assumed to be at a large but finite distance. Waves radiated or scattered by the object, Γ_i, propagate away towards infinity and do not return. This condition that there is no incoming wave is called the radiation condition, which the radiated or scattered wave must satisfy.

2.2 Governing Equation

2.2.1 Helmholtz Equation

The wave equation is the differential equation which governs the time dependent wave problems. Derivation of the wave equation is explained in many text books, such as, in acoustics, by Rayleigh [84] and Morse [76]. The wave equation in a homogeneous and isotropic medium in domain Ω is given by

$$\frac{\partial^2 \Phi}{\partial t^2} = c^2 \nabla^2 \Phi \qquad \text{in } \Omega \qquad (2.1)$$

where t is the time variable, c is the wave speed and ∇^2 is the Laplacian operator. The field variable of interest, Φ can be potential, sound pressure or particle velocity for acoustic problems, and wave elevation, pressure for surface wave problems, among many other possibilities.

For time harmonic problems the field variable Φ can be written by

$$\Phi = \phi e^{-i\omega t} \tag{2.2}$$

where ϕ is the time independent wave potential, $i = \sqrt{-1}$ and ω is the angular frequency. Substituting Equation (2.2) into Equation (2.1) leads to the Helmholtz equation

$$(\nabla^2 + k^2)\phi = 0 \qquad \text{in } \Omega \tag{2.3}$$

where $k = \omega/c$ is the wavenumber.

2.2.2 Boundary Conditions

Boundary conditions are given as one of the following:

(1) Dirichlet Boundary Condition

$$\phi = \bar{\phi} \tag{2.4}$$

where $\bar{\phi}$ is the given value of ϕ. In cases where ϕ is velocity potential or sound pressure in acoustics, this condition is applied when the sound pressure at a boundary is given. The special case of $\bar{\phi} = 0$ means that the boundary acts like an opening to a vacuum where no wave occurs. In this case the wave incident to the boundary is perfectly reflected so that the reflected wave becomes 180° out of phase.

(2) Neumann Boundary Condition

$$\nabla \phi \cdot \mathbf{n} = \bar{u} \tag{2.5}$$

where $\mathbf{n}$ is the outward normal of boundary Γ and $\bar{u}$ are the given values of the normal derivative of ϕ. This condition is widely applied in realistic applications. For example, in many radiation problems, waves are generated by vibrating objects in the domain and the conditions are given by the distribution of the normal velocity $-\bar{u}$ on the surfaces of the objects. In case of $\bar{u} = 0$ where ϕ is the total potential in the field, the boundary is rigid, i.e., the wave is perfectly reflected in phase with the incident wave, which corresponds

21
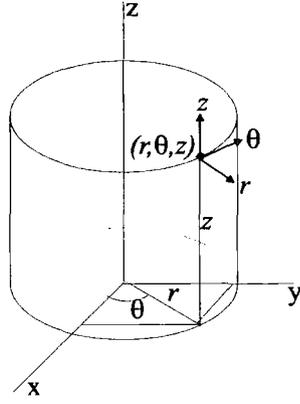
Figure 2.2: Cylindrical co-ordinates.

to many cases of scattering problems where the surface is hard enough and the vibration excited by the wave is negligible.

(3) Robin Boundary Condition

$$\alpha\phi + \beta\nabla\phi \cdot \mathbf{n} = \gamma \tag{2.6}$$

where α, β, and γ are the parameters describing the relationship between ϕ and its normal derivative. The Robin boundary condition is often applied to give local absorbing boundary conditions. For example, in many problems the characteristics of the surfaces are given by acoustic impedance z, which is the ratio of the acoustic pressure to the particle velocity. It can be written in terms of ϕ by

$$z = ik\rho c \frac{\phi}{\nabla\phi \cdot \mathbf{n}} = -ik\rho c\frac{\beta}{\alpha} \tag{2.7}$$

where ρ is the density of the medium in the domain, and ρc is called the characteristic acoustic impedance of the medium. The acoustic impedance z can be applied using the Robin boundary condition by setting parameters α, β and γ in Equation (2.6) as follows:

$$\frac{\beta}{\alpha} = -\frac{z}{ik\rho c}, \qquad \gamma = 0 \tag{2.8}$$

2.3 General Solution of the Helmholtz Equation in Two Dimensions

The Helmholtz equation can be expressed in the cylindrical co-ordinates r, θ, z

$$\left\{ \frac{1}{r}\frac{\partial}{\partial r}\left(r\frac{\partial}{\partial r}\right) + \frac{1}{r^2}\frac{\partial^2}{\partial\theta^2} + \frac{\partial^2}{\partial z^2} \right\}\phi + k^2\phi = 0 \tag{2.9}$$

The separated equations for the factored solution

$$\phi = \phi_r(r)\phi_\theta(\theta)\phi_z(z) \tag{2.10}$$

are

$$\frac{d^2\phi_z}{dz^2} + k_z{}^2\phi_z = 0 \tag{2.11}$$

$$\frac{d^2\phi_\theta}{d\theta^2} + m^2\phi_\theta = 0 \tag{2.12}$$

$$\frac{1}{r}\frac{d}{dr}\left(r\frac{d\phi_r}{dr}\right) + \left(k_r{}^2 - \frac{m^2}{r^2}\right)\phi_r = 0 \tag{2.13}$$

$$k^2 = k_r{}^2 + k_z{}^2 \tag{2.14}$$

The general solution for ϕ_z, is a combination of $\exp(ik_zz)$ and $\exp(-ik_zz)$. The solution for ϕ_θ is $\cos(m\theta)$ or $\sin(m\theta)$, where m is the wavenumber along the circumference and must be an integer for the solution to be continuous at $\theta = 0 = 2\pi$. The solution for the radial equation is a combination of the Bessel function of the first kind $J_m(k_rr)$ and the Bessel function of the second kind, which is also called Neumann function, $Y_m(k_rr)$, as Equation (2.13) is a Bessel's equation.

When $k_z = 0$, the wave is uniform along z-axis and the problem is two-dimensional. The general solution of the Helmholtz equation in two dimensions is thus given by

$$(\alpha_m \cos m\theta + \beta_m \sin m\theta)H_m^{(\ell)}(kr) \tag{2.15}$$

$H_m^{(\ell)}(kr)$ is the Hankel function of the ℓ-th kind of m-th order where ℓ can be 1 or 2, which is given by

$$H_m^{(\ell)}(z) = J_m(z) \pm iY_m(z) \tag{2.16}$$

where $+$ and $-$ on the right hand side is for the case of $\ell = 1$ and $\ell = 2$, respectively. For

large z, these functions can be approximated by the asymptotic forms

$$J_m(z) \cong \sqrt{\frac{2}{\pi z}} \cos\left(z - \frac{2m+1}{4}\pi\right) \qquad (2.17)$$

$$Y_m(z) \cong \sqrt{\frac{2}{\pi z}} \sin\left(z - \frac{2m+1}{4}\pi\right) \qquad (2.18)$$

Therefore, for large kr,

$$H_m^{(\ell)}(kr) \cong \sqrt{\frac{2}{\pi kr}} \, e^{\pm i\left(kr - \frac{2m+1}{4}\pi\right)} \qquad (2.19)$$

and the general solution given by Expression (2.15) becomes, for large kr

$$(\alpha_m \cos m\theta + \beta_m \sin m\theta)\sqrt{\frac{2}{\pi kr}} \, e^{\pm i\left(kr - \frac{2m+1}{4}\pi\right)} \qquad (2.20)$$

This means that the wave oscillates roughly like $\exp(ikr)$ in the radial direction r and that the amplitude decays like $r^{-1/2}$ in two dimensions.

When the time dependence of the wave variables is assumed with $\exp(-i\omega t)$, the Hankel functions of the first kind express the outgoing waves from the source to infinity. On the contrary when $\exp(i\omega t)$ is assumed as the time dependence factor, the Hankel functions of the second kind express the outgoing waves.

2.4 Non Reflecting Boundary Conditions

2.4.1 The Sommerfeld Radiation Condition

In an unbounded domain, the radiated or scattered wave propagates away towards infinity. In the case of scattering problems, the total wave field ϕ can be separated into an *incident* wave ϕ^i and a *scattered* wave ϕ^s

$$\phi = \phi^i + \phi^s \qquad (2.21)$$

The radiated or scattered wave must satisfy the radiation condition at infinity. The radiation condition for the time-harmonic wave problem is called the Sommerfeld radiation condition [88] and is given by

$$\lim_{r \to \infty} r^{\frac{n-1}{2}} \left(\frac{\partial \phi^s}{\partial r} - ik\phi^s\right) = 0 \qquad (2.22)$$

24

where n is the number of dimensions. It is difficult to apply this condition directly in finite elements models because it is given by the form of a limit at infinity. Therefore alternative boundary conditions are necessary to accurately approximate it.

2.4.2 Basic Damper Conditions

When the unbounded domain is truncated by an artificial boundary at a certain finite distance to be dealt with by a domain-based method, it is necessary to apply a suitable boundary condition. As said above, the boundary condition should approximate the Sommerfeld radiation condition at infinity, otherwise the solution inside the domain becomes inaccurate due to the fictitious reflection from the artificial boundary. The condition is often approximated by a local absorbing boundary condition. The locality of the boundary operator and the distance at which it is applied significantly influence the computational efficiency.

(1) Plane Damper Conditions

The simplest local non-reflecting boundary condition is the 'plane damper' boundary condition, which is also called 'ρc impedance boundary condition' in acoustics where 'ρc' is the specific acoustic impedance of the medium. This is derived as follows.

The wave equation in one dimension in a homogeneous and isotropic medium is written by

$$\frac{\partial^2 \phi}{\partial t^2} = c^2 \frac{\partial^2 \phi}{\partial x^2} \tag{2.23}$$

where ϕ is the field variable of interest. The d'Alembert solution takes the form

$$\phi = f_1(x - ct) + g_1(x + ct) \tag{2.24}$$

In Equation (2.24), function f_1 represents the outgoing wave and function g_1 represents the incoming wave. To seek the radiation condition, g_1 can be eliminated and Equation (2.24) becomes

$$\phi = f_1(x - ct) \tag{2.25}$$

On differentiating with respect to t and x,

$$\frac{\partial \phi}{\partial t} = -cf_1' \tag{2.26}$$

25

$$\frac{\partial \phi}{\partial x} = f_1{}' \tag{2.27}$$

By substituting these into Equation (2.23) leads to the relation

$$\frac{\partial \phi}{\partial x} + \frac{1}{c}\frac{\partial \phi}{\partial t} = 0 \tag{2.28}$$

For time-harmonic problems where the time dependence factor is given by $\exp(-i\omega t)$ where ω is the angular frequency,

$$\frac{\partial \phi}{\partial x} - ik\phi = 0 \tag{2.29}$$

This is called the 'plane damper' boundary condition.

This is accurate for a progressive plane wave in one dimension. Because the behaviour of the wave propagating outwards in two or three dimensions become similar to the progressive plane wave as it propagates further, the plane damper boundary condition is also accurate in the far field from a radiating or scattering objects in two or three dimensions. It is important that this condition is applied at a sufficiently large distance from the objects compared to the wavelength, otherwise it gives spurious reflections to the inner field.

(2) Cylindrical Damper Conditions

The finite domain to be treated can be reduced when higher order local non-reflecting boundary condition, such as cylindrical or higher order dampers, are applied.

For two-dimensional problems, the solution can be approximated by

$$\phi = \frac{f_2(x - ct)}{\sqrt{r}} \tag{2.30}$$

because the fundamental solution of the Helmholtz equation in two dimensions has the form of the Hankel function and its amplitude decays roughly in terms of $1/\sqrt{r}$ as seen in the previous section. In the same way as for one dimensional problems, the following simple radiation conditions can be obtained.

$$\frac{\partial \phi}{\partial r} + \frac{1}{2r}\phi + \frac{1}{c}\frac{\partial \phi}{\partial t} = 0 \tag{2.31}$$

26

or

$$\frac{\partial \phi}{\partial r} + \left(\frac{1}{2r} - ik\right)\phi = 0 \tag{2.32}$$

These are called 'cylindrical damper' boundary condition.

These damper conditions are basically exact when applied at infinity. However in the numerical analysis by a domain-based method, they are applied at a finite distance.

2.5   Example Problems in Two-Dimensions

2.5.1   Radiation from a Circular Cylinder
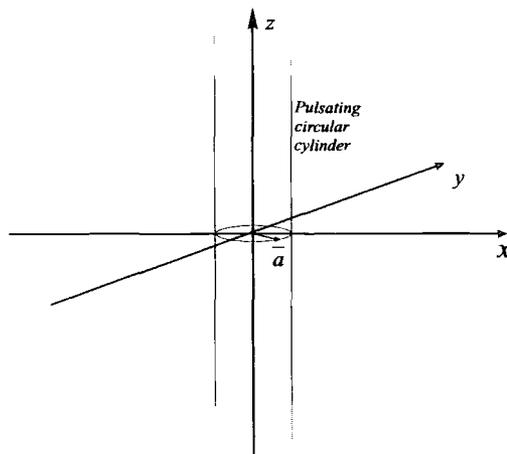
Figure 2.3: Radiation from a pulsating circular cylinder.

The most fundamental wave problem in two dimensions is that of radiation from a circular cylinder in the medium. Suppose there is a long cylinder of radius $\bar{a}$ whose surface is pulsating uniformly normal to the surface with the velocity $u_0 = U_0 \exp(-i\omega t)$ as shown in Figure 2.3. In this case, the wavenumber for the θ direction along the circumference m is zero, i.e., the wave is axisymmetric to the cylinder axis and independent of θ. The wave field thus can be treated as a two dimensional problem in a plane perpendicular to the cylinder axis. The solution takes simple form

$$\alpha_0 H_0^{(1)}(kr) = \alpha_0 \left(J_0(kr) + iY_0(kr)\right) \tag{2.33}$$

The field variable ϕ can be pressure or wave elevation etc., but here we consider the case

where ϕ is velocity potential. Then the velocity u is given by

$$u(r) = -\frac{\partial \phi}{\partial r} = \alpha_0 k H_1^{(1)}(kr)$$ (2.34)

From the velocity at the surface of the cylinder

$$u(\bar{a}) = \alpha_0 k H_1^{(1)}(k\bar{a}) = U_0$$ (2.35)

the amplitudes of the potential α_0 can be written with the amplitude of the velocity U_0

$$\alpha_0 = \frac{U_0}{k H_1^{(1)}(k\bar{a})}$$ (2.36)

and the potential is given by

$$\phi = \frac{U_0 H_0^{(1)}(kr)}{k H_1^{(1)}(k\bar{a})}$$ (2.37)

2.5.2   Scattering by a Circular Cylinder
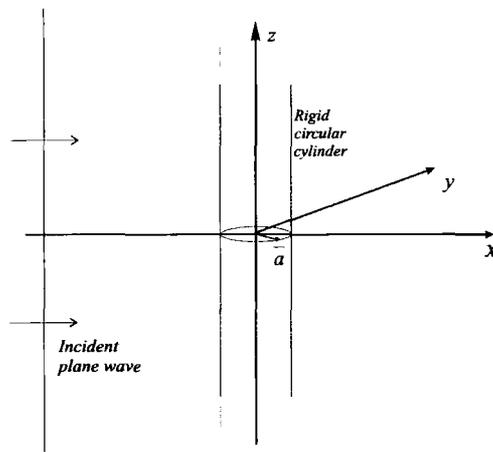
Figure 2.4: Scattering of plane wave by a rigid circular cylinder.

The simplest example of the scattering problems is that an incident plane wave is scattered by a object with simple geometry in the path of propagation. The wave is generated at infinity and results in a plane wave. The problem dealt with here is that a plane wave of unit amplitude is incident perpendicular to the axis of a rigid cylinder. For example, in case of surface waves in water, the incident plane wave propagates horizontally on the surface of water of finite depth and the cylinder is assumed to be vertical. The problem can be treated as a two-dimensional problem.

The geometry of the problem is shown in Figure 2.4. An incident plane wave ϕ^i of unit amplitude progressing from the negative x direction to the positive x direction is written by

$$\phi^i = e^{ikx} \tag{2.38}$$

where k is the wavenumber. This is also expressed by an infinite series of Bessel functions of the first kind

$$\phi^i = \sum_{m=0}^{\infty} i^m \epsilon_m J_m(kr) \cos m\theta \tag{2.39}$$

where r and θ are the polar co-ordinates of any considered point of the domain and $x = r \cos \theta$. The coefficients ϵ_m are $\epsilon_0 = 1$ and $\epsilon_m = 2$ for $m = 1, 2, 3, \cdots$. For the case of surface waves, this problem was first studied by Havelock [55] by considering an infinite depth, and then MacCamy and Fuchs [72] presented a solution for the cases of constant finite depth.

The total potential ϕ is the sum of the incident wave ϕ^i and scattered wave ϕ^s.

$$\phi = \phi^i + \phi^s \tag{2.40}$$

On the rigid surface of the cylinder, the normal derivative of the total potential satisfies

$$\nabla \phi \cdot \mathbf{n} = 0 \tag{2.41}$$

It leads to the boundary condition for the scattered potential

$$\nabla \phi^s \cdot \mathbf{n} = -\nabla \phi^i \cdot \mathbf{n} \tag{2.42}$$

Then the solution of the scattered potential is given by

$$
\begin{aligned}
\phi^s &= -\sum_{m=0}^{\infty} i^m \epsilon_m \frac{J_m'(k\bar{a})}{H_m^{(1)'}(k\bar{a})} H_m^{(1)}(kr) \cos m\theta \\
&= -\sum_{m=0}^{\infty} i^m \epsilon_m \frac{J_{m+1}(k\bar{a}) - J_{m-1}(k\bar{a})}{H_{m+1}^{(1)}(k\bar{a}) - H_{m-1}^{(1)}(k\bar{a})} H_m^{(1)}(kr) \cos m\theta
\end{aligned} \tag{2.43}
$$

where $\bar{a}$ is the radius of the cylinder, $H_m^{(1)}(kr)$ and $J_m(kr)$ are, respectively, the Hankel function of the first kind and the Bessel function of order m, and prime denotes differentiation with respect to r.

Chapter 3

Special Wave Finite Elements

In this chapter the formulations of standard finite elements and special wave finite elements for the wave problems governed by the Helmholtz equation are presented. The special wave finite element formulation employs the plane wave basis to describe the wave field. At each finite element node the potential is expanded in a discrete series of plane waves, each propagating at a specified angle. This enables a single finite element to contain many wavelengths unlike standard finite elements and leads to great reduction in the total number of degrees of freedom of problems and computational costs especially for short wave problems.

In this chapter, firstly the standard finite element formulation using the weighted residual method is described. There are many textbooks on the finite element formulation, for example, one by Zienkiewicz and Taylor [99]. Then the formulation of the special wave finite elements is presented. The special wave finite elements dealt with in this thesis have been developed by Laghrouche and Bettess [67, 69, 71].

3.1 Governing Equations

The Helmholtz equation which governs the wave problems in the frequency domain and the general expressions of boundary conditions are given by Equation (2.3) in Section 2.2.

As explained in the next section, the radiated or scattered potential instead of the total potential is dealt with in this chapter.

3.2 The Weighted Residual Method

By applying the weighted residual method to the Helmholtz equation given by Equation (2.3), we obtain,

$$\int_{\Omega} W(\nabla^2\phi + k^2\phi)d\Omega = 0 \tag{3.1}$$

where Ω is the domain considered and W is the weighting function. This gives the governing finite element integral equation for the problem. Using Green's second identity on Equation (3.1) gives

$$\int_{\Omega} (\nabla W \cdot \nabla\phi - k^2 W\phi)d\Omega - \int_{\Gamma} W\nabla\phi \cdot \mathbf{n}d\Gamma = 0 \tag{3.2}$$

where Γ is the boundary enclosing the domain Ω. This integral equation contains an integral over the domain Ω and an integral over the boundary Γ involving the first derivatives of the unknown function ϕ and the weighting function W. Equation (3.2) contains lower order derivatives than those occurring in Equation (3.1), and is called the *weak* form. From the term of the integral over the boundary Γ, the natural boundary condition arising from this weak form is

$$\nabla\phi \cdot \mathbf{n} = 0 \qquad \text{on } \Gamma \tag{3.3}$$

In order to deal with an unbounded domain by finite elements, the domain needs to be truncated at a finite distance by an artificial boundary Γ_r. As shown in Equation (2.21), the total potential can be written as the sum of the incident potential and the radiated or scattered potential. Because the radiated or scattered potential must satisfy the radiation condition at infinity, the boundary condition which should be applied to these waves on the artificial outer boundary is an absorbing boundary condition to approximate the Sommerfeld radiation condition. On these absorbing boundary conditions, accuracies of some absorbing boundary conditions are reported in comparison with some infinite elements by Shirron and Babuška [87]. However the radiation condition does not apply to the incident wave or the total potential when the incident wave is a progressive plane wave. Therefore only radiated or scattered potential will be dealt with in the finite element formulation hereafter. The boundary condition given by Equation (3.3) is not correct for the radiated or scattered potential and it is necessary to add the terms to give appropriate boundary conditions.

When the boundary Γ_n is the surface of radiating or scattering objects, the Neumann boundary conditions given by Equation (2.5) can be applied to the radiated or scattered potential ϕ. In radiation problems

$$\nabla\phi \cdot \mathbf{n} = \bar{u} \qquad (3.4)$$

where $\bar{u}$ is the given value of normal derivative of the radiated potential. In a simple case of scattering problems when the boundary Γ_n is rigid,

$$\nabla\phi \cdot \mathbf{n} = \bar{u} = -\nabla\phi^i \cdot \mathbf{n} \qquad (3.5)$$

where ϕ^i is the incident wave.

Let us consider the case where, for example, cylindrical damper condition [18] given by Equation (2.32), which corresponds to the first order BGT boundary condition by Bayliss et al. [19], is applied on the artificial boundary Γ_r. The weighted residual equation takes the form

$$\int_{\Omega} W\left(\nabla^2\phi + k^2\phi\right)d\Omega + \int_{\Gamma_n} W\left(\bar{u} - \nabla\phi \cdot \mathbf{n}\right)d\Gamma + \int_{\Gamma_r} W\left\{\left(ik - \frac{1}{2r}\right)\phi - \nabla\phi \cdot \mathbf{n}\right\}d\Gamma = 0 \qquad (3.6)$$

The weak form then becomes

$$\int_{\Omega}\left(\nabla W \cdot \nabla\phi - k^2 W\phi\right)d\Omega + \int_{\Gamma_r}\left(ik - \frac{1}{2r}\right)W\phi d\Gamma = \int_{\Gamma_n} W\bar{u}d\Gamma \qquad (3.7)$$

3.3 Standard Finite Element Formulation

3.3.1 Standard Finite Element Model

The domain Ω is divided into n-node finite elements. The unknown function ϕ within each element is approximated using polynomial shape functions N_j and the nodal values ϕ_j.

$$\phi = \sum_{j=1}^{n} N_j\phi_j = [N]\{\phi\} \qquad (3.8)$$

where

$$[N] = [N_1 \quad N_2 \quad \cdots \quad N_n] \qquad (3.9)$$

$$\{\phi\} = \{\phi_1 \quad \phi_2 \quad \cdots \quad \phi_n\}^T \qquad (3.10)$$

We put a finite set of approximate functions for the weighting function W

$$W = \sum_{j=1}^{n} w_j a_j = [w]\{a\} \tag{3.11}$$

where

$$[w] = [w_1 \quad w_2 \quad \cdots \quad w_n] \tag{3.12}$$

$$\{a\} = \{a_1 \quad a_2 \quad \cdots \quad a_n\}^T \tag{3.13}$$

and a_j are arbitrary parameters. Taking the weighting functions of the same form of the shape functions

$$w_j = N_j \tag{3.14}$$

frequently leads to symmetric matrices and most widely used. This is called the Galerkin (Bubnov-Galerkin) method. On the other hand, taking the weighting functions of the different form from the shape functions

$$w_j \neq N_j \tag{3.15}$$

is called Petrov-Galerkin method.

By applying Bubnov-Galerkin method to the present case, Equation (3.7) leads to

$$\int_{\Omega} \left([\nabla N]^T [\nabla N] - k^2 [N]^T [N] \right) \{\phi\} d\Omega + \int_{\Gamma_r} \left(ik - \frac{1}{2r} \right) \left([N]^T [N] \right) \{\phi\} d\Gamma = \int_{\Gamma_n} [N]^T \bar{u} d\Gamma \tag{3.16}$$

Consequently, a set of discrete equations for each element is written as

$$\left[[\mathbf{K}] - k^2 [\mathbf{M}] + \left(\frac{1}{2r} - ik \right) [\mathbf{C}] \right] \{\phi\} = \{\mathbf{F}\} \tag{3.17}$$

where

$$K_{ij} = \int_{\Omega_e} \nabla N_i \nabla N_j d\Omega_e \tag{3.18}$$

$$M_{ij} = \int_{\Omega_e} N_i N_j d\Omega_e \tag{3.19}$$

$$C_{ij} = \int_{\Gamma_r} N_i N_j d\Gamma_e \tag{3.20}$$

$$F_i = \int_{\Gamma_n} N_i \bar{u}_i d\Gamma_e \qquad (3.21)$$

where i and j are integers equal to $1, 2, ..., n$. The dimension of element matrices is $n \times n$.

3.3.2 Limitations of Standard Finite Elements

As discussed in section 1.3, one of the principle limitations of the standard finite element formulation is the difficulty of resolving spatially oscillating wave-like solutions using node-based interpolation schemes. It has been known for a long time that in order to resolve details of wave problems when using finite elements, it is necessary to use about 10 degrees of freedom per wavelength. This is a 'rule of thumb', needed to obtain results of 'engineering accuracy'. It was also well-known that this fineness of meshing must be maintained throughout the entire domain because it is essential to resolve the wave details everywhere. If this is not done, errors in a zone, not of direct interest can spread into other zones of the problem. This effect is termed *'pollution'*.

In recent years, this approximate rule has been sharpened by mathematical analysis by a number of workers. Ihlenburg and Babuška [61] and Babuška *et al.* [15, 16] show from numerical experiments that for a domain of *unit length* the effects, described above can be summarised in two sources of error, so that

$$e \leq C_1(p) \left(\frac{hk}{2p}\right)^{\bar{m}} + C_2(p)k \left(\frac{hk}{2p}\right)^{\bar{m}+1} \qquad (3.22)$$

where e is the error in H^1-norm, p is the order of the finite element polynomial and called the *approximation degree* of finite element solution, k is the wavenumber, and h is the length of the element and called the *stepsize* of the mesh. $\bar{m}$ is the minimum of p and l, where $l + 1$ is the regularity of the exact solution, meaning that the solution is $l + 1$ times differentiable (in the weak sense) [60]. C_1 and C_2 are constants depending only upon p. The result applies to a domain of unit length. Essentially these results show that there is a *local error* proportional to some power of kh, and a *pollution error* proportional to k multiplied by some power of kh. The latter error must dominate for large wavenumber k. Specifically for linear elements, in which $p = 1$,

$$e \leq C_1(kh) + C_2 k (kh)^2 \qquad (3.23)$$

Further numerical experiments indicate that the larger value of p which is taken, then the smaller both errors become for a given number of degrees of freedom. This is hardly surprising since intuitively the higher the order of the polynomial the closer the approximation to the series form of the trigonometrical functions sin and cosine.

In the most realistic wave problems such as acoustics, surface waves on the sea and electromagnetic wave fields, the wavelength is relatively much smaller than other dimensions of the problem such as the domain considered and the radiating or scattering objects in the domain. For such problems it is required to mesh the domain into a large number of small elements satisfying the limitation above [15, 16] to achieve a sufficient accuracy. This rapidly increases the size of the problem as the wavelength becomes shorter and makes the amount of computation prohibitive.

3.4 Special Wave Finite Element Formulation

3.4.1 Partition of Unity Finite Element Method

To address the limitation of the standard finite element formulation for wave problems, Melenk and Babuška [17, 75] proposed a new finite element method named the partition of unity finite element method (PUFEM). In one variant of this, applied to the Helmholtz equation, finite element shape functions incorporating the wave shape are used, as presented in Bettess and Zienkiewicz infinite elements [27, 95] and the Astley wave envelope elements [1, 10]. But the shape functions of Melenk and Babuška, have the innovation that they include multiple wave directions. They demonstrated that the method works for a plane wave propagating through a square mesh of square finite elements, even when the direction of the incident wave was *not included* in the approximating set of plane waves chosen.

Subsequently Laghrouche and Bettess extended this approach to various finite element types for the solution of the Helmholtz equation and applied them to solve more realistic wave problems such as diffraction problems [67, 71].

The special wave finite elements dealt with in this thesis are the elements developed by Laghrouche and Bettess.

3.4.2 Plane Wave Basis Finite Element Formulation

In the special wave finite element formulation, the field variable ϕ within an n-node finite element is approximated using polynomial shape functions N_j and the local functions ϕ_j to node j.

$$\phi = \sum_{j=1}^{n} N_j \phi_j = [N]\{\phi\} \tag{3.24}$$

The local functions ϕ_j are given by a combination of plane waves propagating in different directions.

$$\phi_j = \sum_{l=1}^{m_j} A_j^l \psi_j^l \tag{3.25}$$

where ψ_j^l are plane waves, A_j^l are the coefficients corresponding to each plane wave, and m_j is the number of approximating plane waves associated with the node j. Then the field variable ϕ is denoted by

$$\phi = \sum_{j=1}^{n} \sum_{l=1}^{m_j} N_j \psi_j^l A_j^l \tag{3.26}$$

These $n \times m_j$ unknowns A_j^l, in a sense, represent the amplitudes of the plane waves ψ_j^l at the node j. Using the Bubnov-Galerkin method, the weighting functions also take the form

$$W_j^l = \sum_{j=1}^{n} \sum_{l=1}^{m_j} N_j \psi_j^l \tag{3.27}$$

where a_j^l are arbitrary parameters.

In case of two-dimensional problems, plane waves ψ_j^l are written as

$$\psi_j^l = e^{i\mathbf{k_j^l} \cdot \mathbf{r}} \tag{3.28}$$

The position vector $\mathbf{r}$ is given by

$$\mathbf{r} = x\,\mathbf{e_x} + y\,\mathbf{e_y} \tag{3.29}$$

where x, y are the global co-ordinates, and $\mathbf{e_x}$, $\mathbf{e_y}$ are the unit vectors in the x and y

36

directions, respectively. The position vector $\mathbf{r}$ can be also written

$$\mathbf{r} = r \left(\cos \alpha \, \mathbf{e_x} + \sin \alpha \, \mathbf{e_y} \right) \tag{3.30}$$

where α is the angle of the radial direction measured from the positive x direction in the global co-ordinates,

$$x = r \cos \alpha \tag{3.31}$$

$$y = r \sin \alpha \tag{3.32}$$

The wavenumber vector $\mathbf{k}_j^l$ is given by

$$\mathbf{k}_j^l = k \left(\cos \theta_j^l \, \mathbf{e_x} + \sin \theta_j^l \, \mathbf{e_y} \right) \tag{3.33}$$

where θ_j^l is the angle of a plane wave ψ_j^l from the positive direction of the global x co-ordinate. Consequently plane waves ψ_j^l can be also written by

$$\psi_j^l = e^{ik(x \cos \theta_j^l + y \sin \theta_j^l)} = e^{ikr \cos (\theta_j^l - \alpha)} \tag{3.34}$$

The scalar variables of r and k are the amplitudes of the vectors $\mathbf{r}$ and $\mathbf{k}_j^l$, respectively.

In the original work by Melenk and Babuška [75, 17], m_j, the number of approximating plane waves are the same for all nodes and the approximating plane waves are equally spaced. This treatment appears reasonable if the actual wave direction is unknown. When the approximating plane waves are equally spaced in the two-dimensional plane, θ_j^l can be written as

$$\theta_j^l = l \frac{2\pi}{m_j} \tag{3.35}$$

where $l = 1, 2, \cdots, m_j$.

However, from an approximating point of view, m_j can vary from node to node and the angles θ_j^l can be arbitrarily set at each node. These angles can be uniformly distributed or may be carefully chosen. They can also be the same for all nodes of the studied mesh or may vary from one node to another. It has been shown that such systems of plane waves form complete sets of functions for the Helmholtz equation [56, 46]. If the wave solution ϕ has a preferred direction, it seems, intuitively to be better, a priori, to cluster the angles θ_j^l

around that direction. For example, to consider the scattering problem, it is supposed that a certain number of directions should be necessary to solve the wave phenomena in the near field of the scattering objects but it should be possible to decrease the number of waves in the far field where the contribution of the component of the scattered wave in the radial direction is expected to become larger as the distance from the objects becomes further. This has been borne out by numerical experiments by Laghrouche and Bettess [68].

3.4.3 New Shape Functions and Unknown Amplitudes

In Equations (3.26) and (3.27), the product of the 'old shape functions' N_j and the plane waves ψ_j^l can be considered as 'new shape functions' corresponding to 'new unknown variables' A_j^l. Then the field variable ϕ through an n-node finite element can be written in a matrix form by

$$\phi = [\mathcal{P}]\{\mathcal{A}\} = \begin{bmatrix} \mathcal{P}_1 & \mathcal{P}_2 & . & . & . & \mathcal{P}_n \end{bmatrix} \begin{Bmatrix} \mathcal{A}_1 & \mathcal{A}_2 & . & . & . & \mathcal{A}_n \end{Bmatrix}^T \qquad (3.36)$$

where the row matrices of the new shape functions corresponding to the node j are

$$\mathcal{P}_j = \begin{bmatrix} P_j^1 & P_j^2 & . & . & . & P_j^{m_j} \end{bmatrix} \qquad (3.37)$$

where

$$P_j^l = N_j \psi_j^l \qquad (3.38)$$

The amplitude vectors $\mathcal{A}_j$ at the node j are

$$\mathcal{A}_j = \begin{Bmatrix} A_j^1 & A_j^2 & . & . & . & A_j^{m_j} \end{Bmatrix} \qquad (3.39)$$

then the potential ϕ is given by

$$\phi = \sum_{j=1}^{n} \sum_{l=1}^{m_j} P_j^l A_j^l \qquad (3.40)$$

3.5 Geometry Mapping

The global co-ordinates x and y of each n-node finite element are related to the local co-ordinates ξ and η using the transformation

$$x = \sum_{j=1}^{n} M_j x_j \qquad y = \sum_{j=1}^{n} M_j y_j \tag{3.41}$$

where x_j and y_j are the nodal co-ordinates and M_j are the shape functions for geometry mapping. Let us take M_j to be the same as the shape functions for field variable N_j, which leads to the isoparametric elements.

The Jacobian matrix J which describes the geometry mapping between the local co-ordinates ξ, η and the global co-ordinates x, y is given by

$$J = \begin{bmatrix} \dfrac{\partial x}{\partial \xi} & \dfrac{\partial y}{\partial \xi} \\ \dfrac{\partial x}{\partial \eta} & \dfrac{\partial y}{\partial \eta} \end{bmatrix} = \begin{bmatrix} \displaystyle\sum_{j=1}^{n} \dfrac{\partial N_j}{\partial \xi} x_j & \displaystyle\sum_{j=1}^{n} \dfrac{\partial N_j}{\partial \xi} y_j \\ \displaystyle\sum_{j=1}^{n} \dfrac{\partial N_j}{\partial \eta} x_j & \displaystyle\sum_{j=1}^{n} \dfrac{\partial N_j}{\partial \eta} y_j \end{bmatrix} \tag{3.42}$$

and the element of surface $dxdy$ is written using the local co-ordinates and the determinant of Jacobian matrix $|J|$ as follows

$$dxdy = |J|\, d\xi\, d\eta \tag{3.43}$$

3.6 Element Matrix

Employing the Bubnov-Galerkin method, leads to

$$\int_{\Omega} \left([\nabla \mathcal{P}]^T [\nabla \mathcal{P}] - k^2 [\mathcal{P}]^T [\mathcal{P}] \right) \{\mathcal{A}\} d\Omega + \int_{\Gamma_r} \left(ik - \frac{1}{2r} \right) ([\mathcal{P}]^T [\mathcal{P}]) \{\mathcal{A}\} d\Gamma = \int_{\Gamma_n} [\mathcal{P}]^T \bar{u} d\Gamma \tag{3.44}$$

Consequently, a set of discrete equations for each element is written as

$$\left[[\mathbf{K}] - k^2 [\mathbf{M}] + \left(ik - \frac{1}{2r} \right) [\mathbf{C}] \right] \{\mathcal{A}\} = \{\mathbf{F}\} \tag{3.45}$$

Components of element matrices are

$$K_{ij} = \int_{\Omega_e} \nabla P_i^m \cdot \nabla P_j^l d\Omega \qquad (3.46)$$

$$= \int_{\Omega_e} \left\{ \frac{\partial P_i^m}{\partial x} \frac{\partial P_j^l}{\partial x} + \frac{\partial P_i^m}{\partial y} \frac{\partial P_j^l}{\partial y} \right\} d\Omega \qquad (3.47)$$

$$M_{ij} = \int_{\Omega_e} P_i^m P_j^l d\Omega \qquad (3.48)$$

$$C_{ij} = \int_{\Gamma_r} P_i^m P_j^l d\Gamma_e \qquad (3.49)$$

$$F_i = \int_{\Gamma_n} P_i^m \bar{u} d\Gamma \qquad (3.50)$$

where i and j are integers corresponding to the m-th wave at node i and the l-th wave at node j, respectively, and given by

$$i = \sum_{\ell=1}^{i-1} m_\ell + m \qquad (3.51)$$

$$j = \sum_{\ell=1}^{j-1} m_\ell + l \qquad (3.52)$$

which are equal to $1, 2, ..., n_p$ and

$$n_p = \sum_{\ell=1}^{n} m_\ell \qquad (3.53)$$

is the total degree of freedom of the element. m_ℓ is the number of waves at node ℓ. The dimension of the element matrix therefore becomes $n_p \times n_p$.

To evaluate the element matrices, the global derivatives of the new shape functions P_r are evaluated from the standard shape functions N_j and the trigonometric functions ψ_j^l

$$\left\{ \begin{array}{c} \frac{\partial P_j^l}{\partial x} \\ \frac{\partial P_j^l}{\partial y} \end{array} \right\} = \left[\left\{ \begin{array}{c} \frac{\partial N_j}{\partial x} \\ \frac{\partial N_j}{\partial y} \end{array} \right\} + ikN_j \left\{ \begin{array}{c} \cos\theta_j^l \\ \sin\theta_j^l \end{array} \right\} \right] \psi_j^l \qquad (3.54)$$

The global derivatives of the standard shape functions are obtained from the local derivatives as follows

$$\left\{ \begin{array}{c} \frac{\partial N_j}{\partial x} \\ \frac{\partial N_j}{\partial y} \end{array} \right\} = \left[\begin{array}{cc} \frac{\partial \xi}{\partial x} & \frac{\partial \eta}{\partial x} \\ \frac{\partial \xi}{\partial y} & \frac{\partial \eta}{\partial y} \end{array} \right] \left\{ \begin{array}{c} \frac{\partial N_j}{\partial \xi} \\ \frac{\partial N_j}{\partial \eta} \end{array} \right\} = J^{-1} \left\{ \begin{array}{c} \frac{\partial N_j}{\partial \xi} \\ \frac{\partial N_j}{\partial \eta} \end{array} \right\}$$

where J is the Jacobian matrix shown in Equation (3.42).

In the case of the standard finite element model described in Section 3.3, the element matrices for an n-node element would be of dimensions $n \times n$ and the unknowns are the nodal values ϕ_j, $j = 1, 2, .., n$. However, the resulting element matrices of special wave finite element derived by this formulation are of dimensions $n_p \times n_p$, and the unknowns of the problem are the amplitudes A_j^l, $j = 1, 2, .., n$ and $l = 1, 2, ..., m_j$. It may appear that this increases the number of degrees of freedom of the nodes, then the dimension of the element matrices, and consequently the dimension of the whole problem. Actually, the element matrices dimension becomes larger unless all m_j are equal to 1. But this special wave finite element can be larger than a wavelength and consequently the number of the elements can be reduced. It will be seen that a significant reduction in the dimensions of the whole problem can usually be achieved [67].

3.7   Numerical Examples

Some numerical results from reference [67] by Laghrouche and Bettess are presented in this section to demonstrate the basic features of the special wave finite elements.

3.7.1   Melenk's Problem
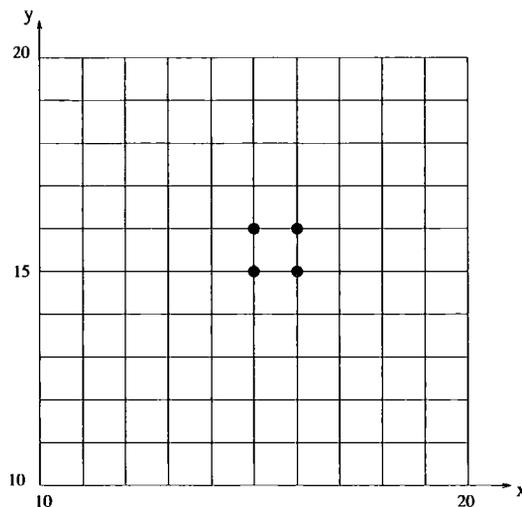
Figure 3.1: Studied example for plane wave problems [67].

Melenk and Babuška [75, 17] considered the Helmholtz equation on a unit square domain $S = [0, 1] \times [0, 1]$ with the Robin boundary condition chosen such that the exact
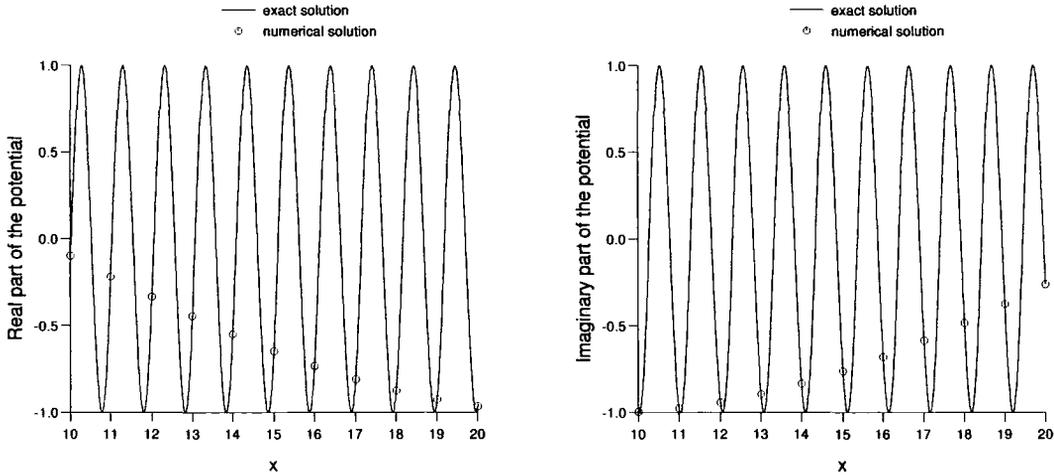
Figure 3.2: Progressive plane wave, real and imaginary parts of the potential at $y/b = 15$, $kb = 2\pi$, $\lambda/b = 1$ [67].

solution of the problem is a progressive plane wave of the form

$$\phi^i = e^{ik(x\cos\frac{\pi}{16} + y\sin\frac{\pi}{16})} \tag{3.55}$$

The solution to the Helmholtz equation was approximated by a system of plane waves excluding the exact solution of the problem. They studied the effect of the mesh size and the order of the approximation, in terms of the number of plane waves used in the system, when the wavenumber is increased.

Laghrouche and Bettess [67] experimented with the number of the approximating plane waves to obtain a satisfactory accuracy for a progressive plane wave problem using almost the same example as that presented by Melenk and Babuška [75, 17].

The mesh model for the problem is shown in Figure 3.1. The domain considered is the square area of $10m \times 10m$ which is divided into a square grid of 11×11 nodal points so that 10×10 4-node bilinear square elements of side length $b = 1m$ fill the studied domain. The boundary condition was given by Robin boundary condition of the form

$$\frac{\partial\phi}{\partial n} + ik\phi = g \tag{3.56}$$

where

$$g = ik\left(n_x\cos\frac{\pi}{16} + n_y\sin\frac{\pi}{16} + 1\right)e^{ik(x\cos\frac{\pi}{16} + y\sin\frac{\pi}{16})} \tag{3.57}$$

42

at all boundary nodes on the boundary which encloses the studied domain. The wavenumber $k = 2\pi$, so the wavelength $\lambda = 1$. A system of 18 plane waves is used in the approximating solution. This means that a single direction is retained every $20°$, so the incident angle of the progressive plane wave at $\pi/16 = 11.25°$ is not included. To evaluate the element matrices, a Gauss-Legendre integration scheme of 10 points was used in each direction.

The numerical results of the real and imaginary parts of the potential at nodes on the line $y/b = 15$ are shown in Figure 3.2 with the analytical solution. Both the interval between nodes b and the wavelength λ are the same value 1, and the numerical results are in good agreement with the analytical solution. This indicates that the limitation of '10 degrees of freedom per wavelength' of the standard finite elements discussed in Section 3.3 does not apply the special wave finite elements.

Laghrouche and Bettess [67] also showed a comparison of the computational cost to solve a wave diffraction problem by the standard finite elements and the special wave finite elements. It is possible to simulate short wave problems for a range of wavenumbers without changing the mesh of the computed domain, and the dramatic reduction in the number of degrees of freedom can be obtained. They conclude that the special wave finite elements are highly competitive with the standard finite elements.

3.7.2   Influence of Number of the Approximating Plane Waves

Laghrouche and Bettess [67] used the similar progressive plane wave problem to investigate the influence of the number of approximating plane waves. They used the same mesh model shown in Figure 3.1 with the plane wave incident from the angle $\pi/4$. The incident progressive plane wave was given by

$$\phi^i = e^{ik(x \cos \frac{\pi}{4} + y \sin \frac{\pi}{4})} \tag{3.58}$$

and the boundary condition was given by Robin boundary condition of the form

$$\frac{\partial \phi}{\partial n} + ik\phi = g \tag{3.59}$$

▼ Relative error of the potential
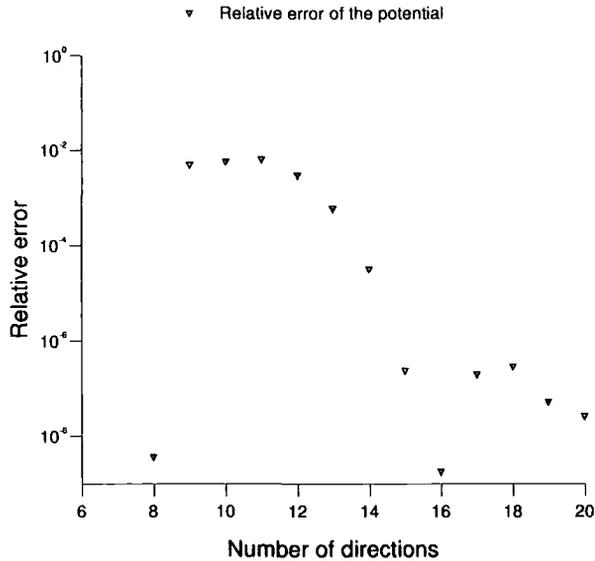
Figure 3.3: Relative error of the potential versus the number of directions of the plane waves system at $x/b = y/b = 15$ [67].

where

$$g = ik\left(n_x \cos\frac{\pi}{4} + n_y \sin\frac{\pi}{4} + 1\right) e^{ik(x\cos\frac{\pi}{4} + y\sin\frac{\pi}{4})} \tag{3.60}$$

at all boundary nodes on the boundary which encloses the studied domain. The wavenumber $k = 2\pi$, so the wavelength $\lambda = 1$. A Gauss-Legendre integration scheme of 10 points was used in each direction for evaluation of the element matrices. The number of the directions of approximating plane waves varies from 8 to 20 and the directions were equally spaced from the positive global x direction.

In Figure 3.3 [67], the relative error in the real part of the potential defined by

$$\frac{\Re(\phi_{exact}) - \Re(\phi_{num})}{\Re(\phi_{exact})} \tag{3.61}$$

evaluated at the node defined by $x/b = y/b = 15$ is shown, where $\Re(\phi_{exact})$ and $\Re(\phi_{num})$ are the real parts of the analytical solution and the numerical results, respectively. The error is about 10^{-2} for the cases where 9 - 12 approximating plane waves are used and then decreases to less than 10^{-6} for the cases where 17 - 20 approximating plane waves are used. Generally the error decreases as the number of the approximating plane waves increases, however it is particularly small when the number of directions is 8 or 16. In these cases the incident angle of the progressive plane wave is included in the directions of approximating plane waves, which results in exceptionally small error.

44
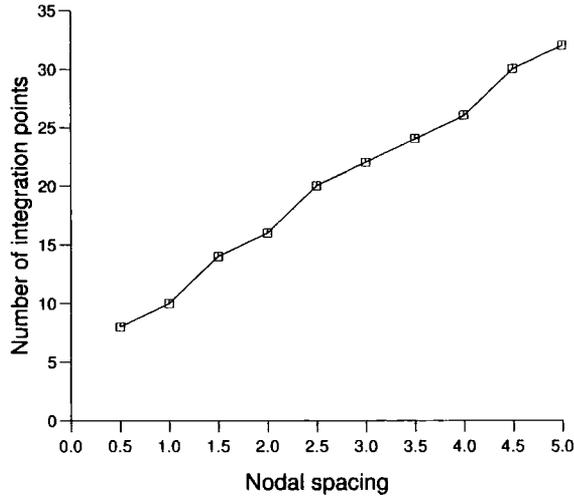
Figure 3.4: Number of integration points versus nodal spacing in term of λ [67].

3.7.3 Influence of Nodal Spacing on Numerical Integration Scheme

In a single special wave finite element, many wavelengths can be contained. When the wavenumber k is large, the integrals required to evaluate the element matrices are highly oscillatory because of the presence of the exponential terms describing plane waves.

Laghrouche and Bettess [67] used Gauss-Legendre numerical integration scheme with up to 120×120 integration points to evaluate these integrals. They presented the results from a series of numerical experiments to find the minimum number of integration points to obtain satisfactory accuracy. They used the similar progressive plane wave problem to investigate the influence of the number of approximating plane waves. They used the same mesh model shown in Figure 3.1 with the plane wave incident from the angle $\pi/18$. The incident progressive plane wave was given by

$$\phi^i = e^{ik(x \cos \frac{\pi}{18} + y \sin \frac{\pi}{18})} \tag{3.62}$$

which was applied by Dirichlet boundary conditions at all boundary nodes. 18 approximating plane waves are used for all nodes. The wavenumber $k = 2\pi$, so the wavelength $\lambda = 1$. Their results is that by increasing the nodal spacing in term of the wavelength the number of the integration points also has to be increased to obtain a wave profile along the line $y/b = 15$ with satisfactory accuracy, and the variation seems to be linear as shown in Figure 3.4. They concluded that about 10 integration points for a nodal spacing of λ, and 30 integration points for a nodal spacing of 5λ are required.

45

3.8 Conclusions

The formulation of the special wave finite elements in which the multiple number of plane waves are included in the shape functions are described. Because of this choice of basis functions, a single finite element can contain many wavelengths, unlike standard finite elements. The shape functions contain oscillatory functions but the element matrix can be evaluated using high order Gauss-Legendre integration.

High accuracy can be obtained by the use of special wave finite elements, which is not limited by the ratio of the element size to the wavelength, unlike standard finite elements. Therefore the mesh can remain the same for a wide range of wavenumbers. Generally the error decreases as the number of the approximating plane waves increases. About 10 integration points for a nodal spacing of one wavelength are required to obtain sufficient accuracy.

One drawback of the method is the high order integration of the element matrices. Applying specialised integration schemes could reduce the number of integration points, which will be discussed in the next two chapters.

Chapter 4

Semi-analytical integration scheme for rectangular and triangular special wave finite elements

In this chapter, the the theory for integrating the element matrices for triangular and rectangular special wave finite elements [26] is presented. The results are compared with those obtained using large numbers of Gauss-Legendre integration points for a range of testing wave problems. The results demonstrate that the method gives correct results, which gives confidence in the procedures, and show that large savings in computation time can be achieved. The integration for quadrilateral special wave finite elements, which is more complicated, is dealt with in the next chapter.

4.1 Introduction

The theory and the formulation for the special wave finite elements developed by Laghrouche and Bettess [67, 71] have been presented in Chapter 3. The special wave finite elements are based on the partition of unity finite element method (PUFEM) proposed by Melenk and Babuška [17, 75]. It can solve short wave problems with a greatly reduced number of active variables. The motivation for the use of these new elements is to escape the limitations of standard finite element procedures for wave problems. However, the integrals required to evaluate the element matrices of the special wave finite elements are highly oscillatory because of the presence of the exponential terms, and the computational cost

of using a conventional numerical integration scheme such as Gauss-Legendre integration becomes relatively expensive.

Let us recall a component of the element matrix

$$K_{ij} - k^2 M_{ij} = \int_{\Omega_e} \left\{ \nabla P_i^m \nabla P_j^l - k^2 P_i^m P_j^l \right\} d\Omega_e \qquad (4.1)$$

where

$$\imath = \sum_{\ell=1}^{i-1} m_\ell + m \qquad (4.2)$$

$$\jmath = \sum_{\ell=1}^{j-1} m_\ell + l \qquad (4.3)$$

and m_ℓ is the number of approximating plane waves at node ℓ. P_j^l are special shape functions which are products of polynomial shape functions N_j and trigonometric functions as written by

$$P_j^l = N_j \psi_j^l \qquad (4.4)$$

and

$$\psi_j^l = e^{ik\hat{e}_j^l \cdot \mathbf{r}} = e^{ik(x \cos \theta_j{}^l + y \sin \theta_j{}^l)} \qquad (4.5)$$

describe plane waves propagating in the angle θ_j^l at node j, and $\hat{e}_j^l$ is a unit vector in this direction. Therefore Equation (4.1) becomes

$$K_{ij} - k^2 M_{ij} = \int_{\Omega_e} \left\{ \nabla (N_i e^{ik\hat{e}_i^m \cdot \mathbf{r}}) \cdot \nabla (N_j e^{ik\hat{e}_j^l \cdot \mathbf{r}}) - k^2 N_i e^{ik\hat{e}_i^m \cdot \mathbf{r}} N_j e^{ik\hat{e}_j^l \cdot \mathbf{r}} \right\} d\Omega_e \qquad (4.6)$$

$$= \int_{\Omega_e} \left\{ (\nabla N_i + ik N_i \hat{e}_i^m) \cdot (\nabla N_j + ik N_j \hat{e}_j^l) - k^2 N_i N_j \right\} e^{ik\hat{e}_i^m \cdot \mathbf{r}} e^{ik\hat{e}_j^l \cdot \mathbf{r}} d\Omega_e \qquad (4.7)$$

Since the wavenumber k may be large, the exponential function in Equation (4.7) may contain many wavelengths. Although this is the great advantage of the method, it causes difficulties when integrating using a conventional numerical integration scheme. Previous authors have resorted to very high order Gauss-Legendre integration when evaluating the above integral. In the examples shown by Laghrouche and Bettess [67] up to 120 by 120 Gauss-Legendre numerical integration is used. So the reduction in the number of active variables, in the system matrix, comes at the price of some computationally intensive numerical integrations over the domain of the elements. The time for these integrations may be comparable with or even exceed the execution time for the system matrix equation

48

solution. The time required for the integrations over the elements may not be prohibitive problem compared to the solution time of the equation from a practical point of view, as the integrations can easily be parallelised. However the Gauss-Legendre integration scheme assumes that the function to be integrated is of a polynomial form, and it is well known that polynomial representations of trigonometrical functions are not accurate and are also expensive to compute [53]. Indeed it seems completely illogical to develop new types of finite elements specially for short waves, which include a knowledge of wave behaviour, and then to ignore this knowledge, and revert to polynomials, at the integration stage.

The challenge then is to develop better integration methods, which incorporate our knowledge of the plane wave functions. This should drastically reduce the time taken to form the element matrices.

4.2   Bi-linear Geometrical Mapping

We introduce the assumption that the local-to-global geometric mapping is a bilinear function of the element co-ordinates, which implies that the edges of the elements are all straight. Higher order mappings could be used, but the integrations would not be exact, which is the case in normal finite elements. For a rectangular or triangular element E_t, the global cartesian co-ordinates $\mathbf{r} = (x, y)$ are related to the local element co-ordinates (ξ, η) by

$$\mathbf{r} = \mathbf{a_t} + \mathbf{b_t}\xi + \mathbf{c_t}\eta \tag{4.8}$$

where the coefficients $\mathbf{a_t}$, $\mathbf{b_t}$ and $\mathbf{c_t}$ are vectors in two dimensions. For a quadrilateral element, the $\xi\eta$ term arises as written by

$$\mathbf{r} = \mathbf{a_t} + \mathbf{b_t}\xi + \mathbf{c_t}\eta + \mathbf{d_t}\xi\eta \tag{4.9}$$

The $\xi\eta$ term complicates the evaluation of the integrals. In this chapter we are firstly concerned with triangular or rectangular finite elements, and then move to quadrilateral finite elements in the next chapter.

In case of rectangular or triangular element, the expression in the curly brackets in Equation (4.7) is a quadratic polynomial in (ξ, η). Consequently, the integral in Equation

49

(4.7) has the form

$$I = \frac{A_t}{\hat{A}} \sum_{p,q=0}^{2} f_{pqi}^{t}{}_{j}^{m\,l} \int_{\hat{E}} \mathcal{L}_{pq}(\xi,\eta) e^{ik\hat{e}_i^m \cdot \mathbf{r}} e^{ik\hat{e}_j^l \cdot \mathbf{r}} d\xi d\eta \qquad (4.10)$$

where

$$\sum_{p,q=0}^{2} f_{pqi}^{t}{}_{j}^{m\,l} \mathcal{L}_{pq}(\xi,\eta) = (\nabla N_i + ik N_i \hat{\mathbf{e}}_i^{\mathbf{m}}) \cdot (\nabla N_j + ik N_j \hat{\mathbf{e}}_j^{\mathbf{l}}) - k^2 N_i N_j \qquad (4.11)$$

A_t is the area of finite element E_t, and $\hat{A}$ is the area of $\hat{E}$, the standard rectangular or triangular element. $\mathcal{L}_{pq}(\xi,\eta)$ is an interpolating polynomial, which takes unit value at an integration point, and is zero at all the others. For rectangular element, and also quadrilateral element discussed in the next chapter, it can be constructed from the product of Lagrange polynomials.

$$L_p(\xi) = \prod_{i=1 \neq p}^{n_L} \left(\frac{\xi - \xi_i}{\xi_p - \xi_i} \right) \qquad L_q(\eta) = \prod_{j=1 \neq q}^{n_L} \left(\frac{\eta - \eta_j}{\eta_q - \eta_j} \right) \qquad (4.12)$$

where n_L is the order of polynomials L_p and L_q. In those cases $\mathcal{L}_{pq}(\xi,\eta) = L_p(\xi)L_q(\eta)$. The values $f_{pqi}^{t}{}_{j}^{m\,l}$ are the coefficients to the interpolating polynomials $\mathcal{L}_{pq}$ and the oscillating functions $\exp(ik\hat{\mathbf{e}}_i^{\mathbf{m}} \cdot \mathbf{r}) \exp(ik\hat{\mathbf{e}}_j^{\mathbf{l}} \cdot \mathbf{r})$ in the integrand. If the same mapping were retained, but higher order interpolation were adopted, the upper limits on p and q would increase.

Substituting Equation (4.3) into Equation (4.10) gives

$$I = \frac{A_t}{\hat{A}} \sum_{p,q=0}^{2} f_{pqi}^{t}{}_{j}^{m\,l} \int_{\hat{E}} \mathcal{L}_{pq}(\xi,\eta) e^{ik\{(\hat{e}_j^l + \hat{e}_i^m) \cdot \mathbf{a}_t + (\hat{e}_j^l + \hat{e}_i^m) \cdot \mathbf{b}_t \xi + (\hat{e}_j^l + \hat{e}_i^m) \cdot \mathbf{c}_t \eta\}} d\xi d\eta \qquad (4.13)$$

By introducing notations

$$C_t = k(\hat{\mathbf{e}}_i^{\mathbf{m}} + \hat{\mathbf{e}}_j^{\mathbf{l}}) \cdot \mathbf{a_t}, \quad F_t = k(\hat{\mathbf{e}}_i^{\mathbf{m}} + \hat{\mathbf{e}}_j^{\mathbf{l}}) \cdot \mathbf{b_t}, \quad G_t = k(\hat{\mathbf{e}}_i^{\mathbf{m}} + \hat{\mathbf{e}}_j^{\mathbf{l}}) \cdot \mathbf{c_t} \qquad (4.14)$$

we obtain a typical form of integration given by

$$I = \frac{A_t}{\hat{A}} e^{iC_t} \sum_{p,q=0}^{2} f_{pqi}^{t}{}_{j}^{m\,l} \int_{\hat{E}} e^{iF_t \xi} e^{iG_t \eta} \mathcal{L}_{pq}(\xi,\eta) \, d\xi d\eta \qquad (4.15)$$

The analysis has now arrived at an integration rule of the following form

$$w_{pq}(F,G) = \int_{\hat{E}} e^{iF\xi}\, e^{iG\eta}\, \mathcal{L}_{pq}(\xi,\eta) d\xi d\eta \tag{4.16}$$

where F and G are constants which are dependent on k, j, l, i, m and $\mathbf{r}$.

For the rectangle, the evaluation of the integration weights is simplified because the integral of products becomes a product of integrals,

$$w_{pq}(F,G) = \int_{-1}^{+1} e^{iF\xi}\, L_p(\xi)\, d\xi \int_{-1}^{+1} e^{iG\eta}\, L_q(\eta)\, d\eta. \tag{4.17}$$

Both integrals on the right-hand side are easily evaluated by repeated application of integration by parts. The evaluation of the integration weights for the standard triangle is more complicated. In this case

$$w_{pq}(F,G) = \int_{0}^{1} \int_{0}^{1-\eta} e^{iF\xi}\, e^{iG\eta}\, L_p(\xi)L_q(\eta)\, d\xi d\eta. \tag{4.18}$$

The inner integral can be evaluated through integration by parts. The outer integral, while complicated, can also be evaluated analytically.

4.3 Theory of Numerical Integration

There are many books and papers devoted on the theory of numerical integration. The necessary theory can be read in, for example, Davis and Rabinowitz [42], Hamming[53], or Ralston[82]. The simple procedure adopted here can be summarised as follows:

- Choose a set of integration abscissæ in two dimensions, distributed over the domain of the finite element. In the present case, the integration abscissæ were chosen to be equally spaced in the ξ and η directions, and to include abscissæ at the finite element vertices. For the rectangle and quadrilateral the ranges were $-1 \le \xi \le 1$ and $-1 \le \eta \le 1$, and for triangles $0 \le \xi \le 1 - \eta$ and $0 \le \eta \le 1$. Equal spacing was chosen because it was simple. It may be possible to select optimal locations for the integration points, as in Gauss-Legendre integration. There is a considerable literature on optimal integration abscissæ for example [82, 42, 53]. However this would be almost impossibly difficult and the optimal locations would be different for every value of F and G. The number of points selected depends upon highest

powers of ξ and η in the element. A bi-linear rectangular element matrix would have highest powers of $\xi^2\eta^2$, by definition. This necessitates three integration points in each direction giving a total of nine points. In general if the highest power of ξ and η is n_L, then $(n_L + 1)^2$ points will be needed. A bi-quadratic element would need 25 integration points.

○ The Lagrange polynomials for each integration point are set up using the classical formula for such polynomials, [82, 53], in both ξ and η directions. The polynomials for each point in the ξ and η directions are found and multiplied together. This is for the rectangle and quadrilateral. The corresponding polynomials are also available for triangles [99]. The next step is to integrate each polynomial over the domain of the element.

⊚ Integrate analytically the product of the Lagrange polynomial and the wave functions over the domain of the finite element, as seen in Equations (4.17) and (4.18) for the rectangle and triangle respectively, to give the weights.

All these operations are ideal for being performed by a computer algebra program. The integration by parts, in two variables, gives rise to a very large number of terms, which are difficult to evaluate by hand. But because they are routine and standardised they are ideal for computer algebra packages. The existence of special cases when $F \to 0$ and $G \to 0$ further complicates the manipulations.

4.4   Integration Scheme Logic

Unlike conventional integration schemes, in which the same integration weights are used for all the terms evaluated at a given integration point, in this case each pair of wave directions requires a different, complex, weight. There is a significant overhead of storage and computation in evaluating and storing these integration weights. However it is still economical compared with conventional Gauss-Legendre integration.

The procedure is as follows. For the finite element all the directions at each node are assembled in a list. A simple example in which nodes 1, 2, 3 and 4 have 3, 2, 5 and 3 directions respectively, is shown below:

● Node 1: θ_1^1, θ_1^2, θ_1^3,

- Node 2: θ_2^1, θ_2^2,

- Node 3: θ_3^1, θ_3^2, θ_3^3, θ_3^4, θ_3^5

- Node 4: θ_4^1, θ_4^2, θ_4^3

where θ_j^l denotes the l-th wave direction at node j.

Let the total number of wave directions in an element be n_p. In the above example there is a total of 13 wave directions. For each pair of directions, that is for $n_p \times (n_p+1)/2$ cases the integration weights are evaluated by a call to a fortran subroutine. In the example above hence $13 \times 14/2 = 91$ cases. The active arguments are the dimensions of the rectangular elements, b_x and b_y, and the exponents F and G, which are evaluated from Equation (4.14) from the wave number and wave directions. The integration weights are stored in a large array of dimension $n_p \times n_p \times (n_L+1) \times (n_L+1)$, where n_L is the highest power of ξ and η encountered. $n_L = 5$ is an appropriate value, if bi-quadratic elements are used. The weights are evaluated prior to the main integration loops.

Each integration loop is more complex than the conventional Gauss-Legendre type integration, because as well as the main loops over all the integration points in the ξ and η directions, it is also necessary to have inner loops over all wave directions. However the total number of multiplications of terms to evaluate the weighted residual is no larger, it is simply partitioned into smaller sections which use different weights. Moreover some terms in the shape function and the derivatives are now present by implication, and not explicitly, so that the formation of the terms corresponding to a single integration point requires less effort than for Gauss-Legendre integration. And, of course, there are, in general, far fewer integration points. In very general terms the logic is as follows:

```
For all ξ integration points do
    For all η integration points do
        For all i wave directions do
            For all j wave directions do
                Form contribution to element matrix at this
                integration point for these directions
                Multiply by weight for this point and these directions
            end do
        end do
    end do
end do
```

4.5　Example Comparisons

Consider a special wave finite element with 36 wave directions at each node and 9 nodes, using 100 by 100 Gauss Legendre integration. At each Gauss point three inner products of shape functions and the derivatives have to be formed to form the contribution to the element matrix. The size of the inner products is number of nodes multiplied by the number of wave directions, that is $36 \times 9 = 324$. Hence the number of floating point multiplications is

$$100 \times 100 \times 3 \times 324 \approx 10,000,000$$

In the case of 5 by 5 set of integration points, the total number of floating point multiplications is

$$5 \times 5 \times 3 \times 324 \approx 25,000$$

So provided the number of operations in evaluating the integration weights is less than 9×10^7, the forming of the integration weights is worthwhile. That is we can afford up to five million floating point multiplications in evaluating the weights for each integration point. With 36 possible directions and $36 \times 37/2 \approx 670$ combinations, even 500 floating point multiplications for each of these, is still worth while. In practice it is often possible to remain well below that figure.

4.6　Rectangular Finite Elements

4.6.1　Theory

In this case the relation between the local ξ, η and global x, y co-ordinates given in Equation (4.8) simply becomes

$$x = \frac{b_x}{2}(1 - \xi) \qquad y = \frac{b_y}{2}(1 - \eta) \tag{4.19}$$

where b_x and b_y are the dimensions of the rectangular element in the x and y directions respectively. The resulting integral is given above as Equation (4.17). As indicated the two integrations in the ξ and η directions can now be carried out in sequence. Now consider

Table 4.1: Different cases for rectangular element.

Cases	F	G
1	$\neq 0$	$\neq 0$
2	≈ 0	$\neq 0$
3	$\neq 0$	≈ 0
4	≈ 0	≈ 0

the simplest case, when $p = 0$. The integral in the ξ direction is simply

$$\int e^{iF\xi} dx = \frac{-ie^{iF\xi}}{F} + C \qquad (4.20)$$

and integrals of terms containing higher order polynomials can be found by integrating by parts. A difficulty arises since it is possible for F to take the value 0. In this case the integral given in Equation (4.20) above must be evaluated using l'Hôpital's rule. If F is small then numerical evaluations based on the Equation (4.20) would also be inaccurate. In such cases it is therefore necessary to adopt a series form for the exponential. This can be integrated term by term. A total of four special cases arises as indicated in Table 4.1.

When the absolute value of F is below some set value, ϵ, the function $\exp{(iF\xi)}$, is replaced by the truncated series

$$e^{iF\xi} \approx \sum_{j=0}^{N} \frac{(iF\xi)^j}{j!} \qquad (4.21)$$

where N denotes the number of terms retained in the approximation. This can be adjusted, using the value ϵ, so that the truncation error in the series is of the order of machine accuracy. The integral of the series in Equation (4.21) is well behaved as $F \to 0$, and so a seamless transition between the integrated form for the exponential and the series should be achieved. A similar consideration applies in the case $G \to 0$.

4.6.2 Numerical Results for Rectangular Element

A program was written which would generate the element matrices using the special integration rules developed here, or many Gauss-Legendre integration points. The element matrices obtained in this way were compared with each other. It was expected that the special integration rule would generate the element matrix accurately, irrespective of the

55

wavenumber, k, whereas the Gauss-Legendre integration scheme would only be accurate if a sufficiently large number of integration points were used. This proved to be the case.

The comparison between the semi-analytical integration and the Gauss-Legendre integration scheme was carried out as follows. The squares of the absolute values of the differences were summed for every term in the two matrices and then divided by the sum of the squares of the absolute values of the terms in the matrix obtained by semi-analytical integration.

$$error = \sqrt{\left(\sum_{i=1}^{n_p}\sum_{j=1}^{n_p}\left|\mathcal{K}_{ij}^{gl} - \mathcal{K}_{ij}^{sa}\right|^2\right) \Big/ \left(\sum_{i=1}^{n_p}\sum_{j=1}^{n_p}\left|\mathcal{K}_{ij}^{sa}\right|^2\right)} \qquad (4.22)$$

where $\mathcal{K}^{gl}$ and $\mathcal{K}^{sa}$ are the element matrices obtained by Gauss-Legendre integration and semi-analytical integration, respectively, n_p is the total number of degrees of freedom in the element. This error is plotted in Figure 4.1.

The element was square, with length of side $2h'$. The program was run for a range of kh' values between 4 and 140, and for a range of conventional Gauss-Legendre integration points between 1 and 120. Values of $kh' = 4$ and $kh' = 140$ approximately correspond to 1.27 and 44.5 wavelengths in an element.

Since the semi-analytical integration should be independent of the wavelength, (apart from the issue of rounding errors at very high values of k), we can predict the behaviour of the results. We should expect the difference between the semi-analytical integrated value for the element matrix, and the numerically integrated value to be small for small values of k. As k increases we should expect the difference, or error, to increase, when the Gauss-Legendre integration scheme no longer has sufficient integration points to resolve the wave details. This is exactly what happens.

Figure 4.1 shows a plot of the error against the wavenumber, k, for a range of numbers of integration points. The semi-analytical and numerical errors increase at a value of k, which increases with the number of integration points. For very low numbers of integration points, between 1 and 10, the element matrix is not resolved at all with any acceptable accuracy. For numbers of points greater than 10, the error is around 10^{-7}, to 10^{-6}, until the wavenumber increases to a value at which the number of integration points cannot resolve the wave details. Then as the wavenumber increases there is a rapid rise in the RMS error, which then plateaus at absurd and unacceptable values of about 10^3. For example this transition takes place for 100 integration points, for k just below 100. For
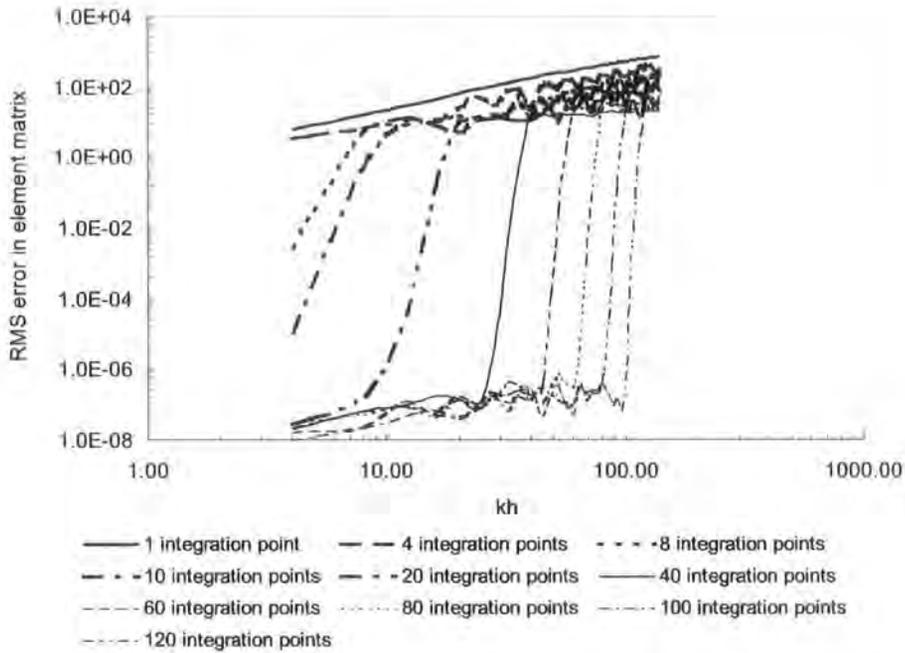
Figure 4.1: RMS errors in the element matrix, as a function of wavenumber and number of integration points.

the results shown, four directions per node were used. Although the results are not shown, the program was also run for a range of different wave directions, and also for the special cases of $F \approx 0$, $G \approx 0$ and $F \approx G \approx 0$ shown in Table 4.1. No significant differences in the results were observed.

4.6.3 Tests and Timing Results for Rectangular Element

The two programs were used to evaluate the element matrices. Of course this is a subjective comparison, since one type of element may be coded more efficiently than the other. The speed-ups varied with the wave length, as shown in Figure 4.2. The time taken to integrate the element matrix semi-analytically has been evaluated using timing routines. This is denoted as T_{sa}. The time to integrate the element matrix numerically has been similarly denoted T_{gl}. The ratio of these two times has been termed, for brevity, 'Ratio of analytical to numerical times for element matrix integration', T_{sa}/T_{gl}. In Figure 4.2 this time is plotted as a function of the number of Gauss-Legendre integration points in ξ and η directions. It demonstrates that the semi-analytical integration scheme gives a considerable benefit, especially for shorter wave lengths. The break-even point is for 10 by 10 Gauss-Legendre integration, which corresponds, roughly, to one wavelength in each direction in the special wave finite element. For 120 by 120 integration, the advantage
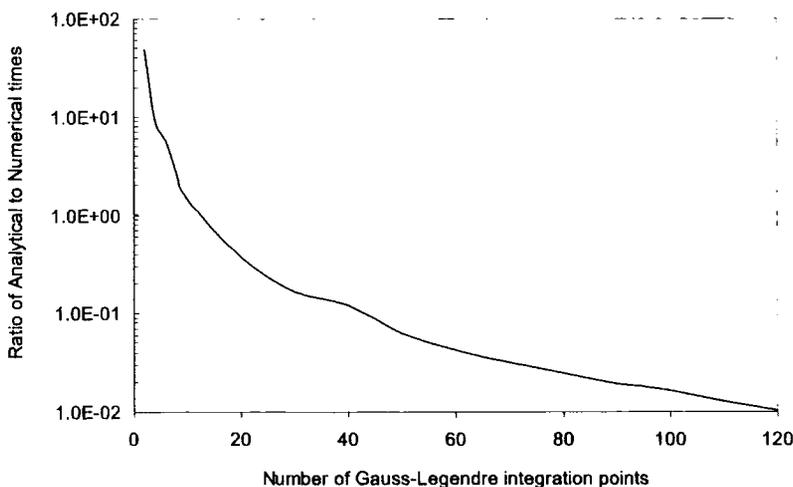
Figure 4.2: Ratio of analytical to numerical times for element matrix integration, T_{sa}/T_{gl}, as a function of number of integration points.

of the semi-analytical integration is a speed-up factor of about 10^2. This is the sort of zone in which the advantages of the special wave finite elements are particularly felt. It should also be noted that no special efforts have been made to 'tweak' the integration code produced by Maple to be optimal. In general, although the code produced by Maple is adequate, it is not particularly efficient. Variables are often defined repeatedly. Also internal symmetries in the calculation of the integration weights have not been exploited. For these, and other reasons, it is felt that the speed-ups shown, are the *minimum* which can be expected from such techniques. (Fortran code produced by Mathematica was much worse than that produced by Maple.)

4.6.4 Numerical Example: Evanescent modes

In order to test the rectangular element integration schemes on a realistic and non-trivial problem the so-called *evanescent mode* problem was solved in the interior of a rectangular domain. While the comparisons given in Figure 4.1 are useful, because of the ill-conditioned nature of the matrices generated by these elements it is *essential* to test the element matrices on a real problem. The solution to this problem is given by Morse and Feshback [77], who demonstrate that the Helmholtz equation can be separated into two equations. By setting

$$\phi = X(x)Y(y) \tag{4.23}$$

58

the Helmholtz equation becomes

$$\frac{1}{X}\frac{d^2 X}{dx^2} + \frac{1}{Y}\frac{d^2 Y}{dy^2} + k^2 = 0 \tag{4.24}$$

k is the wavenumber, given by $k = 2\pi/\lambda$, where λ is the wavelength. After some manipulation this leads to a solution of the form

$$\phi = e^{(i\alpha x + y\sqrt{\alpha^2 - k^2})} \tag{4.25}$$

where the constant α^2 is called the *separation constant*. For values of α smaller than k, the conventional plane wave propagating in a direction defined by the two x and y components is obtained. But if $\alpha > k$, the behaviour in the y direction is exponential, and the apparent wavelength in the x direction is given by $2\pi/\alpha$, and is therefore less than the true wavelength, given by $2\pi/k$. Since the solution in this case has a different wavelength from that assumed in the special element shape functions it is a searching test of the approach. The solution can be further generalised by rotating it through an angle β. The most general form is therefore

$$\phi = a_0 e^{(i\alpha s + t\sqrt{\alpha^2 - k^2})} \tag{4.26}$$

where in the usual notation, with β being the angle of rotation of the wave field

$$\left\{ \begin{array}{c} s \\ t \end{array} \right\} = \left[\begin{array}{cc} \cos\beta & \sin\beta \\ -\sin\beta & \cos\beta \end{array} \right] \left\{ \begin{array}{c} x \\ y \end{array} \right\} \tag{4.27}$$

The boundary condition applied on all four boundaries is the Robin boundary condition [67]

$$\frac{\partial\phi}{\partial n} + ik\phi = g \tag{4.28}$$

where g is the known solution, derived from Equations (4.26) and (4.27) above, and n is the outward normal.

For the numerical solutions, the domain is $0 \le x \le 12$, $0 \le y \le 1.2$. The problem is first solved for the parameters $k = 1$, $\alpha = 1.5$ and $\beta = 30°$. For this case a mesh of 4 by 4 equal sized rectangular elements were used, with 8 wave directions at each node. Figure 4.3 shows the real part of the analytical solution for the evanescent mode.
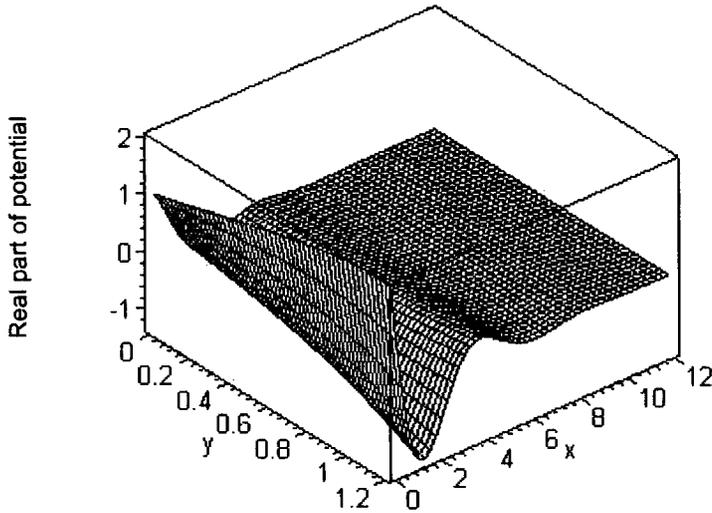
Figure 4.3: Real part of the rotated evanescent mode, for $k = 1$, $\alpha = 1.5$ and $\beta = 30°$, in the domain $0 \leq x \leq 12, 0 \leq y \leq 1.2$.

Analyticalsolution (real) $\cdots\cdots$ Analyticalsolution (imaginary)

■ Gauss-Legendre integration (real)   □ Gauss-Legendre integration (imaginary)

♦ Semi-analytical integration (real)   ◊ Semi-analytical integration (imaginary)
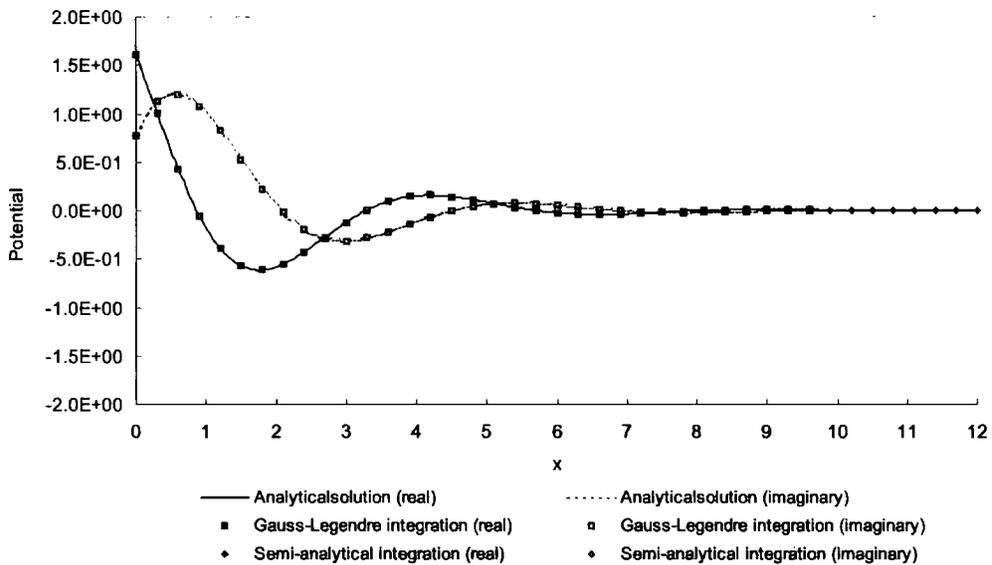
Figure 4.4: Real and imaginary parts of potentials for the rotated evanescent mode, for $k = 1$, $\alpha = 1.5$ and $\beta = 30°$, along the centre-line of the domain, $y = 0.6$.

The real and imaginary potential along the centre line of the domain, $y = 0.6$ is plotted in Figure 4.4, for analytical, and the numerically integrated and the semi-analytically integrated rectangular elements. Figure 4.5 shows the difference between numerical results and analytical solution as the error in the finite element solutions along the same line.

The same evanescent modes problem is next solved for the parameters $k = 3$, $\alpha = 5$ and $\beta = 10°$. The same element mesh was used as before but with 24 wave directions
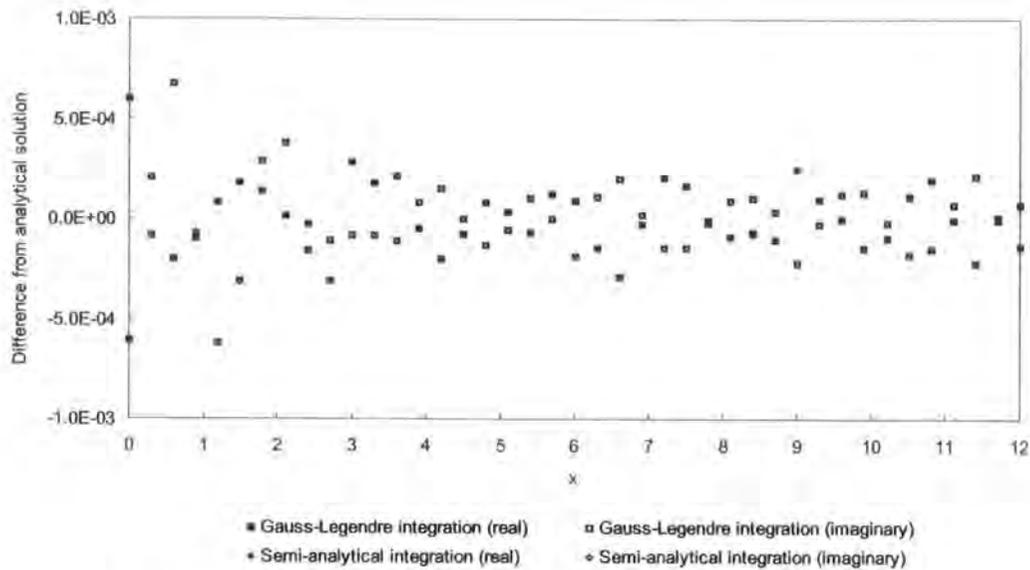
Figure 4.5: Real and imaginary errors in potentials of the rotated evanescent mode, for $k = 1$, $\alpha = 1.5$ and $\beta = 30°$, along the centre-line of the domain, $y = 0.6$.
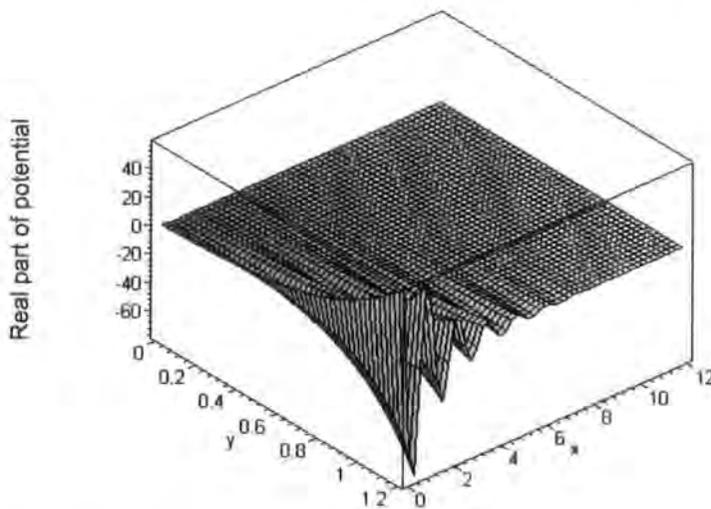
Figure 4.6: Real part of the rotated evanescent mode, for $k = 3$, $\alpha = 5$ and $\beta = 10°$, in the domain $0 \leq x \leq 12, 0 \leq y \leq 1.2$.

at each node. Figure 4.6 shows the real part of the analytical solution for the evanescent mode. For the numerical solutions Robin boundary conditions are used. The real and imaginary potential along the centre line of the domain, $y = 0.6$ is plotted in Figure 4.7, for analytical, and the numerically integrated and the semi-analytically integrated rectangular elements. Figure 4.8 shows the difference between numerical results and analytical solution as the errors in the finite element solutions along the same line. The results are
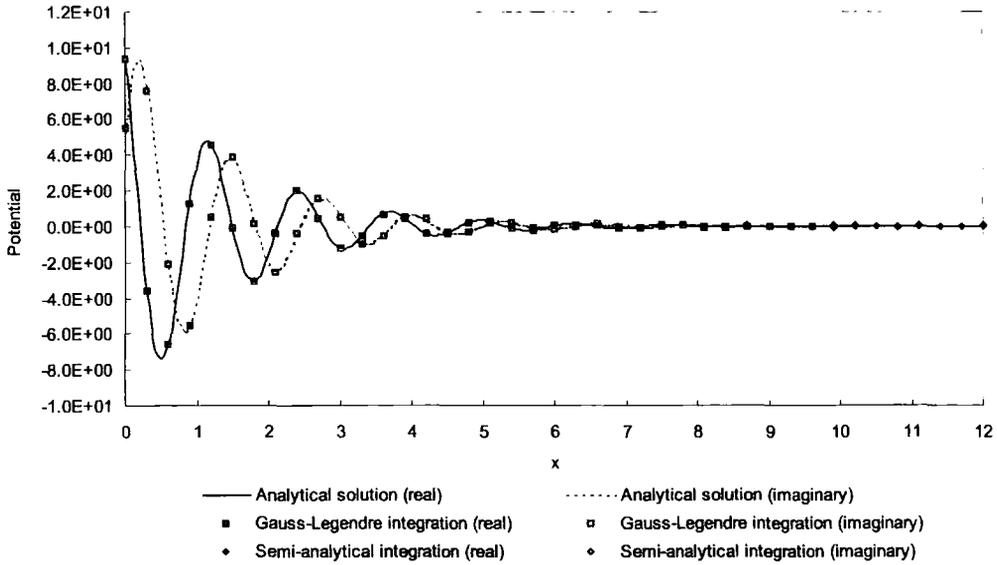
Figure 4.7: Real and imaginary parts of potentials for the rotated evanescent mode, for $k = 3$, $\alpha = 5$ and $\beta = 10°$, along the centre-line of the domain, $y = 0.6$.
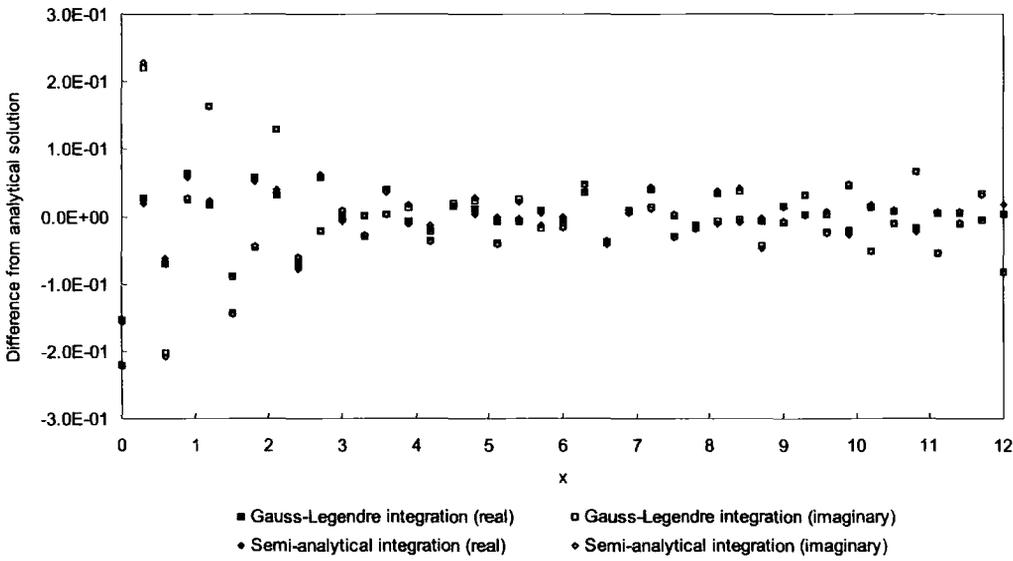
Figure 4.8: Real and imaginary errors in rotated evanescent mode, for $k = 3$, $\alpha = 5$ and $\beta = 10°$, potentials along the centre-line of the domain, $y = 0.6$.

encouraging. Aside from the generally acceptable accuracy of the results, they demonstrate that the results from the numerically integrated elements and the semi-analytically integrated elements are virtually identical. This gives confidence in the scheme for the rectangular element.

4.7 Triangular Finite Elements

4.7.1 Theory
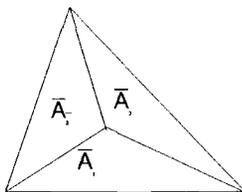
Figure 4.9: Partial areas for area co-ordinates of triangular elements.

Table 4.2: Different cases for triangular element.

Cases	F	G	$F - G$
1	$\neq 0$	$\neq 0$	$\neq 0$
2	$\neq 0$	$\neq 0$	≈ 0
3	$\neq 0$	≈ 0	$\neq 0$
4	≈ 0	$\neq 0$	$\neq 0$
5	≈ 0	≈ 0	≈ 0

The integral for the weights for integration over the triangular finite element is given above as Equation (4.18). The local co-ordinates ξ and η can be identified with the area co-ordinates $\bar{L}_2$ and $\bar{L}_3$ of the triangle respectively, as is well known, and is shown in Figure 4.9.

$$\bar{L}_1 = \bar{A}_1/\bar{A} \quad \bar{L}_2 = \bar{A}_2/\bar{A} \quad \bar{L}_3 = \bar{A}_3/\bar{A} \quad \bar{L}_1 + \bar{L}_2 + \bar{L}_3 = 1 \quad \xi \equiv \bar{L}_2 \quad \eta \equiv \bar{L}_3 \quad (4.29)$$

Because of the limits of integration for the triangle, another special case arises corresponding to that mentioned after Equation (4.18). The case of $F \approx G$ must be considered. Terms of the form $\exp[i(F - G)\eta]$ must then be replaced by the equivalent series. This gives a total of five special cases, listed in Table 4.2.

The polynomials for the triangle must be evaluated in terms of local area, or ξ, η co-ordinates, using expressions which are in standard textbooks [99], and which will not be repeated here. The integration points are chosen to be regularly spaced in ξ and η.

4.7.2 Numerical Example: Scattering Problem

The problem considered consists of a rigid circular cylinder of unit radius. The finite element mesh extends from $r = 1$ to $r = 5$. The mesh is regular, with 36 sectors, each

63
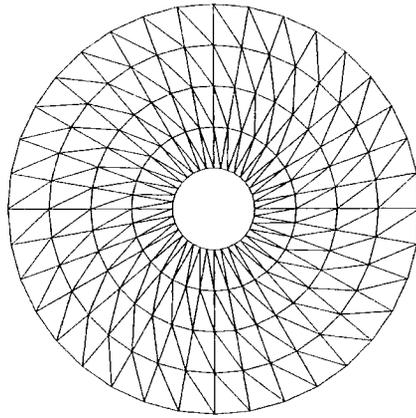
Figure 4.10: Mesh model using triangular finite elements for scattering problem. Inner radius 1, outer radius 5.

subtending 10°. Each sector is modelled using 8 linear triangular elements. (Linear in the sense that the underlying shape function is linear.) The mesh is shown in Figure 4.10.

Figure 4.11 shows the results for plane waves scattered by the cylinder, for $k = 4$, where k is the wavenumber. All the waves considered are incident from the negative x direction, that is from $\theta = 180°$ and $r \to \infty$. They progress towards $\theta = 0°$ and $r \to \infty$. All incident waves have unit amplitude. The numerically integrated elements use a Gauss-Legendre integration scheme involving 8 integration points in two directions. (This unsymmetrical scheme is not entirely satisfactory, but we had no access to higher triangular integration schemes.) The elements on the boundary, used to implement the boundary conditions were integrated using 40 Gauss-Legendre integration points, and so the order of quadrature should not influence the results, as it is so much higher than the minimum requirement. Plane damper boundary conditions were used, since they are simple to implement, and the present investigation is to determine the accuracy of the elements. Both numerically integrated and semi-analytically integrated elements use 8 equally spaced wave directions, i.e., $0°, 45°, \cdots, 315°$.

Figure 4.12 shows the difference between numerical results and analytical solution as the errors in the real and imaginary parts of the complex wave potential as a function of the angle around the cylinder. The results demonstrate that there are virtually no differences between the values obtained by the analytically integrated and numerically integrated elements.

Figure 4.13 shows the results for plane waves scattered by the cylinder, for $k = 16$. The numerically integrated elements use a Gauss-Legendre integration scheme involving 24 integration points in two directions. The same arrangement as before served for boundary
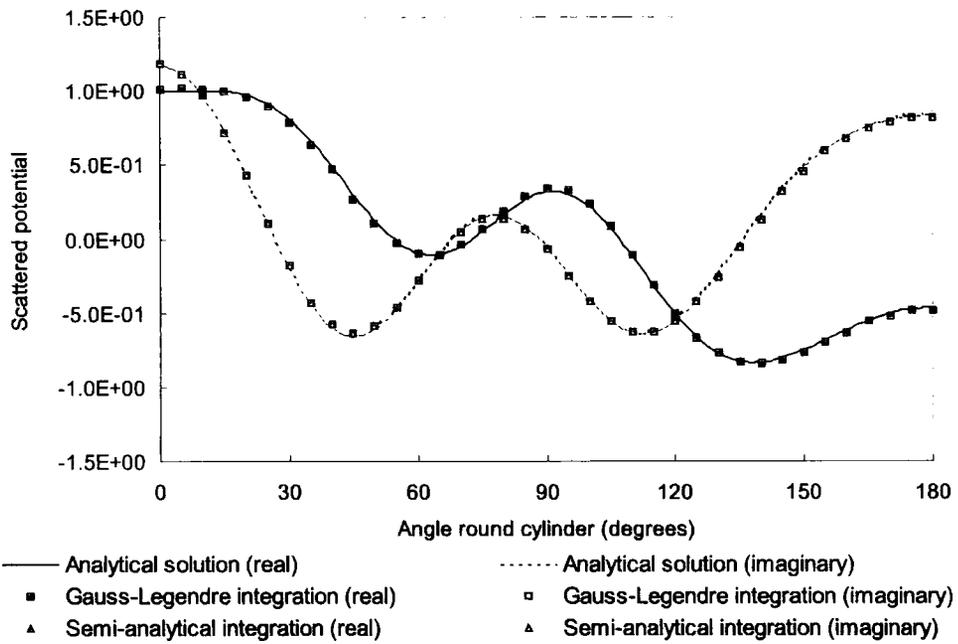
Figure 4.11: Real and imaginary parts of scattered potentials along the circumference of the cylinder, for $k = 4$.
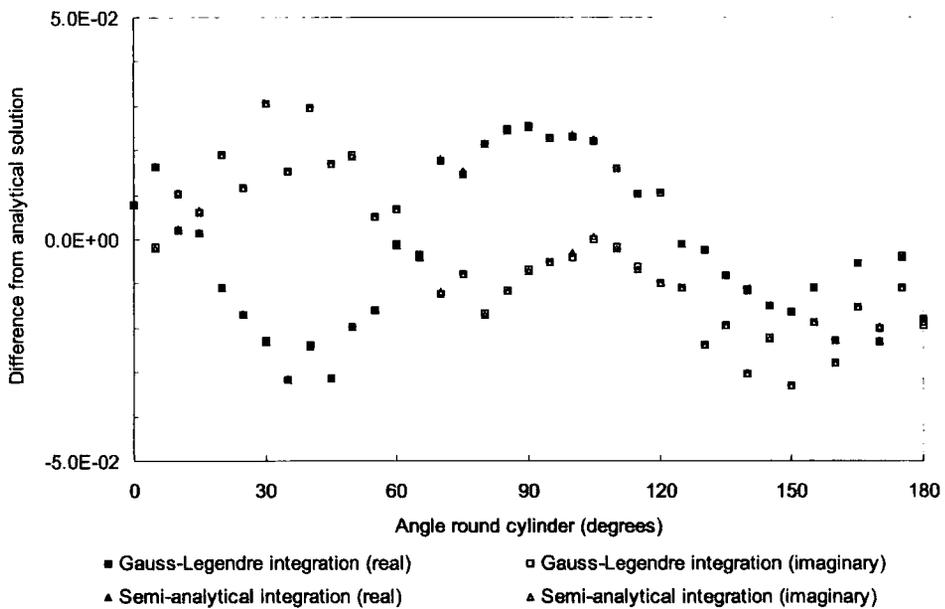
Figure 4.12: Difference from analytical solution in real and imaginary parts of scattered potential along the circumference of the cylinder, for $k = 4$.

elements and plane damper boundary conditions were again used. Both numerically integrated and semi-analytically integrated elements use 18 equally spaced wave directions, for this shorter wave problem i.e., $0°, 20°, \cdots, 340°$.

Figure 4.14 shows the difference between numerical results and analytical solution as
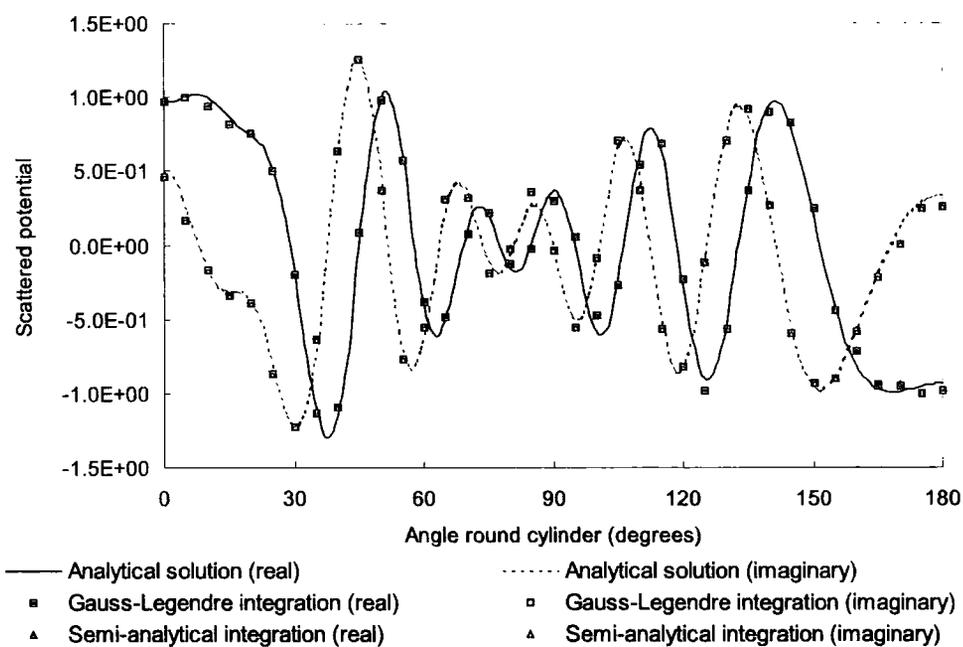
Figure 4.13: Real and imaginary parts of scattered potentials along the circumference of the cylinder, for $k = 16$.
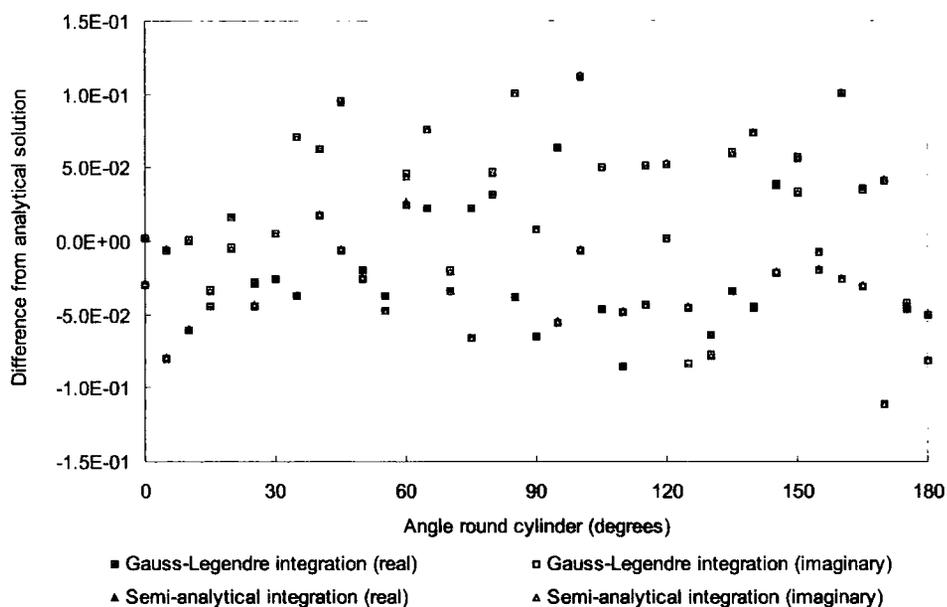
Figure 4.14: Difference from analytical solution in real and imaginary parts of scattered potential along the circumference of the cylinder, for $k = 16$.

the errors in the real and imaginary parts of the complex wave potential as a function of the angle around the cylinder. The results demonstrate that there are virtually no differences between the values obtained by the analytically integrated and numerically integrated elements. For this single example the relative execution times for the formation of the

Table 4.3: Comparison of relative timing.

	Element Matrix Formation	System Matrix Solution
Numerical Elements	14.7377	1.0000
Semi-analytical Elements	0.9836	1.0000

element matrices and the solution of the finite element equations normalised by the time to solve the system matrix are shown in Table 4.3. In the case of the numerically integrated 24 by 24 integration point elements, the time to form the element matrices was about 15 times of the time to solve the system matrix. That for the semi-analytically integrated elements was almost the same as the system matrix solution time. Too much should not be read into one set of figures, but they do indicate that the time for the formation of the element matrices can be brought broadly into line with the time for the solution of the system matrix, which indicates that the method should be competitive. The figure for the semi-analytical integrations should be independent of wavelength. If the criterion of 10 nodes per wavelength, for wave modelling, is used a regular mesh would require 101,859 nodes, and an unstructured mesh 48,892 nodes. This assumes that pollution would not play a role, which might well be optimistic in a problem with over 12 wavelengths in the radial direction. In the present model, with 180 nodes, and 18 directions per node, the total number of degrees of freedom is 3,240. This gives a *factor* of reduction of number of degrees of freedom for the unstructured mesh of roughly 15, and for the structured mesh roughly 31. It is likely that the number of nodes in the present mesh could be reduced if an iso-parametric version of these elements, (which could model more accurately the curved cylinder), were developed, since the nodal spacing circumferentially is much closer than in the radial direction.

4.8 Conclusions

Methods for integrating semi-analytically the element matrices arising from the new schemes of special wave finite elements for the solution of the Helmholtz equation in two dimensions has been presented. The new integration schemes have a number of special cases due to the combination of constants in the exponent of the exponential functions included in the

special shape functions. There are three and four special cases in the cases of rectangular elements and the triangular elements, respectively. In the most general cases, the integration can be dealt with quite simply in an analytical way. In the other special cases, the analytical expression of the integrals were obtained using Taylor's expansion.

The results show that the integration schemes give results which are hardly distinguishable from those obtained using very large numbers of conventional Gauss-Legendre integration points. As expected the element matrix integrations appear to be independent of the wavenumber, as shown by testing. For larger wavenumbers the semi-analytical integrations lead to large savings in execution times, by factors which increase with increasing wavenumber. Preliminary results for some classical wave problems demonstrate that these savings seem to be achieved without any loss of accuracy. At any rate for the elements of simpler geometry, semi-analytical integration seems to be a very promising way forward.

Chapter 5

Semi-analytical integration scheme for quadrilateral special wave finite elements

Following the semi-analytical integration scheme for rectangular and triangular special wave finite elements presented in Chapter 4, the theory for integrating the element matrices for quadrilateral special wave finite elements [92] is presented in this chapter.

5.1 Theory

5.1.1 Basic Form of Integration

In the case of the bi-linear quadrilateral the Jacobian of the mapping from local to global co-ordinates is no longer constant. The integrations will therefore only be approximate. However, it is possible to follow the same procedures as before. An additional term to those of Equations (4.14) is introduced,

$$H_t = k(\hat{\mathbf{e}}_j^l + \hat{\mathbf{e}}_i^m) \cdot \mathbf{d_t} \tag{5.1}$$

In this case, the relation between the local co-ordinates ξ, η and the global co-ordinates x, y is bi-linear, and can be written as

$$x = \alpha_0 + \alpha_1 \xi + \alpha_2 \eta + \alpha_3 \xi \eta$$

$$y = \beta_0 + \beta_1\xi + \beta_2\eta + \beta_3\xi\eta \tag{5.2}$$

where the local co-ordinates ξ and η cover a square domain $-1 \leq \xi \leq 1$, $-1 \leq \eta \leq 1$. α's and β's are real coefficients. The same methodology used for triangular elements is applied, although it is not exact but only approximate because the Jacobian is not constant for quadrilateral elements. The expressions for the weights become

$$w_{pq}(F, G, H) = \int_{\hat{E}} e^{iF\xi} e^{iG\eta} e^{iH\xi\eta} \mathcal{L}_{pq}(\xi, \eta) d\xi d\eta \tag{5.3}$$

This corresponds to Equation (4.16) for a rectangular or triangular element. In the integral of Equation (5.3), the difficulties arise from the presence of the $\xi\eta$ term. However, the integrals, while complicated, can be carried out. In the quadrilateral, there are three constants, F, G and H, and a total of twelve special cases arise, corresponding to these values being zero or non-zero, and to F or G being approximately equal to H, which again causes a problem. When H is non-zero, the weights involve the exponential integral, $\text{Ei}(x)$. This function is not supplied in Fortran, and so it was evaluated in our code in two separate ways. The first method was using the code from Numerical Recipes[81]. The second was by using a code written by Bulirsch [28] and modified by Clark [37]. This code uses Chebychev coefficients to evaluate the Cosine and Sine integrals. Polynomials are evaluated using Clenshaw's algorithm. The values for $\text{Ei}(x)$ obtained from the two codes were checked against each other and against values evaluated to arbitrary precision by Maple.

The evaluation of integration of weights takes the form

$$w_{pq}(F, G, H) = \int_{-1}^{1} \int_{-1}^{1} e^{iF\xi} e^{iG\eta} e^{iH\xi\eta} \mathcal{L}_{pq}(\xi, \eta) d\xi d\eta \tag{5.4}$$

and general term in Equation (5.4) can thus be written as

$$w_{pq}' = \int_{-1}^{1} \int_{-1}^{1} \xi^n \eta^m e^{iF\xi} e^{iG\eta} e^{iH\xi\eta} d\xi d\eta \tag{5.5}$$

where n and m are integers from 0 to the orders of the polynomials of original shape functions in the ξ direction and the η direction, respectively. The integral of any polynomial can be composed from a linear combination of such integrals.

In the integral of Equation (5.5), the difficulties arise from the presence of the $\xi\eta$

term which makes the quadrilateral case more difficult than rectangles and triangles. Also there are cases which need special treatments for numerical calculation depending on the exponent of e in the integration with respect to ξ or η. As seen in Equation (5.5), $F \pm H\eta$ or $G \pm H\xi$ can be considered as the coefficients of ξ or η in the exponent of e respectively, and it can be expected that the numerical calculation will fail or become inaccurate when these coefficients are zero or close to zero. On the other hand, when H is zero Equation (5.5) has no $\xi\eta$ term and this case must be treated separately to avoid numerical inaccuracy.

As a consequence of the above issues, one general case and twelve special cases can be distinguished. They are tabulated in Table 5.1, in which where there is a dash in the table, then the value of the constant is immaterial if the other conditions specified with ≈ 0 and $\neq 0$ in the same row are satisfied.

Table 5.1: Different cases for quadrilateral element.

Cases	H	F	G	$F - H$	$F + H$	$G - H$	$G + H$
1	$\neq 0$	—	—	$\neq 0$	$\neq 0$	$\neq 0$	$\neq 0$
2	≈ 0	$\neq 0$	$\neq 0$	—	—	—	—
3	≈ 0	≈ 0	$\neq 0$	—	—	—	—
4	≈ 0	$\neq 0$	≈ 0	—	—	—	—
5	≈ 0	≈ 0	≈ 0	—	—	—	—
6	$\neq 0$	—	—	≈ 0	$\neq 0$	$\neq 0$	$\neq 0$
7	$\neq 0$	—	—	$\neq 0$	≈ 0	$\neq 0$	$\neq 0$
8	$\neq 0$	—	—	$\neq 0$	$\neq 0$	≈ 0	$\neq 0$
9	$\neq 0$	—	—	$\neq 0$	$\neq 0$	$\neq 0$	≈ 0
10	$\neq 0$	—	—	≈ 0	$\neq 0$	≈ 0	$\neq 0$
11	$\neq 0$	—	—	≈ 0	$\neq 0$	$\neq 0$	≈ 0
12	$\neq 0$	—	—	$\neq 0$	≈ 0	≈ 0	$\neq 0$
13	$\neq 0$	—	—	$\neq 0$	≈ 0	$\neq 0$	≈ 0

5.1.2   General Case 1

In this section, the procedure to integrate over the element for the most general case where

- $H \neq 0$, $F \pm H \neq 0$, $G \pm H \neq 0$

is discussed.

Equation (5.5) is modified by collecting the terms in ξ into the form

$$w_{pq}' = \int_{-1}^{1} \eta^m e^{i\eta G} \left\{ \int_{-1}^{1} \xi^n e^{i\xi(F+H\eta)} d\xi \right\} d\eta \qquad (5.6)$$

71

The integration with respect to ξ can be written as

$$\int_{-1}^{1} \xi^n e^{i\alpha\xi} d\xi \tag{5.7}$$

where $\alpha = F + H\eta$. Note that $n \geq 0$. When $\alpha \neq 0$, the integration is simply carried out by using integration by parts

$$\int \xi^n e^{i\alpha\xi} d\xi = \frac{e^{i\alpha\xi}}{i\alpha} \sum_{k=0}^{n} (-1)^k \frac{n!\xi^{n-k}}{(n-k)!(i\alpha)^k} \tag{5.8}$$

and then Equation (5.6) becomes

$$w_{pq}' = \int_{-1}^{1} \eta^m e^{i\eta G} \sum_{k=0}^{n} \left\{ \frac{i^{k-1}n!}{(n-k)!} \frac{e^{i\alpha}}{\alpha^{k+1}} - (-1)^{n-k} \frac{i^{k-1}n!}{(n-k)!} \frac{e^{-i\alpha}}{\alpha^{k+1}} \right\} d\eta \tag{5.9}$$

The first term in the summation corresponds to the upper limit of the integration with respect to ξ, and the second term corresponds to the lower limit of ξ. Then the integration with respect to α instead of η will be considered. When $H \neq 0$, η is written with α as

$$\eta = \frac{\alpha - F}{H} \tag{5.10}$$

By using this relationship, Equation (5.9) is transformed into the form

$$
\begin{aligned}
w_{pq}' &= \frac{e^{iF} e^{-i\frac{G+H}{H}F}}{H^{m+1}} \sum_{k=0}^{n} \left[\frac{i^{k-1}n!}{(n-k)!} \sum_{l=0}^{m} \left\{ \frac{m!}{(m-l)!l!} (-F)^{m-l} \int_{F-H}^{F+H} \alpha^{l-k-1} e^{i\frac{G+H}{H}\alpha} d\alpha \right\} \right] \\
&\quad - \frac{e^{-iF} e^{-i\frac{G-H}{H}F}}{H^{m+1}} \sum_{k=0}^{n} \left[(-1)^{n-k} \frac{i^{k-1}n!}{(n-k)!} \sum_{l=0}^{m} \left\{ \frac{m!}{(m-l)!l!} (-F)^{m-l} \right. \right. \\
&\quad \left. \left. \times \int_{F-H}^{F+H} \alpha^{l-k-1} e^{i\frac{G-H}{H}\alpha} d\alpha \right\} \right]
\end{aligned} \tag{5.11}
$$

and the integration is simplified.

Now it can be seen that the assumption $\alpha \neq 0$ implies $F - H \neq 0$ corresponding to $\eta = -1$, the lower limit of the integration with respect to α, or $F + H \neq 0$ corresponding to $\eta = 1$, the upper limit of α.

The integrations with respect to α have similar forms to Equation (5.7) as

$$\int_{F-H}^{F+H} s^p e^{i\gamma s} ds \tag{5.12}$$

where $p = l - k - 1$. Considering that $0 \leq k \leq n$ and $0 \leq l \leq m$, p can take a value in the range of $-n - 1 \leq p \leq m - 1$. As seen in Equation (5.11), γ is $(G - H)/H$ corresponding to -1, the lower limit of the integration with respect to ξ, and $(G + H)/H$ corresponding to 1, the upper limit of ξ.

When $\gamma \neq 0$, the integration takes the form depending on the value of p

$$
\int s^p e^{i\gamma s} ds =
\begin{cases}
\dfrac{e^{i\gamma s}}{i\gamma} \displaystyle\sum_{r=0}^{p} (-1)^r \dfrac{p! s^{p-r}}{(p-r)!(i\gamma)^r} & \text{when } \gamma \neq 0, p \geq 0 \\[4mm]
Ei(i\gamma s) & \text{when } \gamma \neq 0, p = -1 \\[4mm]
\dfrac{-e^{i\gamma s}}{(-p-1)!} \displaystyle\sum_{r=1}^{-p-1} \dfrac{(-p-r-1)!(i\gamma)^{r-1}}{s^{-p-r}} + \dfrac{(i\gamma)^{-p-1}}{(-p-1)!} Ei(i\gamma s) & \\[4mm]
& \text{when } \gamma \neq 0, p \leq -2
\end{cases}
\tag{5.13}
$$

5.1.3 Special Cases 2-5

The conditions for the general case discussed in the previous section are not always satisfied. Therefore the other special cases will be discussed in this and the next sections. First of all, the exponential term including $\xi\eta$ in Equation (5.5) disappears when exactly $H = 0$, but we must also consider the special cases where $H \approx 0$ in this section.

When $H \approx 0$, applying Taylor's expansion

$$
e^{iH\xi\eta} = \sum_{r=0}^{\infty} \frac{(iH\xi\eta)^r}{r!} \cong \sum_{r=0}^{r_{max}} \frac{(iH\xi\eta)^r}{r!}
\tag{5.14}
$$

to Equation (5.5) leads to

$$
\begin{aligned}
w_{pq}' &= \int_{-1}^{1}\int_{-1}^{1} \xi^n \eta^m e^{iF\xi} e^{iG\eta} \sum_{r=0}^{r_{max}} \frac{(iH\xi\eta)^r}{r!} d\xi d\eta \\
&= \sum_{r=0}^{r_{max}} \frac{i^r H^r}{r!} \int_{-1}^{1} \xi^{n+r} e^{iF\xi} d\xi \int_{-1}^{1} \eta^{m+r} e^{iG\eta} d\eta
\end{aligned}
\tag{5.15}
$$

instead of Equation (5.6) for the general case, where r_{max} must be chosen large enough for the accuracy. This can be done by setting the $r_{max} + 1$ term in the expansion, Equation (5.14), to the machine accuracy, say 10^{-15}, and solving for r_{max}.

The integration can be evaluated as the product of each integration with respect to ξ and η of the form

$$
\int_{-1}^{1} s^p e^{i\gamma s} ds
\tag{5.16}
$$

73

where s is ξ or η, γ is F or G and p is $n+r$ or $m+r$ respectively. Because of $n \geq 0$, $m \geq 0$ and $0 \leq r \leq r_{max}$, $n+r \geq 0$ and $m+r \geq 0$ and then $p \geq 0$.

In this case each integration can be evaluated in two ways subject to the value of γ. When $\gamma \neq 0$, it becomes

$$\int s^p e^{i\gamma s} ds = \frac{e^{i\gamma s}}{i\gamma} \sum_{r=0}^{p} (-1)^r \frac{p! s^{p-r}}{(p-r)!(i\gamma)^r} \qquad \text{when } \gamma \neq 0, p \geq 0 \qquad (5.17)$$

and when $\gamma \approx 0$, by applying Taylor's expansion to $\exp(i\gamma s)$, it becomes

$$\int s^p e^{i\gamma s} ds \cong \sum_{j=0}^{jmax} \frac{(i\gamma)^j}{j!(p+j+1)} s^{p+j+1} \qquad \text{when } \gamma \approx 0, p \geq 0 \qquad (5.18)$$

In these special cases where $H \approx 0$, there are 4 cases in total subject to the value of F and G.

- $H \approx 0$, $F \neq 0$ and $G \neq 0$

- $H \approx 0$, $F \approx 0$ and $G \neq 0$

- $H \approx 0$, $F \neq 0$ and $G \approx 0$

- $H \approx 0$, $F \approx 0$ and $G \approx 0$

These cases can be evaluated by combinations of the forms discussed in this section.

5.1.4 Special Cases 6-13

When the assumptions $H \neq 0$ and $F \pm H \neq 0$ are satisfied, the first integration with respect to ξ is carried out as shown for the general case. However when $\gamma \approx 0$ in the integral of Equation (5.12) corresponding to the lower or upper limit of the integration with respect to ξ, more special cases arise which must be compared during the integration with respect to η.

For the case where $\gamma \approx 0$, applying Taylor's expansion to $\exp(i\gamma s)$ leads to

$$\int s^p e^{i\gamma s} ds \quad \cong \quad \int \sum_{j=0}^{jmax} \frac{(i\gamma s)^j}{j!} s^p ds \qquad \text{when } \gamma \approx 0 \qquad (5.19)$$

$$= \begin{cases} \sum_{j=0}^{jmax} \frac{(i\gamma)^j}{j!(p+j+1)} s^{p+j+1} & \text{when } \gamma \approx 0, j+p \neq -1 \\ \sum_{j=0}^{jmax} \frac{(i\gamma)^j}{j!} \ln s & \text{when } \gamma \approx 0, j+p = -1 \end{cases} \qquad (5.20)$$

where $p = l - k - 1$ and $-n - 1 \le p \le m - 1$.

We recall the original expression, Equation (5.5) in which the relationship of F to ξ and G to η are identical. Therefore essentially it should be possible to alter the order of the integrations. Thus the integration can be evaluated by replacing F with G and ξ with η in the procedure shown above in order to deal with the special case when $F - H \approx 0$ or $F + H \approx 0$.

After all, in these special cases where $H \ne 0$, there are some cases requiring different treatments due to the relationship between F and H, or G and H.

- $H \ne 0$, $F - H \approx 0$, $F + H \ne 0$, $G - H \ne 0$, $G + H \ne 0$

- $H \ne 0$, $F - H \ne 0$, $F + H \approx 0$, $G - H \ne 0$, $G + H \ne 0$

- $H \ne 0$, $F - H \ne 0$, $F + H \ne 0$, $G - H \approx 0$, $G + H \ne 0$

- $H \ne 0$, $F - H \ne 0$, $F + H \ne 0$, $G - H \ne 0$, $G + H \approx 0$

In addition, there are more special cases caused by the combination of these conditions. If $H \ne 0$, it can be assumed that $F - H \approx 0$ and $F + H \approx 0$ do not occur at the same time unless $F \approx 0$, which was already discussed. In the same way, it can be assumed that $G - H \approx 0$ and $G + H \approx 0$ do not occur at the same time. However, it is possible that one of $F \pm H$ and one of $G \pm H$ become 0 at the same time. The resulting special cases are

- $H \ne 0$, $F - H \approx 0$, $F + H \ne 0$, $G - H \approx 0$, $G + H \ne 0$

- $H \ne 0$, $F - H \approx 0$, $F + H \ne 0$, $G - H \ne 0$, $G + H \approx 0$

- $H \ne 0$, $F - H \ne 0$, $F + H \approx 0$, $G - H \approx 0$, $G + H \ne 0$

- $H \ne 0$, $F - H \ne 0$, $F + H \approx 0$, $G - H \ne 0$, $G + H \approx 0$

These cases should be evaluated by the combination of the expressions which have already been discussed above.
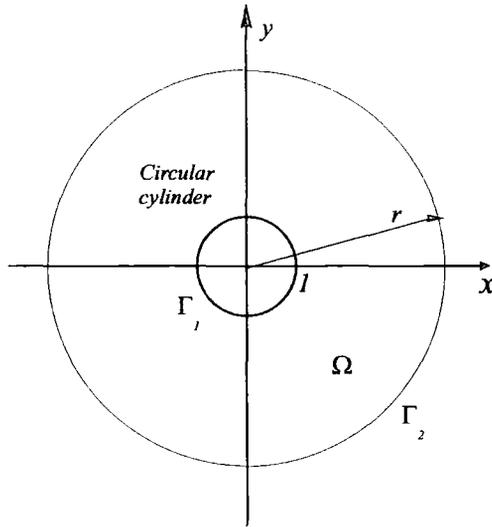
Figure 5.1: Geometry of scattering problem in two dimensions.
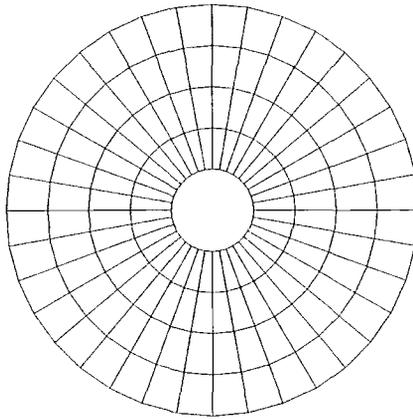
Figure 5.2: Mesh model using quadrilateral finite elements for scattering problem. Inner radius 1, outer radius 5.

5.2 Numerical Example: Scattering Problem

In order to test the semi-analytical quadrilateral element integration schemes presented in previous sections, a realistic problem was solved. The geometry of the problem is shown in Figure 5.1.

The problem is that of a circular cylinder of unit radius and infinite length. The surface of the cylinder is rigid and the plane wave of unit amplitude is incident perpendicular to the cylinder axis from the angle $\theta = 180°$. The wave field can be treated as a two dimensional problem in a plane perpendicular to the cylinder axis. The finite element mesh using quadrilateral elements is shown in Figure 5.2. The cylindrical domain over $1 \leq r \leq 5$ is divided into 36 sectors of 10 degrees each, and each sector is divided into four 4-node quadrilateral elements in the radial direction. To verify the integration scheme,
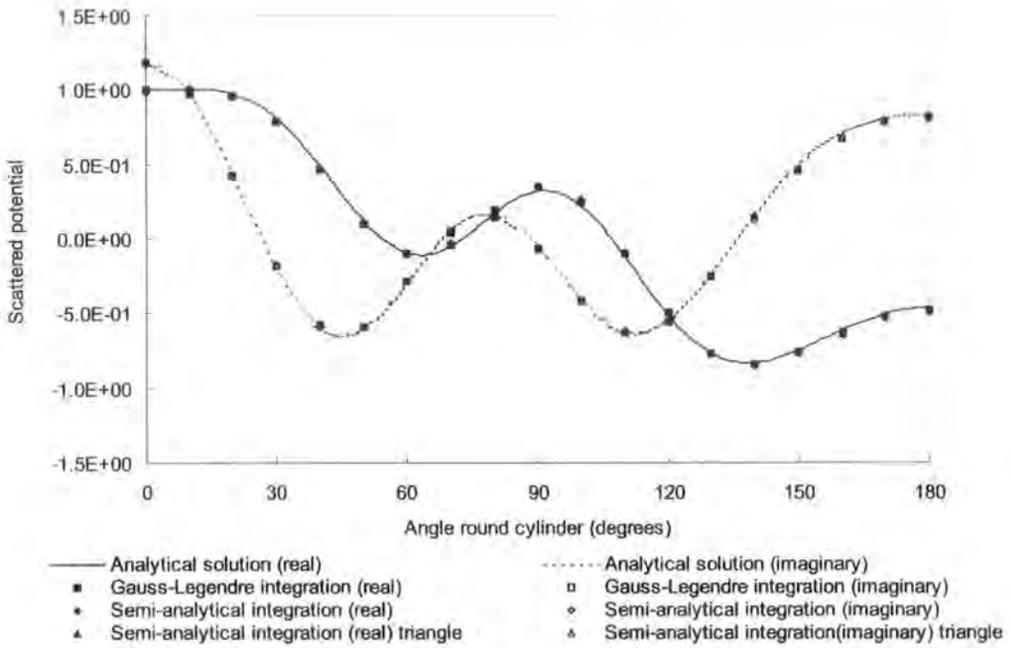
Figure 5.3: Real and imaginary parts of scattered potentials along the circumference of the cylinder, for $k = 4$.
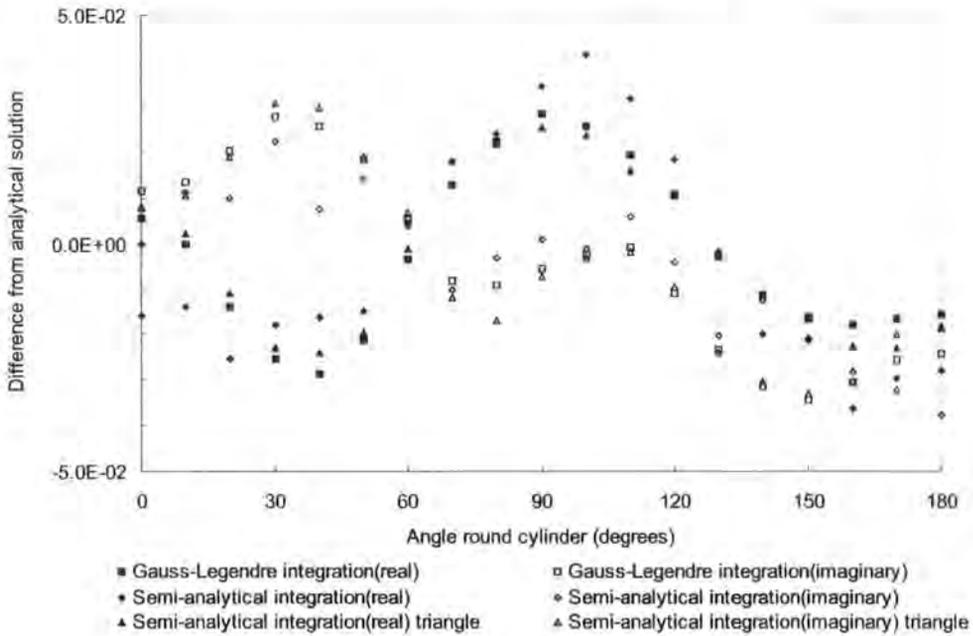
Figure 5.4: Difference from analytical solution in real and imaginary parts of scattered potential along the circumference of the cylinder, for $k = 4$.

quadrilateral elements were integrated using the semi-analytical scheme presented in the previous section or Gauss-Legendre integration scheme. To compare the results with those obtained by mesh model using triangular elements, each quadrilateral element in Figure 5.2 was divided into two triangular elements, so that the number of elements was doubled. The
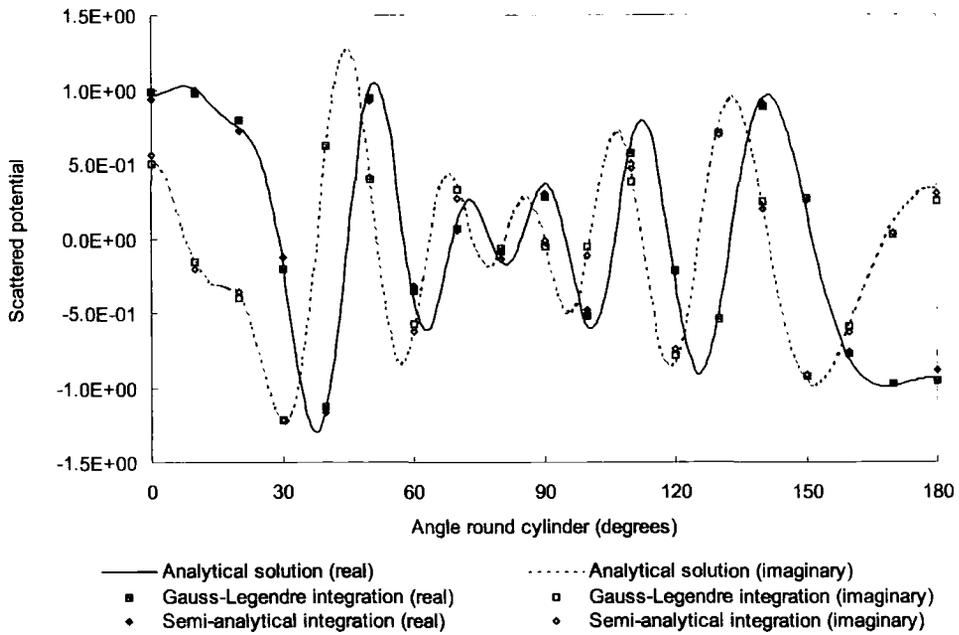
Figure 5.5: Real and imaginary parts of scattered potentials along the circumference of the cylinder, for $k = 16$.
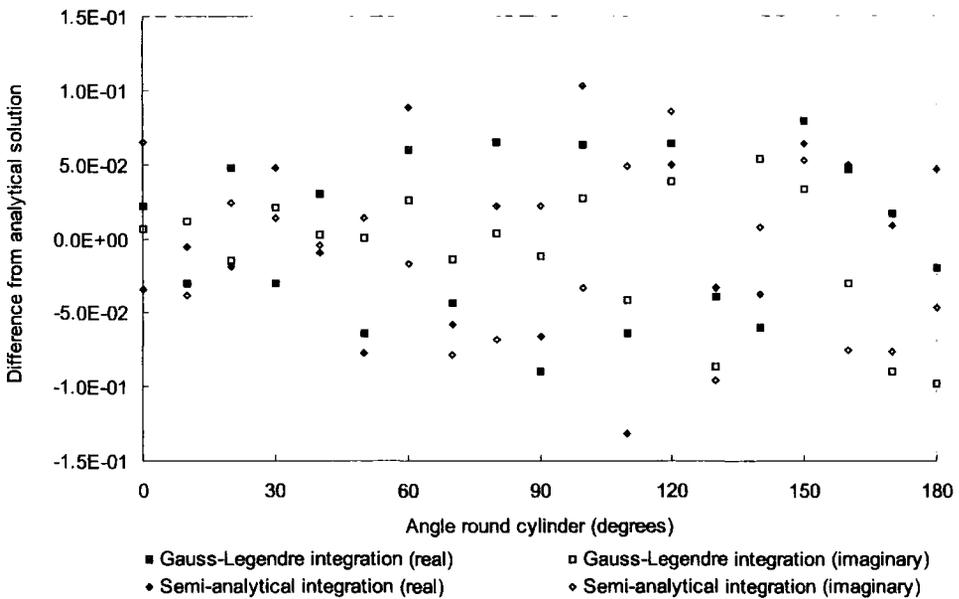
Figure 5.6: Difference from analytical solution in real and imaginary parts of scattered potential along the circumference of the cylinder, for $k = 16$.

mash model using triangular elements is the same as that shown in Figure 4.10. Triangular elements were integrated using semi-analytical scheme discussed in Section 4.7.

On the inner boundary at $r = 1$ the normal derivatives of scattered potential were given as the Neumann boundary condition and on the outer boundary at $r = 5$ plane

damper boundary condition was applied. Ortiz and Sanchez [78] showed the boundary condition of Higdon [57] behaves perfectly non-reflecting for each approximating plane wave if its direction is included in the condition. It should be quite accurate in plane wave bases finite elements if the directions of approximating plane waves are optimal or the number of plane waves is large enough so that the wave field is approximated in a good accuracy. However here we applied the simple plane damper to the scattered potential as the total of contributions of all plane waves at each node on the outer boundary because of its simplicity.

The problem was solved for the wavenumbers $k = 4$ and 16. The approximating plane waves were equally spaced from the direction of the positive global x-axis. At each node eight plane waves of the angle $0°, 45°, \cdots, 315°$, were applied for the case of $k = 4$, and eighteen plane waves of the angle $0°, 20°, \cdots, 340°$ were applied for the case of $k = 16$. For the case using Gauss-Legendre integration, the number of integration points in each direction was eight for the case of $k = 4$ and twenty four for the case of $k = 16$ due to the shorter wavelength. To implement the boundary conditions forty integration points were used so that the order of quadrature should not influence the results, as it is so much higher than the minimum requirement.

Figure 5.3 shows the scattered potential by the cylinder, for $k = 4$ as a function of the angle around the cylinder. The numerical results obtained by quadrilateral mesh are shown with those by triangular mesh and the analytical solution. Figure 5.4 shows the differences between numerical results and analytical solution as the errors in the real and imaginary parts of the complex scattered potential as a function of the angle around the cylinder. The maximum error of the scattered potential by quadrilateral mesh model using semi-analytical integration is slightly larger than that by triangular mesh model using semi-analytical integration or that by the same quadrilateral mesh model but with Gauss-Legendre integration. But the accuracies obtained by each integration methods vary against the angle, and they are of the same order.

Figure 5.5 shows the scattered potential by the cylinder, for $k = 16$ as a function of the angle around the cylinder. The numerical results obtained by quadrilateral mesh are shown with the analytical solution. Figure 5.6 shows the differences between numerical results and analytical solution as the errors in the real and imaginary parts of the complex scattered potential as a function of the angle around the cylinder. Again the sufficient

accuracy was achieved by using the semi-analytical integration, and the accuracies of the numerical results obtained by the semi-analytical integration and the Gauss-Legendre integration are of the same order.

A single special wave finite elements can contain many wavelengths, unlike the standard elements, because of the choice of basis function containing trigonometric functions. However it is necessary to increase the integration points in an element for shorter wave problems when a conventional numerical integration scheme is used to obtain element matrices. On the contrary, the computational cost of the semi-analytical integration scheme presented in this and previous chapter does not depend upon the wavelength. It means that it becomes more beneficial, as the waves become shorter, to use this semi-analytical integration scheme, which was already shown for triangular elements in the previous chapter.

In the case of the straight edged triangular elements, described previously [26], the Jacobian matrix which maps from local to global co-ordinates is constant. This means that it does not contribute any errors to the integration process. In the present case of quadrilateral, the Jacobian matrix is not constant. The terms are rational polynomials. It is in the nature of large members of Gauss-Legendre integration points, that a good approximation to the variation of the Jacobian matrix would be obtained. In the present scheme one might expect errors, due to the reduced number of integration points. However the errors have not increased, in comparison with the triangular element, which is very satisfactory. In the results shown in Figure 5.4, the errors for both the triangle and the quadrilateral are of the same order. We will leave aside the errors caused by modelling the cylinder as a straight edged polygon, as these are the same in both cases. It seems that for this case the errors in the quadrilateral element caused by the varying Jacobian are compensated by the higher order polynomial in the quadrilateral, due to the presence of the $\xi\eta$ term. More definite conclusions will have to await further numerical testing.

5.3 Conclusions

A method for integrating semi-analytically the element matrices of a straight edged quadrilateral element arising from the new schemes of special wave finite elements for the solution of the Helmholtz equation in two dimensions has been presented. In the same way as done in the previous chapter, the integration was dealt with quite simply in an analytical way

in the most general case, and Taylor's expansion was applied in the special cases. Because of the presence of the term including the product of both co-ordinates in the exponent, it is more complicated to deal with quadrilateral elements than rectangular or triangular elements. There are 12 special cases in the case of quadrilateral elements.

The results show, again, that the semi-analytical integration scheme gives results which have the accuracy of the same order as those obtained using very large numbers of conventional Gauss-Legendre integration points, and that the element matrix integrations appear to be independent of the wavenumber, as well as the results of rectangular and triangular elements.

Chapter 6

Mapped Wave Infinite Elements

In this chapter the formulation of the mapped wave infinite elements for the wave problems governed by the Helmholtz equation is described, and then the theory of coupling of them to standard finite elements is discussed [89].

The infinite elements scheme is an extension of the concept of finite elements in which the elements have an infinite extent in one or more directions. Because the radiated or scattered wave must satisfy the Sommerfeld radiation condition at infinity in unbounded domain problems, the shape functions of infinite elements are chosen to describe the suitable behaviour. Therefore infinite elements make it unnecessary to truncate the domain by the artificial boundary, or to apply the absorbing boundary condition to approximate the radiation condition. They are easily implemented together with finite elements and the system matrix remains banded.

The original unconjugated mapped wave infinite element theory for periodic wave problems was developed by Bettess *et al.* [25] and Zienkiewicz *et al.* [93], which concentrated only on circular problems. The extension of the mapping so as to allow infinite elements to be placed on arbitrary boundary was applied to unconjugated wave infinite elements by Bettess and Bettess [21]. A detailed survey of infinite element formulations is presented in Chapter 1.

The mapped wave infinite elements dealt with in this thesis are based on the Bettess formulation [21].
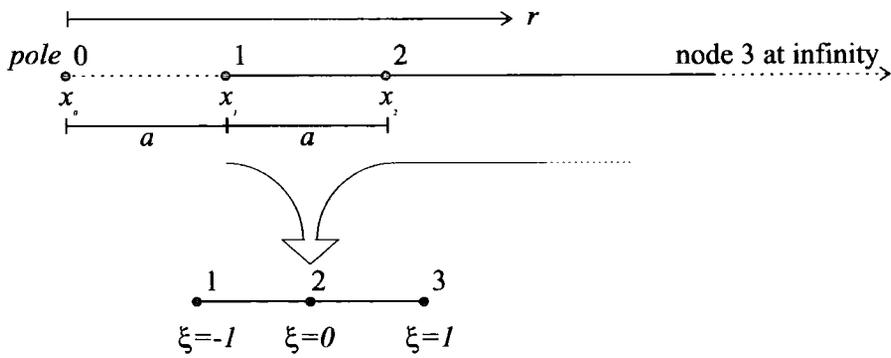
Figure 6.1: Infinite element mapping in one dimension.

6.1 Governing Equations

The Helmholtz equation which governs the wave problems in the frequency domain and the general expressions of boundary conditions are given by Equation (2.3) in Section 2.2.

Because the infinite element shape functions are defined so as to satisfy the radiation condition, the radiated or scattered potential is dealt with in the formulations in this chapter.

6.2 Infinite Element Mapping

6.2.1 One-Dimensional Mapping

Now we discuss the two dimensional case of an infinite element extending to infinity in the radial direction and finite in the angular direction. The essential effect of using a mapped infinite element is that the finite domain $-1 \leq \xi \leq 1$ in the local co-ordinates is mapped onto an unbounded domain $a \leq r \leq \infty$ in the global co-ordinates, where r is the distance from the 'pole' of the infinite element and a is the distance from the 'pole' to the inner edge of the infinite element.

Most of the infinite elements developed to date use some kind of mapping concept. Often two mappings are involved, one for the shape function and one for the numerical integration, usually Gauss-Legendre scheme. The Zienkiewicz mapping [96, 97] identifies the two mappings and has a great advantage that the original Gauss-Legendre integration abscissae and weights are retained. The only change needed to a finite element routine to make the element infinite is a new computation of the Jacobian matrix.

Consider first the geometry of one-dimensional problem shown in Figure 6.1. For the

case of a quadratic element whose geometry is defined by three nodes, the element is assumed to extend from point x_1 through x_2 to x_3, which at infinity. x_0 is taken to be the 'pole' of the radial behaviour. x_1 can be at anywhere in the interval x_0 to x_2, as written by

$$x_1 = \gamma x_2 + (1 - \gamma) x_0 \qquad (6.1)$$

where $0 < \gamma < 1$. In this work x_1 is defined at the midpoint between x_0 and x_2, i.e., $\gamma = 1/2$, so that

$$x_1 = \frac{x_0 + x_2}{2} \qquad (6.2)$$

A suitable mapping expression is

$$x = \tilde{N}_0(\xi) x_0 + \tilde{N}_2(\xi) x_2 \qquad (6.3)$$

where

$$\tilde{N}_0(\xi) = \frac{-\xi}{1 - \xi} \qquad (6.4)$$

$$\tilde{N}_2(\xi) = 1 + \frac{\xi}{1 - \xi} \qquad (6.5)$$

In some respect it is more convenient to relate the mapping to the element nodes, which was achieved by Marques and Owen [73]. A similar procedure was suggested by Kumar [62].

In the Marques and Owen formulation, $\tilde{N}_0$ and $\tilde{N}_2$ are replaced by mapping functions $M_1(\xi)$ and $M_2(\xi)$ so that

$$x = M_1(\xi) x_1 + M_2(\xi) x_2 \qquad (6.6)$$

where

$$M_1(\xi) = -\frac{2\xi}{1 - \xi} \qquad (6.7)$$

$$M_2(\xi) = \frac{1 + \xi}{1 - \xi} \qquad (6.8)$$
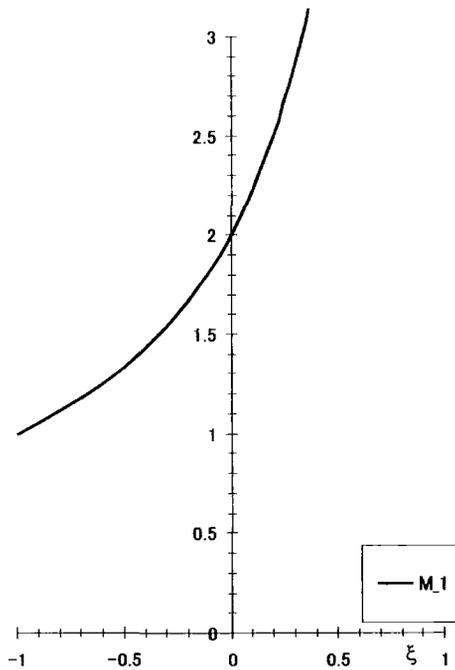
(a) Mapping for linear element
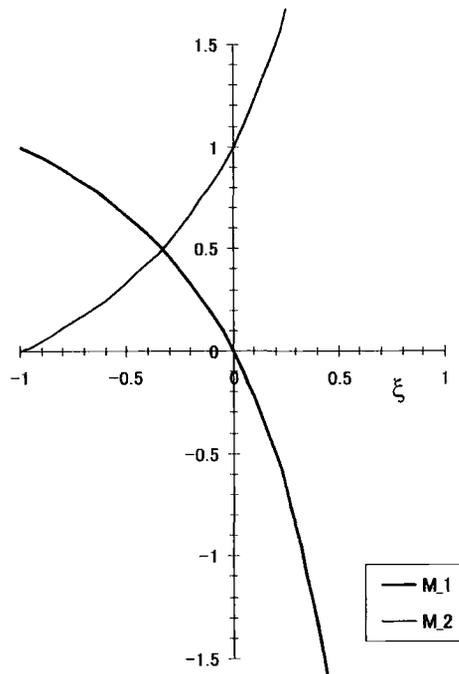
ξ		-1	1
$M_1(\xi)$	$2/(1-\xi)$	1	∞

(b) Mapping for quadratic element

ξ		-1	0	1
$M_1(\xi)$	$-2\xi/(1-\xi)$	1	0	∞
$M_2(\xi)$	$(1+\xi)/(1-\xi)$	0	1	$-\infty$

Figure 6.2: One-dimensional infinite mapping functions for linear and quadratic elements.

They satisfy

$$M_1(\xi) + M_2(\xi) = 1 \tag{6.9}$$

and take the values shown in Figure 6.2. In the same way, the mapping function for a linear one dimensional element is given by

$$M_1(\xi) = \frac{2}{1-\xi} \tag{6.10}$$

Let r be the distance from the 'pole', and the mapping between ξ and x is written as

$$r = x - x_0 = \frac{2a}{1-\xi} \tag{6.11}$$

where

$$a = \frac{x_2 - x_0}{2} = x_1 - x_0 \tag{6.12}$$

a is the distance from the 'pole' to the inner edge of the infinite element. The implication

of this is that the inner half of the infinite element has the extent of a.

6.2.2 Circular Mapping in Two Dimensions

This infinite geometry mapping can be easily extended to two and three dimensional geometries. For a two-dimensional infinite element of one infinite direction, the element mapping function is derived from the one-dimensional mapping function in the ξ direction, as shown in the previous section, and the usual shape function such as Lagrange polynomials in the η direction. The mapping functions for the infinite ξ direction are shown in Equations (6.7) and (6.8) for the quadratic case and in Equation (6.10) for the linear case. The mapping in the radial direction from ξ to r is given by the same form of Equation (6.11), i.e.,

$$r = \frac{2a}{1 - \xi} \tag{6.13}$$

where a, the distance between the 'pole' and the inner edge of the infinite element, is constant. As infinite elements in this formulation have a common 'pole', the inner edges of the infinite elements are located on a circular boundary of radius a. On the other hand, Lagrange polynomials of n-th order used as the shape functions in the η direction are given by

$$L_i^n(\eta) = \prod_{\substack{j=1 \\ j \neq i}}^{n} \frac{\eta - \eta_j}{\eta_i - \eta_j} \tag{6.14}$$

In the Marques and Owen formulation [73], the mapping functions for the ξ direction and the polynomial shape functions are simply multiplied to form the element mapping functions in two dimensions. When the number of nodes in the ξ direction is n_ξ and that in the η direction is n_η, the element mapping function $\mathcal{M}(\xi, \eta)$ becomes

$$\mathcal{M}_l(\xi, \eta) = M_i^{n_\xi}(\xi) L_j^{n_\eta}(\eta) \tag{6.15}$$

where $n = n_\xi \times n_\eta$, $i = 1, \cdots, n_\xi$, $j = 1, \cdots, n_\eta$, and $l = 1, \cdots, n$. Integer l denotes the node number in a two dimensional element, and integers i and j are the node numbers in each ξ and η direction as used in the definitions in the mapping functions in the ξ direction and the shape functions in the η direction, respectively. For example, infinite elements derived from a linear 4 node parent element and a quadratic 9 node parent element are

Table 6.1: Infinite element mapping functions for linear element in two dimensions.

Node,i	ξ_i	η_i	$\mathcal{M}_i^2$
1	-1	-1	$(1-\eta)/(1-\xi)$
2	-1	1	$(1+\eta)/(1-\xi)$

Table 6.2: Infinite element mapping functions for quadratic element in two dimensions.

Node,i	ξ_i	η_i	$\mathcal{M}_i^6$
1	-1	-1	$\eta(1-\eta)\xi/(1-\xi)$
2	0	-1	$-\eta(1-\eta)(1+\xi)/2(1-\xi)$
3	0	0	$(1-\eta^2)(1+\xi)/(1-\xi)$
4	0	1	$\eta(1+\eta)(1+\xi)/2(1-\xi)$
5	-1	1	$-\xi\eta(1+\eta)/(1-\xi)$
6	-1	0	$-2\xi(1+\eta)(1-\eta)/(1-\xi)$
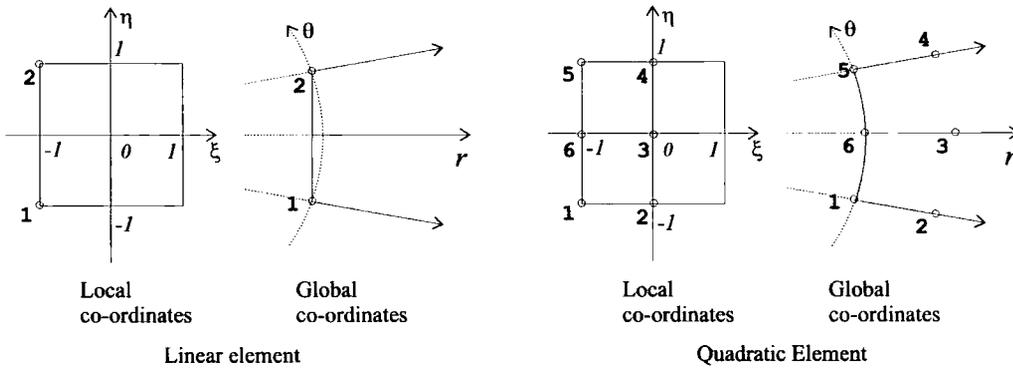
Figure 6.3: Infinite element mappings for linear and quadratic elements in two dimensions.

shown in Figure 6.3 and their mapping functions are shown in Tables 6.1 and 6.2. Because mapping functions for the nodes at $\xi = 1$ in the parent element, which are mapped onto infinity, are not defined, the element mapping functions are shown for 2 nodes and 6 nodes for linear and quadratic elements respectively.

Consequently global co-ordinates x and y of each n-node finite element are related to the local co-ordinates ξ and η using the transformation

$$x = \sum_{j=1}^{n} \mathcal{M}_j x_j \qquad y = \sum_{j=1}^{n} \mathcal{M}_j y_j \tag{6.16}$$

where x_j and y_j are the nodal co-ordinates. Here j denotes the node number in two

dimensions. Then the Jacobian matrix J which describes the geometry mapping between the local co-ordinates ξ, η and the global co-ordinates x, y is given by

$$J = \begin{bmatrix} \dfrac{\partial x}{\partial \xi} & \dfrac{\partial y}{\partial \xi} \\ \dfrac{\partial x}{\partial \eta} & \dfrac{\partial y}{\partial \eta} \end{bmatrix} = \begin{bmatrix} \displaystyle\sum_{j=1}^{n} \dfrac{\partial \mathcal{M}_j}{\partial \xi} x_j & \displaystyle\sum_{j=1}^{n} \dfrac{\partial \mathcal{M}_j}{\partial \xi} y_j \\ \displaystyle\sum_{j=1}^{n} \dfrac{\partial \mathcal{M}_j}{\partial \eta} x_j & \displaystyle\sum_{j=1}^{n} \dfrac{\partial \mathcal{M}_j}{\partial \eta} y_j \end{bmatrix} \tag{6.17}$$

and the element of surface $dxdy$ is written in terms of the local co-ordinates and the determinant of Jacobian matrix $|J|$ as follows

$$dxdy \quad = \quad |J|\, d\xi\, d\eta \tag{6.18}$$

Since the derivatives of mapping functions with respect to ξ and η can be easily obtained, the Jacobian matrix can also be obtained and the element matrix can be formed. To describe the unknown function within the element, standard shape functions can be used, but some special shape function containing the feature of the outgoing wave in the radial direction from the node is used for the wave infinite element discussed in this work. The details of the shape functions are described in the Section 6.3. The order of shape function must match the number of nodes in the η direction of the element to ensure continuity. In the infinite ξ direction the shape function can be of any order.

6.2.3 Non-circular Mapping in Two Dimensions

In the original mapped infinite element theory for periodic wave problems by Bettess *et al.* [25] and Zienkiewicz *et al.* [93], a was a constant, which means that infinite elements had a common 'pole' and they had to be placed on a circular mesh in the two dimensional case and a spherical mesh in the three dimensional case.

The extension of the mapping so as to allow infinite elements to have arbitrary pole locations so that they can be placed on arbitrary boundary, first applied to wave envelope elements by Astley *et al.* [14], Cremers *et al.* [40] and Cremers and Fyfe [39], was also applied to unconjugated mapped wave infinite elements by Bettess and Bettess [21]. In the Bettess formulation for two-dimensional problems [21], the mapping in the radial direction from ξ to r is given by

$$r = \frac{A(\eta)}{1 - \xi} \tag{6.19}$$

88

where $A(\eta)$ is equal to $2a$ in Equation (6.11). However, it varies with respect to η, the local co-ordinate corresponding to the angular direction in the global co-ordinate. Function $A(\eta)$ is interpolated by using $L_i(\eta)$, the shape functions in the η direction and A_i, twice the distance from the 'pole' to the i-th node which defines the element geometry on the inner edge of the infinite element,

$$A(\eta) = \sum_i L_i(\eta) A_i \tag{6.20}$$

$$\frac{\partial A(\eta)}{\partial \eta} = \sum_i \frac{\partial L_i(\eta)}{\partial \eta} A_i \tag{6.21}$$

A_i are applied to any points on the same straight lines from the 'pole', i.e., the points corresponding to the same local η co-ordinate. The nodes are located at $\eta = -1$ and $+1$ for elements that are linear in the angular direction, and at $\eta = -1$, 0 and $+1$ for those that are quadratic in the angular direction. On each line of these η values, the x and y co-ordinates are used to calculate A_i,

$$A_i = 2\sqrt{(x_i - x_0)^2 + (y_i - y_0)^2} \tag{6.22}$$

where (x_0, y_0) is the global co-ordinates of the 'pole', and

$$x_i = \sum_{j=1}^{n} \mathcal{M}_j(-1, \eta_i) x_j \tag{6.23}$$

$$y_i = \sum_{j=1}^{n} \mathcal{M}_j(-1, \eta_i) y_j \tag{6.24}$$

Thus $A(\eta)$ varies between and within each element, which allows different infinite elements to have different 'poles' and to be placed on an arbitrary boundary. The shape functions $L_i(\eta)$ are defined on the inner edge of the infinite element only. For linear and quadratic elements, the $L_i(\eta)$ take the well known forms

$$\text{linear:} \quad L_1(\eta) = -\frac{1}{2}(\eta - 1) \quad L_2(\eta) = \frac{1}{2}(\eta + 1) \tag{6.25}$$

$$\text{quadratic:} \quad L_1(\eta) = \frac{1}{2}\eta(\eta - 1) \quad L_2(\eta) = 1 - \eta^2 \quad L_3(\eta) = \frac{1}{2}\eta(\eta + 1) \tag{6.26}$$

6.3 Shape Functions for Coupling with Standard Finite Element

6.3.1 Amplitude Decay and Wave Component

As shown in Section 2.3, the general solution of the Helmholtz equation in two dimensions is given by expression (2.15). This shows that the wave oscillates roughly like $\exp(ikr)$ in the radial direction r and that the amplitude decays in $r^{-1/2}$ in two dimensions. This needs to be considered in the mapped wave infinite element formulation.

The first step to obtain the mapped wave infinite element model is the same as the standard finite element formulation. The field variable ϕ within an n-node infinite element is approximated using polynomial shape functions N_j and the nodal values ϕ_j

$$\phi = \sum_{j=1}^{n} N_j(\xi, \eta) \phi_j \tag{6.27}$$

This takes the form of a polynomial in powers of ξ

$$\phi = \alpha_0 + \alpha_1 \xi + \alpha_2 \xi^2 + \cdots \tag{6.28}$$

where coefficients α_j include some constants and powers of η. When the mapping between ξ and r shown in Equation (6.19) is applied, Equation (6.28) yields a polynomial in inverse powers of r

$$\phi = \beta_0 + \beta_1 \frac{1}{r} + \beta_2 \frac{1}{r^2} + \cdots \tag{6.29}$$

where β_j can be determined by α's and $A(\eta)$. If the polynomial is required to decay to zero at infinity then $\beta_0 = 0$. Equation (6.29) shows that when the shape function is mapped onto a infinite element in the global co-ordinates, the expression of the field variable ϕ contains a decay term of the form $1/r$. This is suitable to describe the decay of outgoing waves in three dimensional exterior problems, because their dominant term is of the form $\exp(ikr)/r$.

In two dimensions, however, the wave oscillates roughly like $\exp(ikr)$ in the radial direction r and that the amplitude decays in $r^{-1/2}$ as mentioned above. In order to describe the amplitude decay in two dimensions, the shape function needs to be multiplied by $r^{1/2}$, and to include the wave-like oscillation, a periodic component of the form $\exp(ikr)$ also

needs to be introduced into the shape function. The suitable shape functions for a mapped wave infinite element $S_j(\xi, \eta)$ are therefore the standard polynomial shape functions shown in Equation 6.27 multiplied by $r^{1/2} \exp(ikr)$, that is

$$
\begin{aligned}
S_j(\xi, \eta) &= N_j(\xi, \eta) r^{1/2} e^{ikr} & (6.30) \\
&= N_j(\xi, \eta) \left[\frac{A(\eta)}{1 - \xi} \right]^{1/2} e^{ikA(\eta)/(1-\xi)} & (6.31)
\end{aligned}
$$

which gives the required two dimensional behaviour. The expression for the field variable ϕ is

$$
\phi = \sum_{j=1}^{n} S_j(\xi, \eta) \phi_j \tag{6.32}
$$

6.3.2 Compatibility of Shape Functions

To ensure the continuity of amplitudes and phases between standard finite element and mapped wave infinite element, the amplitude of the shape function must be normalized to unity and the phase must be set to zero on the finite element/infinite element interface [25]. On the interface, i.e., on the inner edge of the infinite element where $\xi = -1$, the shape function $S_j(\xi, \eta)$ takes the value

$$
S_j(-1, \eta) = N_j(-1, \eta) \left[\frac{A(\eta)}{2} \right]^{1/2} e^{ikA(\eta)/2} \tag{6.33}
$$

thus the shape function $S_j(\xi, \eta)$ needs to be multiplied by a term

$$
\left[\frac{2}{A(\eta)} \right]^{1/2} e^{-ikA(\eta)/2} \tag{6.34}
$$

consequently the shape function $S_j(\xi, \eta)$ becomes

$$
S_j(\xi, \eta) = N_j(\xi, \eta) \left[\frac{2}{A(\eta)} \right]^{1/2} \left[\frac{A(\eta)}{1 - \xi} \right]^{1/2} e^{-ikA(\eta)/2} e^{ikA(\eta)/(1-\xi)} \tag{6.35}
$$

In terms of ξ and η the shape function and the derivatives simplify to become

$$
S_j(\xi, \eta) = N_j(\xi, \eta) \left[\frac{2}{1 - \xi} \right]^{1/2} e^{-ikA(\eta)/2} e^{ikA(\eta)/(1-\xi)} \tag{6.36}
$$

91
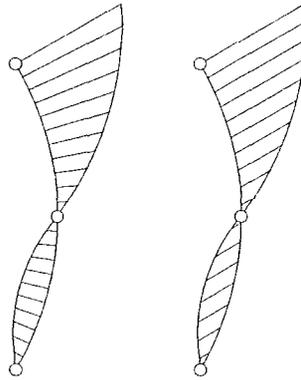
Figure 6.4: Wave directions in mapped wave infinite element(left) and in special wave finite element(right).

$$\frac{\partial S_j(\xi,\eta)}{\partial \xi} = \left[\frac{2}{1-\xi}\right]^{1/2}\left[\frac{\partial N_j(\xi,\eta)}{\partial \xi} + \frac{N_j(\xi,\eta)}{2(1-\xi)} + \frac{ikA(\eta)N_j(\xi,\eta)}{(1-\xi)^2}\right]$$
$$\times \quad e^{-ikA(\eta)/2}e^{ikA(\eta)/(1-\xi)} \tag{6.37}$$

$$\frac{\partial S_j(\xi,\eta)}{\partial \eta} = \left[\frac{2}{1-\xi}\right]^{1/2}\left[\frac{\partial N_j(\xi,\eta)}{\partial \eta} + \frac{ik}{2}\frac{1+\xi}{1-\xi}N_j(\xi,\eta)\frac{\partial A(\eta)}{\partial \eta}\right]$$
$$\times \quad e^{-ikA(\eta)/2}e^{ikA(\eta)/(1-\xi)} \tag{6.38}$$

6.4 Shape Functions for Coupling with Special Wave Finite Element

As described in the previous section, it is necessary to include a correction term in the shape functions of the mapped wave infinite elements to be coupled to standard finite elements. In case of the coupling of the mapped wave infinite elements to the special wave finite elements, the theory becomes slightly different because the shape functions of the special wave finite elements also contain trigonometric functions describing wave behaviour.

As seen in chapters 3 and 6, both types of elements use special shape functions which contain trigonometric functions to describe wave behaviour. However care must be taken when coupling these different types of elements, because the wave directions between nodes on the finite element/infinite element interface can be incompatible. This is because of the difference of the wave direction settings of these elements. Firstly, although an arbitrary number of approximating plane waves can be used for special wave finite elements, only the radial wave is assumed for mapped wave infinite elements. Because of this limitation, only the radial approximating plane wave can be applied at the nodes shared by these

92

finite and infinite elements. Secondly, although for special wave finite elements the wave directions are defined with fixed angles relative to the x-axis of the global co-ordinates, for mapped wave infinite elements the wave direction is radial from the 'pole'. This means that wave directions are normally globally constant between nodes within a special wave finite element but the radial direction varies between nodes within a mapped wave infinite element as shown in Figure 6.4. The wave directions between nodes can thus be incompatible. In order to eliminate this internode incompatibility, it has been decided to force the waves associated with nodes on the interface to be strictly radial for both types of elements. This is only one of several possible choices, such as introducing additional constraints, for example, applying constraints by Lagrange multipliers.

In this section, the waves associated with nodes on the finite element/infinite element interface are forced to be strictly radial. This necessitates a simple modification to the evaluation of the terms in Equation (3.26)

$$\phi = \sum_{j=1}^{n} \sum_{l=1}^{m_j} N_j \psi_j^l A_j^l$$

so that the wave directions which form part of shape functions for the finite element for interface nodes are now radial. This eliminates internode incompatibility between the two types of elements. To be more precise, for nodes with plane waves, the wave function is $\exp[i(k_x x + k_y y)]$ where k_x and k_y are the constant components of the wavenumber ($k = [k_x^2 + k_y^2]^{1/2}$) and for the cylindrical wave the function is $\exp(ikr)$ where the radial direction r varies.

In case where only one approximating plane wave in the radial direction is used for a special wave finite element, the nodal variable ϕ is written as

$$\phi = \sum_{j=1}^{n} N_j e^{ikr} A_j \tag{6.39}$$

The wave-like oscillating behaviour is described by the term $\exp(ikr)$, where r is the radial direction from the 'pole' of the coupled infinite element. On the other hand, in the infinite element formulation the nodal variable ϕ is written as

$$\phi = \sum_{j=1}^{n} C_j N_j r^{1/2} e^{ikr} \phi_j \tag{6.40}$$

where C_j is an extra term which ensures continuity of finite elements and infinite elements [25, 95]. In case of infinite elements to be coupled with standard finite elements, it is written as

$$C_j = \left[\frac{2}{A(\eta)}\right]^{1/2} e^{-ikA(\eta)/2} \qquad (6.41)$$

as shown in the previous section. However, in case of infinite elements to be coupled with special wave finite elements, as shape functions of both types of elements have the factor $\exp(ikr)$, the continuity of the phase is automatically ensured. Therefore the term $\exp(-ikA(\eta)/2)$ is no longer needed. Because the amplitude of the shape functions of the mapped wave infinite elements needs to be normalised in order to ensure a unit absolute value of the shape function at the node and the continuity between finite and infinite elements, the factor $\{2/A(\eta)\}^{1/2}$ is still needed for two dimensional case. Consequently, the correction term becomes

$$C_j = \left[\frac{2}{A(\eta)}\right]^{1/2} \qquad (6.42)$$

and

$$\phi = \sum_{j=1}^{n} \left[\frac{2}{A(\eta)}\right]^{1/2} N_j(\xi,\eta) r^{1/2} e^{ikr} \phi_j \qquad (6.43)$$

The shape functions for the mapped wave infinite element become

$$S_j(\xi,\eta) = \left[\frac{2}{A(\eta)}\right]^{1/2} r^{1/2} N_j(\xi,\eta) e^{ikr} \qquad (6.44)$$

In terms of ξ and η the shape function and the derivatives simply to become

$$S_j(\xi,\eta) = \left[\frac{2}{1-\xi}\right]^{1/2} N_j(\xi,\eta) e^{\frac{ikA(\eta)}{1-\xi}} \qquad (6.45)$$

$$\frac{\partial S_j(\xi,\eta)}{\partial \xi} = \left[\frac{2}{1-\xi}\right]^{1/2} \left[\frac{\partial N_j(\xi,\eta)}{\partial \xi} + \frac{N_j(\xi,\eta)}{2(1-\xi)} + \frac{ikA(\eta)}{(1-\xi)^2} N_j(\xi,\eta)\right] e^{\frac{ikA(\eta)}{1-\xi}} \qquad (6.46)$$

$$\frac{\partial S_j(\xi,\eta)}{\partial \eta} = \left[\frac{2}{1-\xi}\right]^{1/2} \left[\frac{\partial N_j(\xi,\eta)}{\partial \eta} + \frac{ik}{1-\xi} N_j(\xi,\eta) \frac{\partial A(\eta)}{\partial \eta}\right] e^{\frac{ikA(\eta)}{1-\xi}} \qquad (6.47)$$

$A(\eta)$ varies with respect to η, the local co-ordinate corresponding to the angular direction in the global co-ordinate, and is independent of ξ, the local co-ordinate corresponding to the radial direction in the global co-ordinate. For the current case, in order to keep

the wave directions defined on the finite/infinite element interface strictly radial, $A(\eta)$ is evaluated on each radial line of a value of η using the global co-ordinates (x, y) of every point on the inner edge.

$$A(\eta) = 2\left\{(x - x_0)^2 + (y - y_0)^2\right\}^{1/2} \tag{6.48}$$

$$\frac{\partial A(\eta)}{\partial \eta} = \frac{2}{\{(x - x_0)^2 + (y - y_0)^2\}^{1/2}} \left(x\frac{\partial x}{\partial \eta} + y\frac{\partial y}{\partial \eta}\right) \tag{6.49}$$

where

$$x = \sum_{j=1}^{n} \mathcal{M}_j(-1, \eta)x_j \tag{6.50}$$

$$y = \sum_{j=1}^{n} \mathcal{M}_j(-1, \eta)y_j \tag{6.51}$$

η derivatives of x and y are components of the Jacobian matrix given by Equation (6.17).

6.5   Element Matrix

The element matrix formulation for a mapped wave infinite element is similar to that of a finite element shown in Chapter 3. It should be noted that the mapping functions are used to obtain the Jacobian matrix instead of the shape functions. The formulation is basically the same for the infinite elements to be coupled with standard finite elements and those to be coupled with special wave finite elements. The only difference comes from the shape functions and the derivatives shown in Equations (6.35)-(6.38) and (6.45)-(6.47) due to the existence of the phase correction term.

6.5.1   The Weighted Residual Method

In the same way as the finite element formulation, the weak form for infinite elements is obtained. Firstly by applying the weighted residual method to the Helmholtz equation given by Equation (2.3), we obtain,

$$\int_{\Omega} W(\nabla^2\phi + k^2\phi)d\Omega = 0 \tag{6.52}$$

95

where Ω is the domain considered and W is the weighting function. Using Green's second identity on Equation (6.52) gives the weak form

$$\int_\Omega (\nabla W \nabla \phi - k^2 W \phi) d\Omega - \int_\Gamma W \nabla \phi \cdot \mathbf{n} d\Gamma = 0 \qquad (6.53)$$

where Γ is the boundary enclosing the domain Ω. The natural boundary condition arising from this weak form is

$$\nabla \phi \cdot \mathbf{n} = 0 \qquad \text{on } \Gamma \qquad (6.54)$$

Because only the radiated or scattered wave, which satisfies the Sommerfeld condition at infinity, is dealt with as ϕ in the infinite element formulation in this chapter, the boundary condition given by Equation (6.54) is not suitable. Therefore it is necessary to add the terms to give appropriate boundary conditions. It is the Neumann boundary conditions given by

$$\nabla \phi \cdot \mathbf{n} = \bar{u} \qquad (6.55)$$

where $\bar{u}$ is the given value of normal derivative of the radiated or scattered potential. This boundary condition is applied to the boundary Γ_n, the surface of radiating or scattering objects.

In the mapped wave infinite element formulation, due to the decay characteristics of the amplitude along the distance from the 'pole' given to the shape functions, the radiation condition is automatically satisfied at infinity. However, applying the radiation condition on the outer boundary Γ_∞ by the form

$$\nabla \phi \cdot \mathbf{n} - ik\phi = 0 \qquad \text{on } \Gamma_\infty \qquad (6.56)$$

clarify the evaluation of the terms at infinity as explained below.

By including these boundary conditions, given by Equations (6.55) and (6.56), the weighted residual equation for infinite elements takes the form

$$\int_\Omega W \left(\nabla^2 \phi + k^2 \phi \right) d\Omega + \int_{\Gamma_n} W \left(\bar{u} - \nabla \phi \cdot \mathbf{n} \right) d\Gamma + \int_{\Gamma_\infty} W \left(ik\phi - \nabla \phi \cdot \mathbf{n} \right) d\Gamma = 0 \quad (6.57)$$

The weak form then becomes

$$\int_\Omega \left(\nabla W \nabla \phi - k^2 W \phi \right) d\Omega - \int_{\Gamma_\infty} ik W \phi d\Gamma = \int_{\Gamma_n} W \bar{u} d\Gamma \qquad (6.58)$$

96

where the domain Ω has an infinite extent and the boundary Γ_∞ is at infinity.

Using shape functions given by Equation (6.35) or Equation (6.44) for infinite elements, derived in the previous sections, results in giving a term of undefined integral

$$\int_B^\infty e^{iu}du \qquad (6.59)$$

arising from the integral over the domain Ω, where B is a constant. This integral is undefined because of the oscillating value at the upper limit of the integral. However, another term arising from the integral over the boundary at infinity Γ_∞ cancels out this undefined oscillating value. The integral over the boundary at infinity results in this cancelling term and the terms which become zero as r goes to infinity. Although this was uncertain in the first paper on mapped wave infinite elements by Zienkiewicz *et al.* [93], it was first clarified by Astley *et al.* [9] for a spherically symmetric case in three dimensions by forming the problem in a finite domain and looking at the limiting case as the domain extends to infinity. Then Bettess considered several special cases in one, two and three dimensions in Appendices D and E in reference [24]. The matter was also considered by Burnett [29] and Gerdes [48].

Therefore, in forming the element matrix, it is possible to set both the undefined oscillating term mentioned above and the integral over the boundary at infinity to zero, and only the remaining terms from the 'stiffness' part of the residual statement can be necessary to be considered. The special integration scheme for the evaluation of these terms in this way are developed and listed in Zienkiewicz *et al.* [93], and available on a diskette with Bettess [24]. This special integration scheme is specialised for the mapped wave infinite element using the radial wave from the 'pole'.

6.5.2 Mapped Wave Infinite Element Model

The domain Ω is divided into n-node infinite elements. The unknown function ϕ within each element is approximated using the shape functions S_j and the nodal values ϕ_j.

$$\phi = \sum_{j=1}^n S_j \phi_j = [S]\{\phi\} \qquad (6.60)$$

We put a finite set of approximate functions for the weighting function W

$$W = \sum_{j=1}^{n} w_j a_j = [w]\{\delta a\} \tag{6.61}$$

where a_j are arbitrary parameters.

Applying Bubnov-Galerkin method to the present case, i.e., employing the weighting functions of the same form of the shape functions

$$w_j = S_j \tag{6.62}$$

leads to the unconjugated infinite elements.

Comparison of various formulations of infinite elements by Gerdes [48] and Shirron and Babuška [87] showed the results that the unconjugated elements act as a highly accurate boundary condition on the inner boundary of infinite elements but fail to provide an accurate approximation of the solution in the exterior domain, i.e., inside the infinite elements. Therefore in this work the domain in the near field of radiating or scattering objects are discretised by finite elements. Infinite elements are not directly attached to the objects but placed outside the finite element layers. This makes the integral over the boundary Γ_n in Equation (6.58), which gives the Neumann boundary condition on the surface of the radiating or scattering objects, unnecessary in the infinite element formulation dealt with in this thesis. Consequently, the weak form becomes

$$\int_{\Omega} \left(\nabla W \nabla \phi - k^2 W \phi \right) d\Omega - \int_{\Gamma_{\infty}} ik W \phi d\Gamma = 0 \tag{6.63}$$

6.5.3 Element Matrix

By applying the unconjugated mapped wave infinite element model shown above, the weak form given by Equation (6.63) becomes

$$\int_{\Omega} \left([\nabla S]^T [\nabla S] - k^2 [S]^T [S] \right) \{\phi\} d\Omega - ik \int_{\Gamma_{\infty}} [S]^T [S] \{\phi\} d\Gamma = 0 \tag{6.64}$$

Consequently, a set of discrete equations for each element is written by

$$\left[[\mathbf{K}] - k^2 [\mathbf{M}] - ik [\mathbf{C}] \right] \{\phi\} = \{\mathbf{0}\} \tag{6.65}$$

where

$$K_{ij} = \int_{\Omega_e} \nabla S_i \nabla S_j d\Omega \qquad (6.66)$$

$$= \int_{\Omega_e} \left\{ \frac{\partial S_i}{\partial x}\frac{\partial S_j}{\partial x} + \frac{\partial S_i}{\partial y}\frac{\partial S_j}{\partial y} \right\} d\Omega \qquad (6.67)$$

$$M_{ij} = \int_{\Omega_e} S_i S_j d\Omega \qquad (6.68)$$

$$C_{ij} = \int_{\Gamma_\infty} S_i S_j d\Gamma \qquad (6.69)$$

where i and j are integers equal to $1, 2, ..., n$. The dimension of element matrices is $n \times n$.

The global derivatives of the shape functions are obtained by

$$\left\{ \begin{array}{c} \frac{\partial S_i(\xi,\eta)}{\partial x} \\ \frac{\partial S_i(\xi,\eta)}{\partial y} \end{array} \right\} = \left[\begin{array}{cc} \frac{\partial \xi}{\partial x} & \frac{\partial \eta}{\partial x} \\ \frac{\partial \xi}{\partial y} & \frac{\partial \eta}{\partial y} \end{array} \right] \left\{ \begin{array}{c} \frac{\partial S_i(\xi,\eta)}{\partial \xi} \\ \frac{\partial S_i(\xi,\eta)}{\partial \eta} \end{array} \right\} = J^{-1} \left\{ \begin{array}{c} \frac{\partial S_i(\xi,\eta)}{\partial \xi} \\ \frac{\partial S_i(\xi,\eta)}{\partial \eta} \end{array} \right\} \qquad (6.70)$$

where the local derivatives are given by Equations (6.37) and (6.38) or (6.46) and (6.47) depending on the type of the finite elements to be coupled with, and the Jacobian matrix J is given by Equation (6.17).

6.6 Numerical Examples

6.6.1 Hankel Source Problem

(1) Computational Model

In order to test the coupling of the special wave finite and mapped wave infinite elements, a simple problem of radiation from a cylinder, named Hankel Source Problem, was considered. The geometry of the problem is the same as that shown in Figure 2.3.

The problem is that of a circular cylinder of unit radius and infinite length in the domain filled with some medium. When the normal velocity of the surface of the cylinder is uniform, the wave field can be treated as a two dimensional problem in a plane perpendicular to the cylinder axis. The radiated outgoing wave $\phi^r(kr)$ is represented by the Hankel function of the first kind of order zero as shown in Equation (2.37). Suppose the amplitude is unity, it is given by

$$\phi^r(kr) = H_0^{(1)}(kr) \qquad (6.71)$$
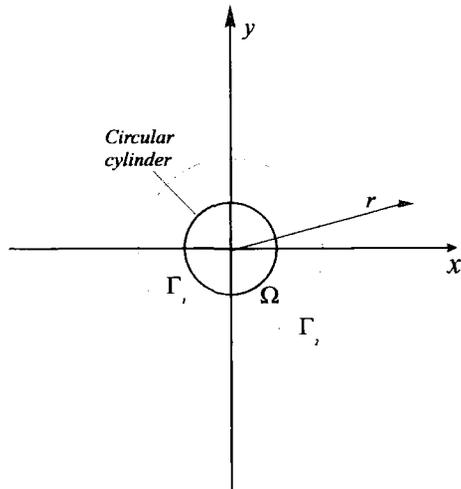
Figure 6.5: Geometry of Hankel source problem in two dimensions.
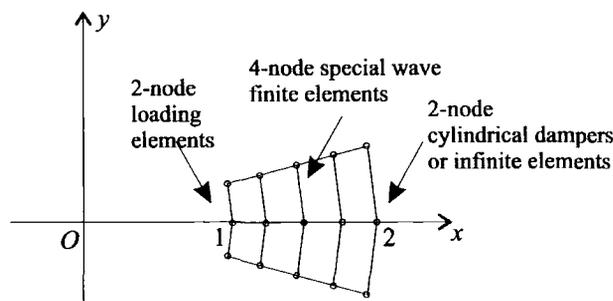
Figure 6.6: Mesh model for Hankel source problem.

The domain considered around the cylinder in two-dimensions is shown in Figure 6.5. The domain between boundaries Γ_1 at $r = 1$ and Γ_2 at $r = 2$ is a finite element domain, and the domain further from Γ_2 at $r = 2$ is modelled by infinite elements, or a damper condition is applied on Γ_2. From the axisymmetric nature of the problem in the two dimensional plane, the domain around the cylinder was modelled by a sectorial mesh bounded by straight radii at $-10°$ and $10°$. The finite/infinite element mesh model is shown in Figure 6.6. The sectorial domain over $1 \le r \le 2$ is divided into 2 sectors of 10 degrees each, and each sector is divided into four 4-node quadrilateral finite elements in the radial direction. On the inner boundary $r = 1$ the normal derivatives of radiated potential were given as the Neumann boundary condition, and on the outer boundary at $r = 2$, 2-node linear mapped wave infinite elements or cylindrical dampers are applied for comparison.

The problem was solved for the wavenumber $k = 4$ and 8. For the nodes in $1 \le r < 2$, 8 equally spaced approximating plane waves are applied. The wave directions are $0°, 45°, \cdots, 315°$, where $0°$ is the radial direction at each node. For the nodes at $r = 2$,

100

single wave in the radial direction at each node is applied. 24 Gauss-Legendre integration points are used in each direction for finite elements, and angular direction for infinite elements.

(2) Results

Figures 6.7 and 6.8 show the numerical results of the potential using finite elements and infinite elements or cylindrical dampers with analytical solution, and the difference between numerical results and the analytical solution, respectively, as a function of the distance from the axis of the cylinder, for the case of $k = 4$. Figures 6.9 and 6.10 show the potential and the error respectively for the case of $k = 8$.

The damper results are good close to the cylinder, but at the far field boundary diverge from the analytical solution. This is probably because at this boundary the field is only represented by a single radial wave. By contrast the infinite element errors remain at about 10^{-4} throughout the domain. Overall the results indicate that the special wave finite element and infinite element combination works well. Results were obtained for higher values of k, and were broadly similar, so have not been shown.
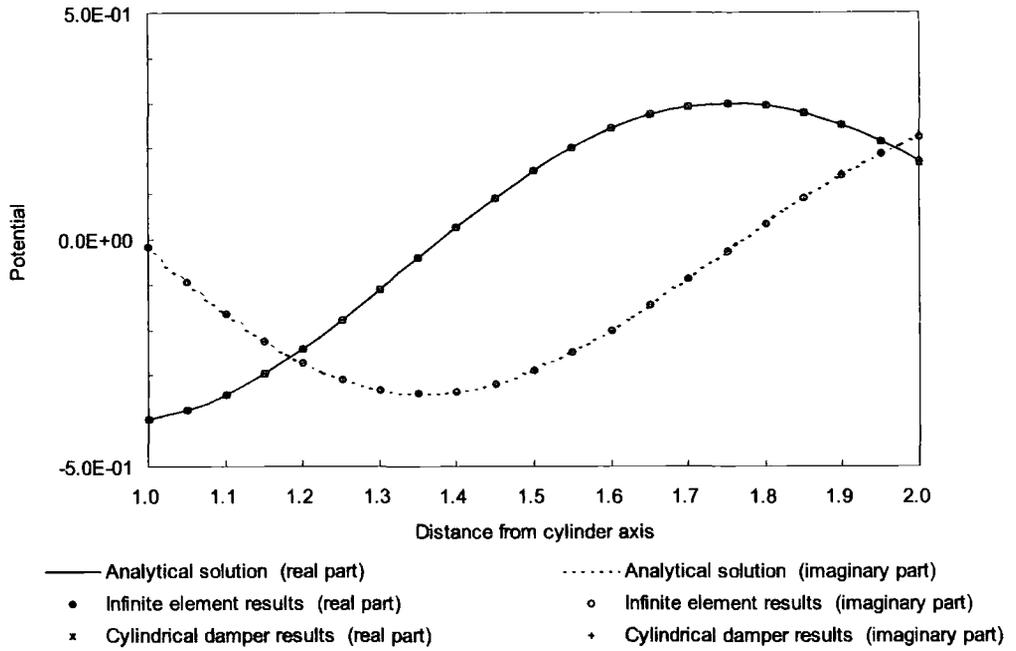
Figure 6.7: Real and imaginary parts of potentials of Hankel source problem as function of distance from cylinder axis, for $k = 4$.
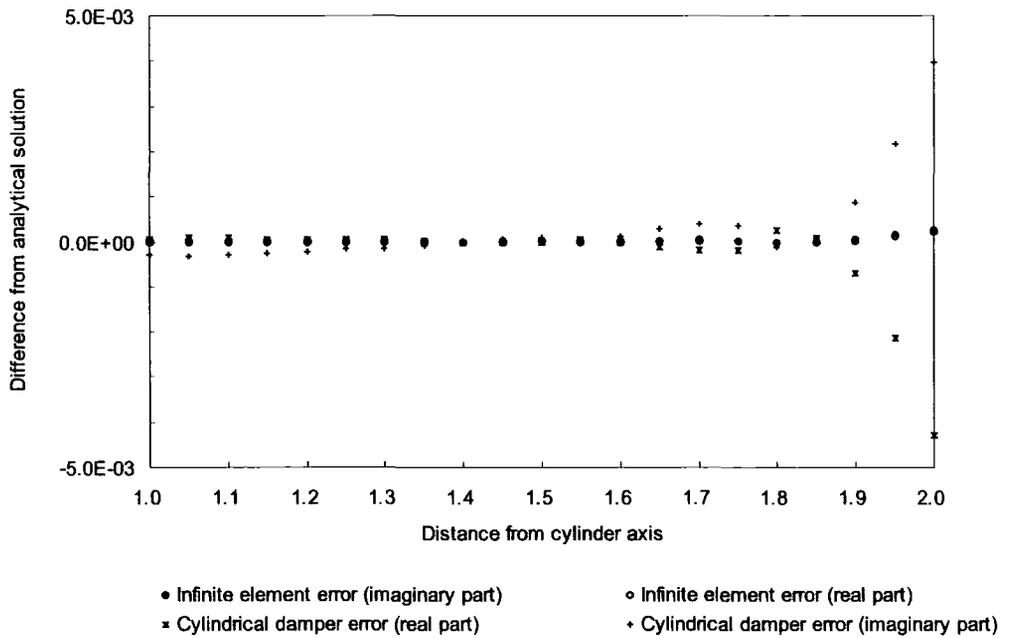
Figure 6.8: Difference from analytical solution in real and imaginary parts of potential of Hankel source problem using infinite elements or dampers as function of distance from cylinder axis, for $k = 4$.
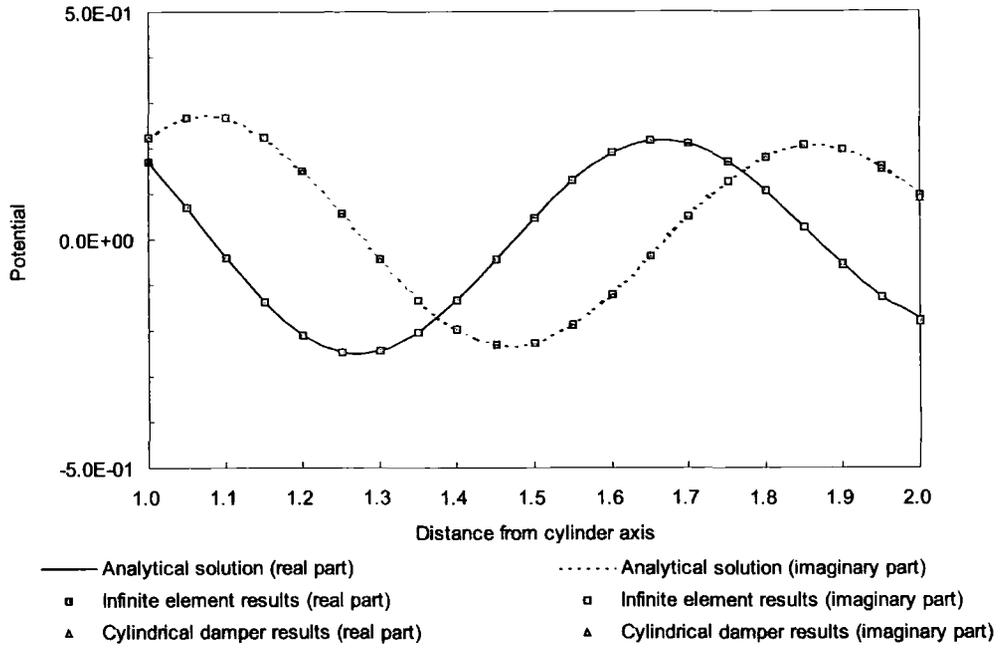
Figure 6.9: Real and imaginary parts of potentials of Hankel source problem as function of distance from cylinder axis, for $k = 8$.
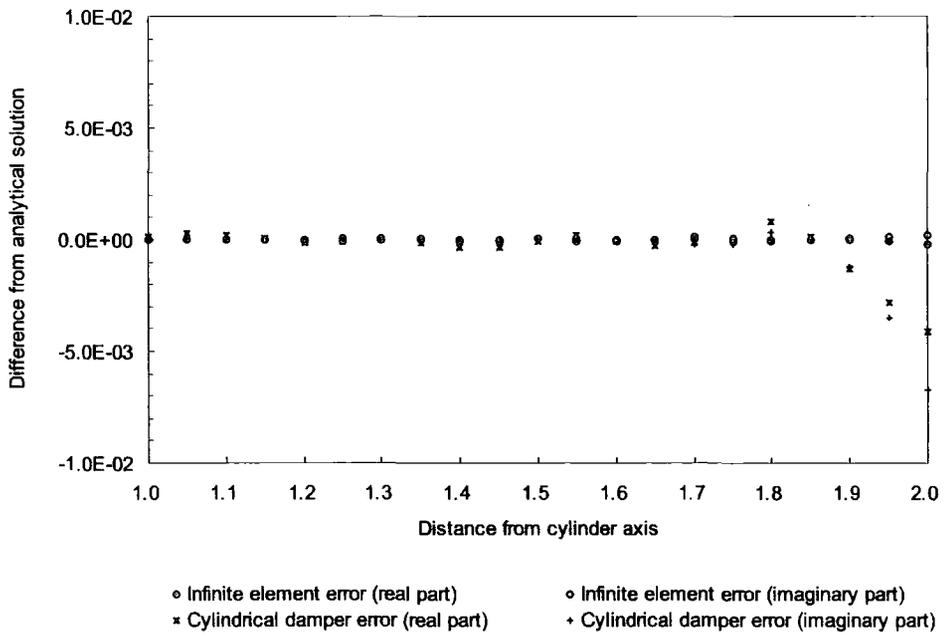
Figure 6.10: Difference from analytical solution in real and imaginary parts of potential of Hankel source problem using infinite elements or dampers as function of distance from cylinder axis, for $k = 8$.

6.6.2 Scattering Problem

(1) Computational Model
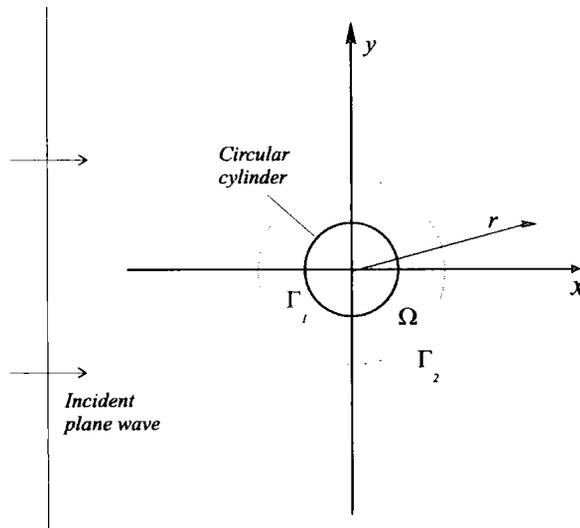
Figure 6.11: Geometry of scattering problem in two dimensions.
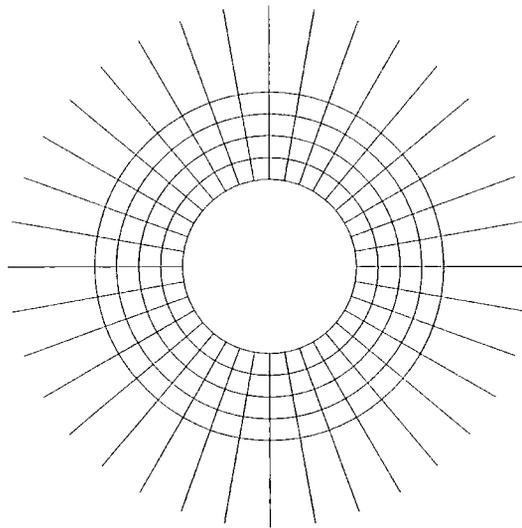
Figure 6.12: Finite/inifnite element mesh model for scattering problem. Inner radius 1, radius of finite/infinite element interface 2.

The problem of plane wave scattered by a circular cylinder was also considered. The problem is that of a circular cylinder of unit radius and infinite length, and the plane wave of unit amplitude is incident perpendicular to the cylinder axis from the negative x-direction. Again, the wave field can be treated as a two dimensional problem in a plane perpendicular to the cylinder axis.

The domain considered is shown in Figure 6.11, and the finite and infinite element mesh model is shown in Figure 6.12. The cylindrical domain over $1 \leq r \leq 2$ is divided

into 36 sectors of 10 degrees each, and each sector is divided into four 4-node quadrilateral elements in the radial direction. On the inner boundary $r = 1$ the normal derivatives of scattered potential were given as the Neumann boundary condition, and on the outer boundary at $r = 2$, 2-node linear mapped wave infinite elements or cylindrical dampers are applied for comparison.

The problem was solved for the wavenumber $k = 4$ and 8. For the nodes in $1 \leq r < 2$, 8 equally spaced approximating plane waves are applied. The directions are $0°, 45°, \cdots, 315°$, where $0°$ is the radial direction at each node. For the nodes at $r = 2$, one plane wave in the radial direction at each node is applied. 24 Gauss-Legendre integration points are used in each direction for finite elements, and the angular direction for infinite elements.

(2) Results

Figures 6.13 and 6.14 show the numerical results of the scattered potential with analytical solution, and the difference between numerical results and the analytical solution, respectively, as a function of the angle around the cylinder, for the case of $k = 4$. In the same way, Figures 6.15 and 6.16 show the scattered potential and the error respectively for the case of $k = 8$.

For the case of $k = 4$, the infinite element errors remain at about or less than 10^{-3}. On the other hand the damper errors are larger than the infinite element errors for almost all the angles. The maximum errors for the dampers are about 5×10^{-2} and located between $0°$ and $90°$. For the case of $k = 8$, both the infinite element errors and the damper errors are large compared to the previous case. This may be because of the small number of approximating waves. For both cases of $k = 4$ and 8, eight approximating plane waves were used in the special wave finite elements, which may not be enough to model the scattered field for the higher wavenumber of $k = 8$. However the infinite element errors still remain at about the same or less than the damper errors.

The mapped wave infinite element used here are the simplest linear one, which has the same number of degrees of freedom as the damper element used here. It is expected that the better accuracy can be obtained using infinite elements of higher order in the radial direction. But it is shown that even the linear infinite elements work more accurately with the special wave finite elements than cylindrical dampers.

105
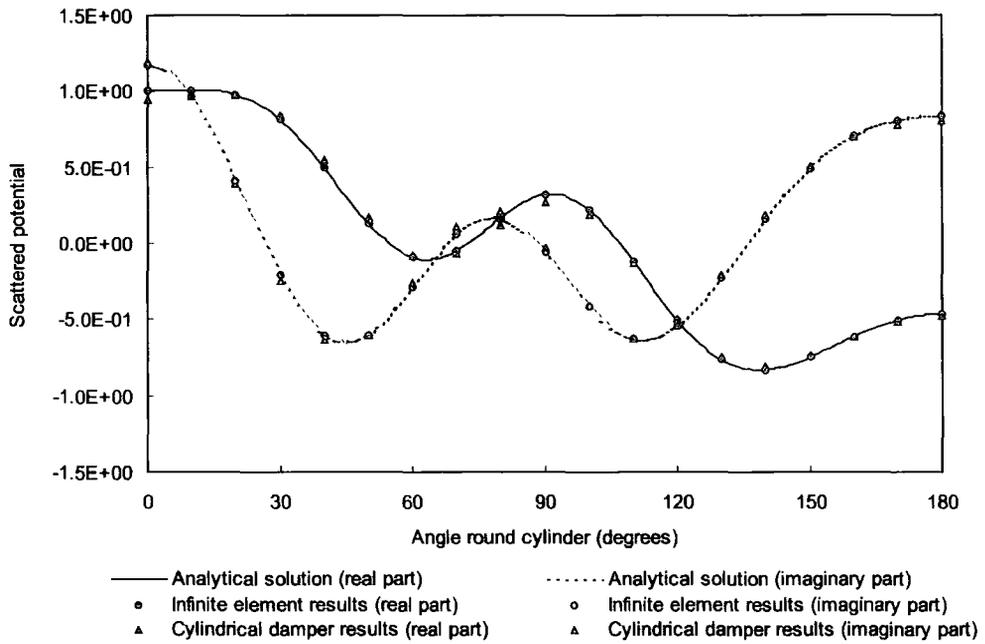
Figure 6.13: Real and imaginary parts of scattered potentials along the circumference of the cylinder, for $k = 4$.
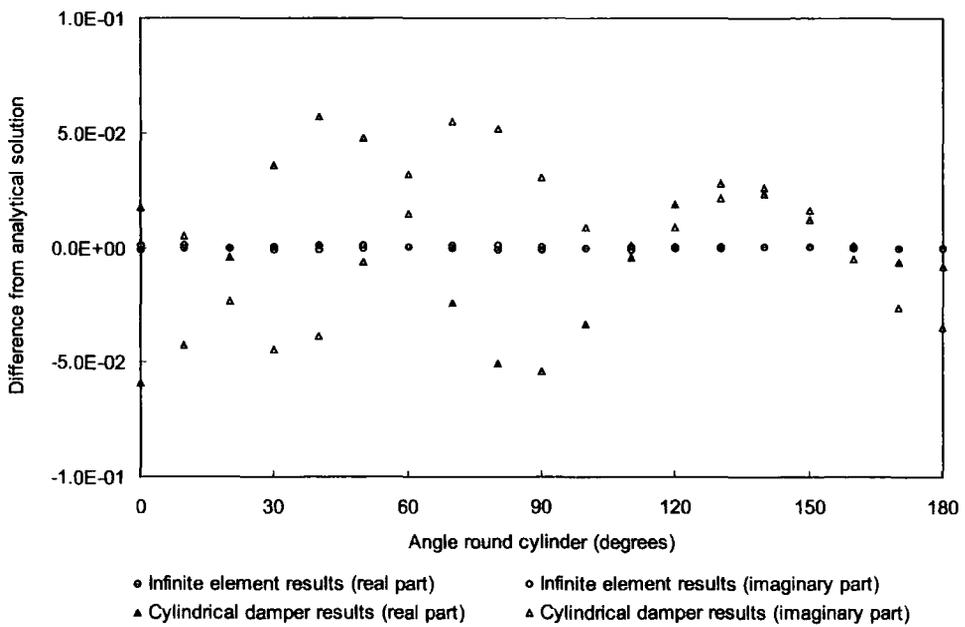
Figure 6.14: Difference from analytical solution in real and imaginary parts of scattered potential using infinite elements or dampers along circumference of cylinder, for $k = 4$.
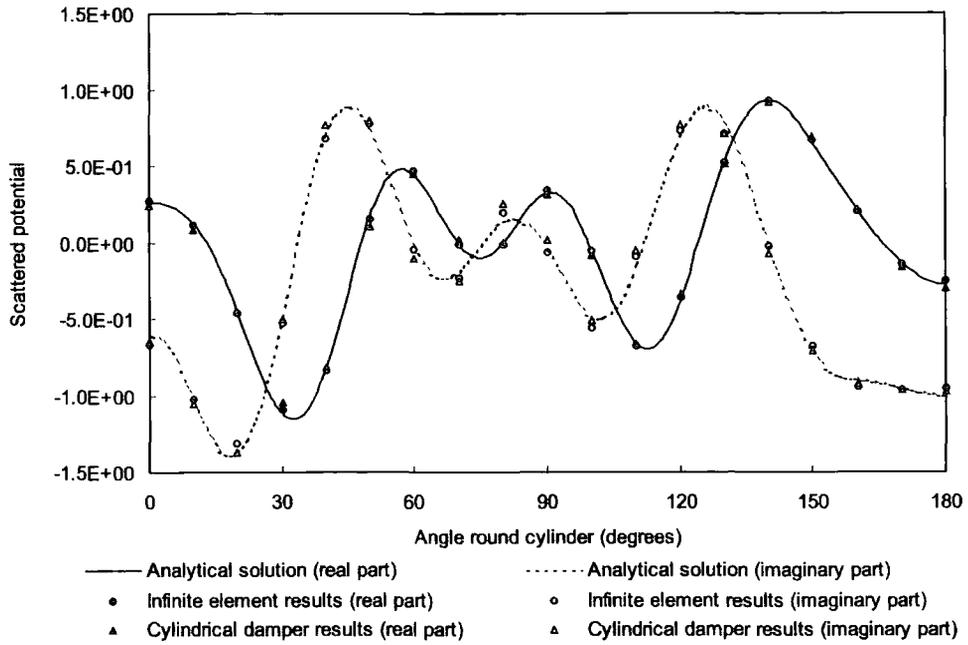
Figure 6.15: Real and imaginary parts of scattered potentials along the circumference of the cylinder, for $k = 8$.
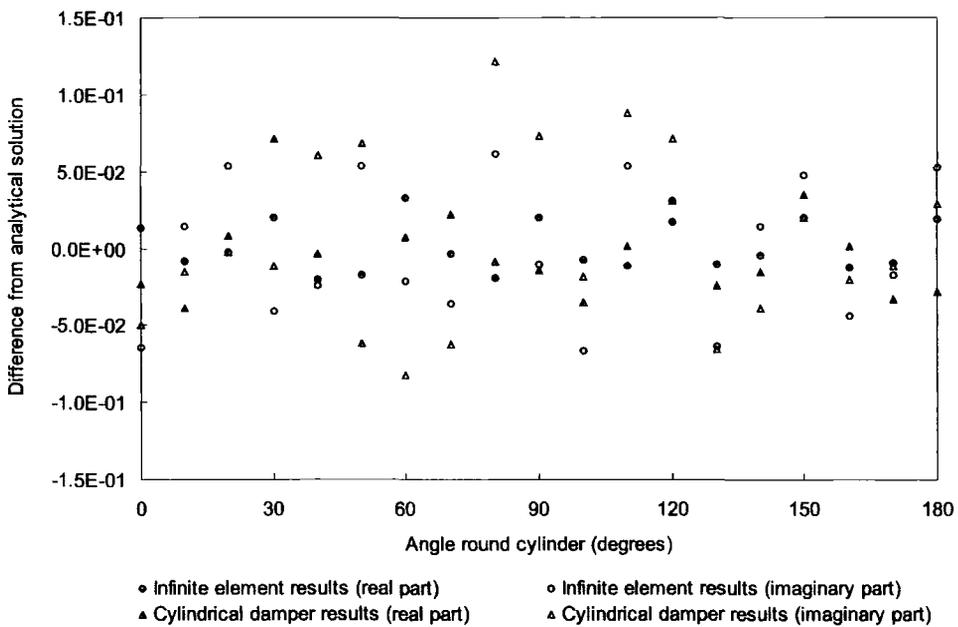
Figure 6.16: Difference from analytical solution in real and imaginary parts of scattered potential using infinite elements or dampers along the circumference of the cylinder, for $k = 8$.

6.7 Conclusions

The formulation of the conventional mapped wave infinite elements for the Helmholtz equation in unbounded domain was described, and then the theory of coupling of them to special wave finite elements was discussed. The applications to the Hankel source problem and a problem of plane wave scattered by a circular cylinder were presented. Special wave finite elements allow an element to contain many wavelengths rather than having many finite elements per wavelength, which should be a great advantage for short wave problems. Mapped wave infinite elements can be applied to boundaries of arbitrary shape, although presently they can have only a single radial wave direction. The wave direction on the finite/infinite element interface and within the mapped wave infinite elements were forced to be strictly radial from the 'pole' of the infinite elements to ensure compatibility between the two different types of elements. The main conclusion of this chapter is that the mapped wave infinite elements can be successfully coupled with the special wave finite elements to achieve solutions to wave problems in unbounded domain of high accuracy.

It can be conjectured that the special wave finite elements could also be combined with other, more recent wave infinite elements which have more general mappings, due to Astley [14], Cremers *et al.* [40, 39], Burnett and Holford [30] and others. It would be necessary to match the directions of wave propagation at the special wave finite/infinite element interface.

As presented in this chapter, the mapped wave infinite elements enable us to deal with wave problems without truncation of the unbounded domain and are easily implemented together with special wave finite elements as well as with standard finite elements. If the mapped wave infinite elements which include multiple waves propagating in different directions like special wave finite elements are developed, they become a straightforward extension of the special wave finite elements for unbounded domain problems. This will be discussed in the next chapter.

Chapter 7

Special Wave Infinite Elements

In this chapter, the formulation of the special wave infinite elements is developed [91]. The special wave infinite elements are the new concept of mapped wave infinite elements in which multiple waves propagating in different directions are considered. The conventional mapped wave infinite elements, in which only a single wave propagating in the radial direction is allowed, are successfully coupled to the special wave finite elements in Chapter 6. The special wave infinite elements should, however, be a more straightforward extension for use with the special wave finite elements for unbounded problems.

Because the shape functions of the special wave infinite elements are defined so as to satisfy the radiation condition, the radiated or scattered potential is dealt with in the formulations in this chapter.

7.1 Special Wave Infinite Element Formulation

7.1.1 Non-radial Wave in Infinite Elements

(a) Wave Function

In the conventional mapped wave infinite element formulation when coupled to the special wave finite elements as discussed in Chapter 6, the function

$$\left[\frac{2}{A(\eta)}\right]^{1/2} r^{1/2} e^{ikr} \tag{7.1}$$

is multiplied by the standard polynomial shape functions, where $A(\eta)$ is twice the distance between 'pole' and the inner edge of the infinite element. The function $r^{1/2} \exp{(ikr)}$
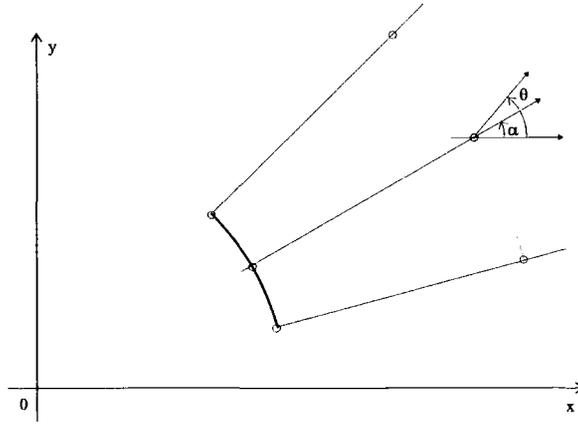
Figure 7.1: Definition of angles of radial direction and non-radial wave direction.

gives shape functions suitable behaviour of a wave propagating in the radial direction in two dimensions. The coefficient $[2/A(\eta)]^{1/2}$ normalises the amplitude of the shape functions so as to ensure compatibility on the finite/infinite element interface. Because the wave direction is strictly forced to be radial on the finite/infinite element interface, the compatibility of the phase is automatically satisfied.

To consider a wave which propagates in a direction at angle θ, which can be different from the radial direction, let us introduce the position vector $\mathbf{r}$ and the wavenumber vector $\mathbf{k}_\theta$. As dealt with in Chapter 3 for the special wave finite elements, the position vector $\mathbf{r}$ is given by

$$\mathbf{r} = x\,\mathbf{e_x} + y\,\mathbf{e_y} = r\,(\cos\alpha\,\mathbf{e_x} + \sin\alpha\,\mathbf{e_y}) \tag{7.2}$$

where x, y are the global co-ordinates, and $\mathbf{e_x}$, $\mathbf{e_y}$ are the unit vectors in the x and y directions, respectively. α is the angle of the radial direction measured from the positive x direction in the global co-ordinates. The wavenumber vector $\mathbf{k}_\theta$ is given by

$$\mathbf{k}_\theta = k(\cos\theta\,\mathbf{e_x} + \sin\theta\,\mathbf{e_y}) \tag{7.3}$$

Thus the term which supplies the wave behaviour to the shape functions takes the form

$$r^{1/2}e^{i\mathbf{k}_\theta\cdot\mathbf{r}} = r^{1/2}e^{ik(x\cos\theta+y\sin\theta)} = r^{1/2}e^{ikr\cos(\theta-\alpha)} \tag{7.4}$$

This expression is justified to some extent by the Hankel function series for exterior wave solutions.

(b) Amplitude Correction Term

The amplitude correction term when coupled with the special wave finite elements is

$$\left[\frac{2}{A(\eta)}\right]^{1/2} \tag{7.5}$$

This is the same as that for the conventional mapped wave infinite elements as the amplitude correction term $r^{1/2}$ is the same.

(c) Phase Correction Term

When only a single wave direction is defined at the nodes on the finite/infinite element interface for both types of elements and the directions are the same for finite and infinite elements, the compatibility of the phase is automatically satisfied, because the shape functions of the elements of both types include the same term $\exp\left[ik(x\cos\theta + y\sin\theta)\right]$. Therefore the phase correction term is no longer needed.

(d) New Shape Functions and Potential Expression

The suitable new shape functions thus take the form

$$N_j(\xi,\eta)\left[\frac{2}{A(\eta)}\right]^{1/2} r^{1/2}e^{ik(x\cos\theta + y\sin\theta)} \tag{7.6}$$

and with these new shape functions, the variables are no longer the nodal values but those corresponding to the complex amplitudes of the wave propagating at angle θ at node j. Let us denote them by B_j where $j = 1, \cdots, n$. The expression for the potential ϕ thus becomes

$$\phi = \sum_{j=1}^{n} N_j(\xi,\eta)\left[\frac{2}{A(\eta)}\right]^{1/2} r^{1/2}e^{ik(x\cos\theta + y\sin\theta)} B_j \tag{7.7}$$

The local functions ϕ_j, which correspond to the nodal values in the standard finite element formulation, are given by

$$\phi_j = \left[\frac{2}{A(\eta)}\right]^{1/2} r^{1/2}e^{ik(x\cos\theta + y\sin\theta)} B_j \tag{7.8}$$

The formulation becomes that of the conventional mapped wave infinite elements when the angle $\theta = \alpha$.

111

7.1.2 Multiple Waves in Infinite Elements

(a) Wave Function

To extend the formulation to use multiple waves which propagate in different directions, like the special wave finite elements, the local functions ϕ_j is given as the summation of the wave components propagating in each direction by

$$\phi_j = \sum_{l=1}^{m_j} \left[\frac{2}{A(\eta)} \right]^{1/2} r^{1/2} e^{ik(x \cos \theta_j^l + y \sin \theta_j^l)} B_j^l \tag{7.9}$$

where m_j is the number of the waves associated with node j, and θ_j^l and B_j^l are the angle of the direction and the amplitude of the l-th wave, respectively. B_j^l corresponds to A_j^l in the special wave finite element formulation in Chapter 3. The wave functions for each direction θ_j^l have the form

$$r^{1/2} e^{ik(x \cos \theta_j^l + y \sin \theta_j^l)} \tag{7.10}$$

(b) Amplitude Correction Term

The amplitude correction term is again

$$\left[\frac{2}{A(\eta)} \right]^{1/2} \tag{7.11}$$

This is the same as that for the conventional mapped wave infinite elements as the amplitude correction term $r^{1/2}$ is the same.

(c) Phase Correction Term

When the number and the directions of the waves given for finite and infinite elements at the common nodes on the finite/infinite element interface are the same, A_j^l for the finite elements and B_j^l for the infinite elements must be the same. The compatibility of the phase regarding each wave direction is automatically satisfied because the elements of both types include the same term of $\exp[ik(x \cos \theta_j^l + y \sin \theta_j^l)]$. Therefore, as before, the phase correction term is no longer needed.

(d) New Shape Functions and Potential Expression

Consequently the special shape functions $S_j^l(\xi, \eta)$ are of the form

$$S_j^l(\xi, \eta) = \left[\frac{2}{A(\eta)}\right]^{1/2} N_j(\xi, \eta) r^{1/2} e^{ik(x \cos \theta_j^l + y \sin \theta_j^l)} \tag{7.12}$$

which can be also written

$$S_j^l(\xi, \eta) = \left[\frac{2}{A(\eta)}\right]^{1/2} N_j(\xi, \eta) r^{1/2} e^{ikr \cos(\theta_j^l - \alpha)} \tag{7.13}$$

And the potential ϕ is given by

$$\phi = \sum_{j=1}^{n} \sum_{l=1}^{m_j} N_j(\xi, \eta) \left[\frac{2}{A(\eta)}\right]^{1/2} r^{1/2} e^{ik(x \cos \theta_j^l + y \sin \theta_j^l)} B_j^l \tag{7.14}$$

This can be written in terms of the special shape functions S_j^l and the new nodal variables B_j^l in the form

$$\phi = \sum_{j=1}^{n} \sum_{l=1}^{m_j} S_j^l B_j^l = [\mathcal{S}]\{\mathcal{B}\} = [\mathcal{S}_1 \quad \mathcal{S}_2 \quad \cdots \quad \mathcal{S}_n] \{\mathcal{B}_1 \quad \mathcal{B}_2 \quad \cdots \quad \mathcal{B}_n\}^T \tag{7.15}$$

where the row matrices of the new shape functions corresponding to the node j are

$$\mathcal{S}_j = \begin{bmatrix} S_j^1 & S_j^2 & \cdots & S_j^n \end{bmatrix} \tag{7.16}$$

$$\mathcal{B}_j = \left\{ B_j^1 \quad B_j^2 \quad \cdots \quad B_j^n \right\} \tag{7.17}$$

In terms of ξ and η, the shape functions and the derivatives take the forms of

$$S_j^l(\xi, \eta) = \left[\frac{2}{1-\xi}\right]^{1/2} N_j(\xi, \eta) e^{\frac{ikA(\eta)}{1-\xi} \cos(\theta_j^l - \alpha)} \tag{7.18}$$

$$\frac{\partial S_j^l(\xi, \eta)}{\partial \xi} = \left[\frac{2}{1-\xi}\right]^{1/2} \left[\frac{\partial N_j(\xi, \eta)}{\partial \xi} + \frac{N_j(\xi, \eta)}{2(1-\xi)} + \frac{ikA(\eta)}{(1-\xi)^2} \cos(\theta_j^l - \alpha) N_j(\xi, \eta)\right]$$
$$\times e^{\frac{ikA(\eta)}{1-\xi} \cos(\theta_j^l - \alpha)} \tag{7.19}$$

$$\frac{\partial S_j^l(\xi, \eta)}{\partial \eta} = \left[\frac{2}{1-\xi}\right]^{1/2} \left[\frac{\partial N_j(\xi, \eta)}{\partial \eta} + \frac{ik \cos(\theta_j^l - \alpha)}{1-\xi} \frac{\partial A(\eta)}{\partial \eta} N_j(\xi, \eta)\right]$$
$$\times e^{\frac{ikA(\eta)}{1-\xi} \cos(\theta_j^l - \alpha)} \tag{7.20}$$

Finite element   *Infinite element*
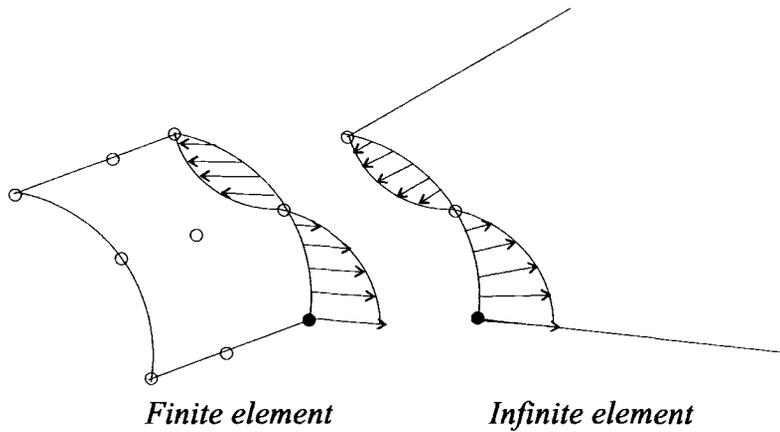
Figure 7.2: Incompatible wave directions between finite and infinite elements by normal definition.

Finite element   *Infinite element*
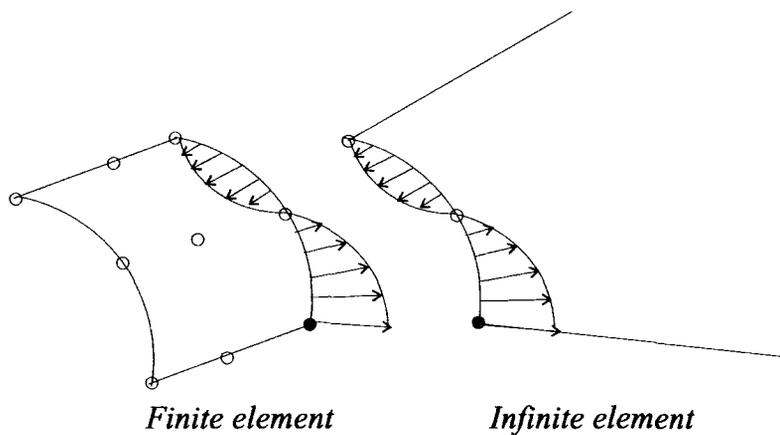
Figure 7.3: Wave directions forced to be compatible on finite/infinite element interface.

The formulation of the conventional mapped wave infinite elements can be considered as the special case where $m_j = 1$ and the angle $\theta_j^l = \alpha$ for all nodes.

7.2 Compatibility of Wave Directions between Finite and Infinite Elements

The new shape functions and the derivatives given by Equation (7.18)-(7.20) are based on the assumption that the number and the directions of the waves given for finite and infinite elements at the common nodes on the finite/infinite element interface are the same. Moreover, special attention is required to deal with wave directions of these two types of elements to ensure continuity on the interface.

The wave directions are normally globally constant between nodes within a special wave finite element but the radial direction varies between nodes within a mapped wave

114

infinite element. Figure 7.2 shows a possible discrepancy of the wave directions between two different element types included in the shape functions defined at the common nodes indicated by closed circle. This discrepancy leads to the incompatibility of the wave directions between nodes of the finite/infinite element interface. This problem was discussed in Chapter 6 for the case where the wave on the interface is restricted to be only a single radial wave for the coupling of the conventional mapped wave infinite elements to the special wave finite elements, where the waves associated with nodes on the interface are forced to be strictly radial for both types of elements in order to eliminate this internode incompatibility.

In the same way, throughout in this Chapter, all wave directions are forced to vary so that the relative angles from the radial direction are kept to be the values specified on the finite/infinite element interface and within infinite elements, as shown in Figure 7.3.

7.3 Element Matrix

The element matrix formulation for a special wave infinite element is basically the same as that of the conventional mapped wave infinite element presented in Chapter 6.

The weak form is

$$\int_{\Omega} \left(\nabla W \nabla \phi - k^2 W \phi \right) d\Omega - \int_{\Gamma_\infty} ik W \phi d\Gamma = 0 \qquad (7.21)$$

where the domain Ω has an infinite extent and the boundary Γ_∞ is at infinity. W is the weighting function and k is the wavenumber.

By using the Bubnov-Galerkin method, a finite set of functions for the weighting functions is chosen to be the same as the shape functions. Therefore the weak form leads to a discrete set of equations for the element

$$\int_{\Omega} \left([\nabla \mathcal{S}]^T [\nabla S] - k^2 [\mathcal{S}]^T [\mathcal{S}] \right) \{ \mathcal{B} \} d\Omega - ik \int_{\Gamma_\infty} [\mathcal{S}]^T [\mathcal{S}] \{ \mathcal{B} \} d\Gamma = 0 \qquad (7.22)$$

Consequently, a set of discrete equations for each element is written by

$$\left[[\mathbf{K}] - k^2 [\mathbf{M}] - ik [\mathbf{C}] \right] \{ \mathcal{B} \} = \{ \mathbf{0} \} \qquad (7.23)$$

where

$$K_{ij} = \int_{\Omega_e} \nabla S_i^m \nabla S_j^l d\Omega \tag{7.24}$$

$$= \int_{\Omega_e} \left\{ \frac{\partial S_i^m}{\partial x} \frac{\partial S_j^l}{\partial x} + \frac{\partial S_i^m}{\partial y} \frac{\partial S_j^l}{\partial y} \right\} d\Omega \tag{7.25}$$

$$M_{ij} = \int_{\Omega_e} S_i^m S_j^l d\Omega \tag{7.26}$$

$$C_{ij} = \int_{\Gamma_\infty} S_i^m S_j^l d\Gamma \tag{7.27}$$

where i and j are integers corresponding to the m-th wave at node i and the l-th wave at node j, respectively, and the relations are given by

$$i = \sum_{\ell=1}^{i-1} m_\ell + m \tag{7.28}$$

$$j = \sum_{\ell=1}^{j-1} m_\ell + l \tag{7.29}$$

which are equal to $1, 2, ..., n_p$ and

$$n_p = \sum_{\ell=1}^{n} m_\ell \tag{7.30}$$

is the total degree of freedom of the element. m_ℓ is the number of waves at node ℓ. The dimension of the element matrix therefore becomes $n_p \times n_p$.

7.4 Undefined Oscillatory Terms

The 'undefined' oscillatory terms arise in each integrals consisting of the element matrix given by Equations (7.24)-(7.27). These terms are theoretically 'undefined' because of the upper limit of the integration $\xi = 1$, which corresponds to $r = \infty$, however, they cancel out each other, as discussed in Chapter 6. This is taken into account in the special integration scheme by Zienkiewicz *et al.* [93] for the conventional mapped wave infinite elements.

On the other hand, in forming the element matrix by Gauss-Legendre integration scheme, it is impossible to integrate the infinite domain. Therefore it is necessary to consider a sufficiently large area of an element and to apply sufficient integration points to integrate the area accurately. Because the upper limit of the integration with respect to r becomes not the infinity but a finite value, the 'undefined' oscillatory terms are no longer 'undefined' but can be numerically evaluated. These terms are included in the numerically

evaluated values of each of the 'stiffness', 'mass' and 'damper' matrices, and cancel out by summing up all these element matrices.

The 'damper' term of the element matrix shows the radiation condition is applied on the outer boundary Γ_∞, which needs to be replaced by the boundary Γ_R at a finite distance R. Although the radiation condition is automatically satisfied at infinity because of the decay behaviour along the distance of the shape functions as explained in Chapter 6, it is not clear when the element area is truncated. Therefore the application of the radiation condition is necessary in the formulation to avoid unnecessary reflection.

When the infinite element area is truncated by the outer boundary Γ_R instead of Γ_∞, the element matrix is given by

$$\mathcal{K}_{ij}^{IE} \simeq \int_{\Omega_R} \left(\nabla S_i^m \nabla S_j^l - k^2 S_i^m S_j^l \right) d\Omega - ik \int_{\Gamma_R} S_i^m S_j^l d\Gamma \tag{7.31}$$

where Ω_R is the truncated finite area of the element. In terms of the local co-ordinates ξ, η, it takes the form

$$\mathcal{K}_{ij}^{IE} \simeq \int_{-1}^{1} \int_{-1}^{\xi_R} \left(\nabla S_i^m \nabla S_j^l - k^2 S_i^m S_j^l \right) |J| d\xi d\eta - ik \int_{-1}^{1} S_i^m S_j^l \left(\frac{\partial y}{\partial \eta} - \frac{\partial x}{\partial \eta} \right) d\eta \tag{7.32}$$

where $|J|$ is the determinant of the Jacobian matrix J given by Equation (6.17), which relates the global x, y and the local ξ, η co-ordinates, and ξ_R is the local co-ordinate value corresponding to $r = R$, i.e.,

$$\xi_R = 1 - \frac{A(\eta)}{R} \tag{7.33}$$

7.5 Gauss-Legendre Integration for Mapped Wave Infinite Elements

The conventional mapped wave infinite elements are integrated by the special integration scheme by Zienkiewicz *et al.* [93], in which the wave propagates in an infinite element is restricted to a single wave which propagates in the radial direction only. However, in the special wave infinite elements to be developed in this study, multiple waves which propagate in different directions are to be included. Therefore another method is required to evaluate the integrals appearing in the special wave infinite element formulation. It

may be possible to develop a new special integration scheme which can integrate shape functions including multiple wave directions. However it is also possible to apply some general integration schemes which do not restrict the wave directions in infinite elements. For example, a Gauss-Legendre integration scheme has been successfully applied to the special wave finite elements in spite of their oscillating shape functions containing multiple number of wave directions.

In this section, the application of a Gauss-Legendre integration scheme to the mapped wave infinite elements is discussed, as a preparation for the development of special wave infinite elements.

7.5.1   Application of Gauss-Legendre Integration to Wave Elements

In Gauss-Legendre numerical integration, the abscissae and weights are chosen to get the most accurate results for the integration of functions of polynomial form. The details and tables of the abscissae and the weights are given in many references such as Davis and Rabinowitz [42].

The n-order Gauss Legendre integration of function $f(\xi)$ is given by the form

$$\int_{-1}^{1} f(\xi)d\xi = \sum_{p=1}^{n} f(\xi_p)w(\xi_p) \tag{7.34}$$

where ξ_p are abscissae and $w(\xi_p)$ are the corresponding weights. This scheme can integrate a polynomial up to the degree of $2n-1$. It assumes the polynomial form of the function. However it has been successfully applied to obtain element matrices of the special wave finite elements in spite of the oscillating behaviour of their shape functions if more than ten integration points are used for a length of a wavelength as shown in Section 3.7. The same requirement as the rule of the application of the Gauss-Legendre Integration scheme to the special wave finite elements should be applied to its application to the mapped wave infinite elements, as they also have similar oscillating behaviour due to the special shape functions containing trigonometric functions. The difference between the shape functions and the derivatives of the special wave finite elements and the mapped wave infinite elements are that the amplitude of the functions of the infinite elements decay along the distance from the 'pole' in the radial direction.

Figure 7.4 shows the infinite mapping of the integration points from the local to the global co-ordinates for one dimensional case. The upper limit $\xi = 1$ is mapped onto

118
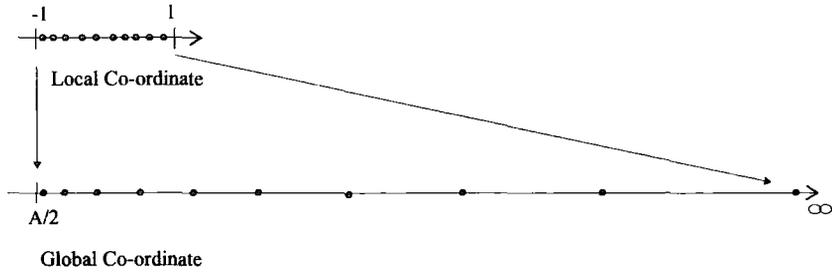
Figure 7.4: One dimensional infinite mapping of integration points.

$r = \infty$. Because of this mapping, a constant distance in the local ξ co-ordinate is mapped onto a larger distance in the r direction in the global co-ordinates as ξ increases from -1 to 1. Consequently the interval between two adjacent integration points in the global co-ordinates becomes relatively larger as r becomes larger, and the requirement of the ratio of the interval of two adjacent integration points to the wavelength will not be satisfied at large r. Actually this requirement can not be satisfied over the entire element by using finite number of integration points because an infinite element extends to infinity.

However, as the waves decay along in the radial direction in two or three dimensions, the contribution to the integral of the very far field becomes negligible. Thus the problem of the larger interval can be ignored in the further field, beyond a certain distance from the 'pole' and radiating or scattering objects. Consequently it should be possible to evaluate the integral over an entire infinite element by only taking into account a certain finite area. Therefore it is important to investigate how much area of an element should be considered and to apply sufficient integration points to integrate this area accurately.

7.5.2 Dividing Infinite Element into Subelements in Infinite Direction

To integrate an element in the infinite direction accurately using many integration points, the element is divided into many subelements in the radial direction so that each subelement has the same length r_{div} in the global co-ordinates, and a Gauss-Legendre integration scheme of the same order is applied to integrate each subelement. The whole integral is obtained as the sum of the integrals of each subelement. When the element is divided into n_{div} subelements in the infinite direction, the integration with respect to ξ can be obtained from

$$\int_{-1}^{1} f(\xi, \eta)d\xi = \sum_{s=1}^{n_{div}} \int_{-1}^{1} f(\xi, \eta)d\bar{\xi} \qquad (7.35)$$

119
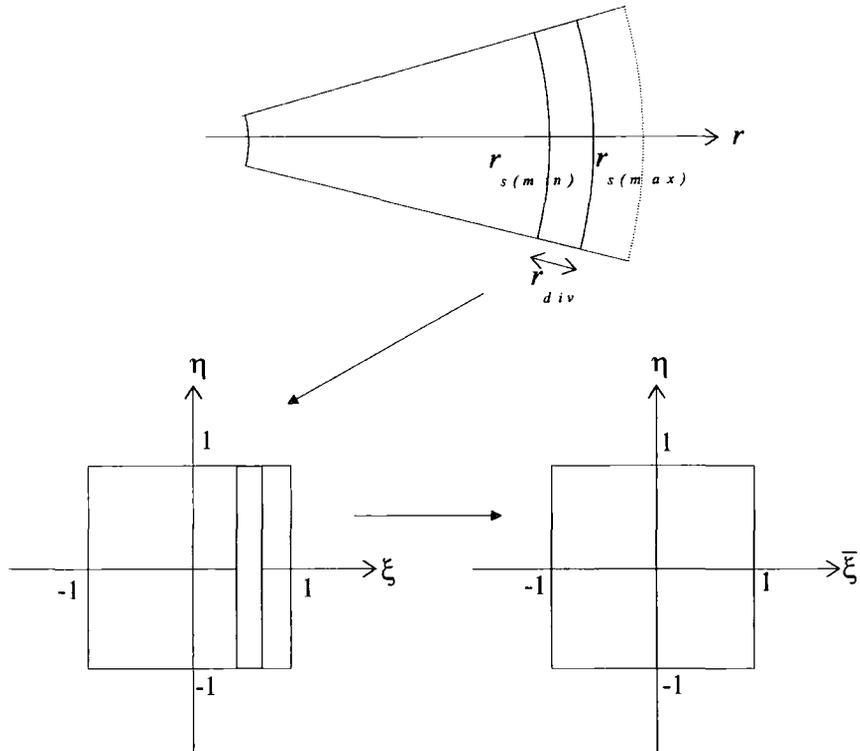
Figure 7.5: Dividing infinite element into subelements for the use of Gauss-Legendre integration.

Although n_{div}, the number of subelements becomes infinity if we integrate over the complete area of the infinite element, satisfactory accuracy should be achieved with a finite number of subelements. This is more practical than applying the Gauss-Legendre integration of very high order to the whole integration area of the element.

In s-th subelement in the infinite direction, the smallest and the largest values of r denoted by $r_{s(min)}$ and $r_{s(max)}$, respectively, are given by

$$r_{s(min)} = \frac{A(\eta)}{2} + (s-1)r_{div} \tag{7.36}$$

$$r_{s(max)} = \frac{A(\eta)}{2} + s\, r_{div} \tag{7.37}$$

where $A(\eta)/2$ is the distance from the 'pole' to the inner edge of the infinite element. When the local co-ordinate $\bar{\xi}$ is defined to be $-1 \leq \bar{\xi} \leq 1$ in each subelement, as shown in Figure 7.5, the relation between r and $\bar{\xi}$ in the s-th subelement is given by

$$r = r_{s(min)} + \frac{r_{div}}{2} + \frac{r_{div}}{2}\bar{\xi} \tag{7.38}$$

120

The derivatives $\partial r / \partial \bar{\xi}$ and $\partial \xi / \partial \bar{\xi}$ are

$$\frac{\partial r}{\partial \bar{\xi}} = \frac{r_{div}}{2} \tag{7.39}$$

$$\frac{\partial \xi}{\partial \bar{\xi}} = \frac{r_{div}}{2} \frac{(1-\xi)^2}{A(\eta)} \tag{7.40}$$

The distance from the 'pole' to the outer boundary of the most distant subelement, denoted by $R(\eta)$, is given by the subelement length r_{div} and the number of subelements n_{div} by

$$R(\eta) = \frac{A(\eta)}{2} + n_{div} r_{div} \tag{7.41}$$

The original infinite extent of the element $A(\eta)/2 \le r < \infty$ is truncated to a finite area $A(\eta)/2 \le r \le R(\eta)$. It is necessary to consider the outer boundary Γ_R at $r = R(\eta)$ to obtain element matrices.

7.5.3 Numerical Integration

To integrate over an element domain Ω by using a Gauss-Legendre integration scheme of n_ξ points in the ξ direction and n_η points in the η direction,

$$\int_\Omega f(\xi,\eta) d\Omega = \int_{-1}^{1} \int_{-1}^{1} f(\xi,\eta)|J| d\xi d\eta \tag{7.42}$$

By using Gauss-Legendre integrations of the n_ξ order in ξ direction, and the n_η order in η direction, respectively, the integral is numerically calculated by

$$\int_\Omega f(\xi,\eta) d\Omega = \sum_{q=1}^{n_\eta} \sum_{p=1}^{n_\xi} f(\xi_p, \eta_q)|J| w(\xi_p) w(\eta_q) \tag{7.43}$$

where ξ_p and η_q are abscissae in the ξ and the η directions, respectively and $w(\xi_p), w(\eta_q)$ are corresponding weights. Dividing the element area into n_{div} subelements in ξ direction leads to the form

$$\int_\Omega f(\xi,\eta) d\Omega = \sum_{q=1}^{n_\eta} \sum_{s=1}^{n_{div}} \sum_{p=1}^{n_{\bar{\xi}}} f(\xi_p, \eta_q)|\bar{J}| w(\bar{\xi}_p) w(\eta_q) \tag{7.44}$$

where $n_{\bar{\xi}}$ is the number of the integration points applied to the $\bar{\xi}$ direction of subelement, $w(\bar{\xi}_p)$ are the corresponding weights, and $|\bar{J}|$ is the determinant of the Jacobian matrix $\bar{J}$, which relates the global x, y and the local $\bar{\xi}$, η co-ordinates instead of the local ξ, η co-ordinates. The Jacobian matrix $\bar{J}$ is obtained from the original Jacobian matrix J and $\partial\xi/\partial\bar{\xi}$ by

$$\bar{J} = \begin{bmatrix} \dfrac{\partial x}{\partial \bar{\xi}} & \dfrac{\partial y}{\partial \bar{\xi}} \\ \dfrac{\partial x}{\partial \eta} & \dfrac{\partial y}{\partial \eta} \end{bmatrix} = \begin{bmatrix} \dfrac{\partial x}{\partial \xi}\dfrac{\partial \xi}{\partial \bar{\xi}} & \dfrac{\partial y}{\partial \xi}\dfrac{\partial \xi}{\partial \bar{\xi}} \\ \dfrac{\partial x}{\partial \eta} & \dfrac{\partial y}{\partial \eta} \end{bmatrix} \tag{7.45}$$

Thus the element matrix is obtained by

$$\mathcal{K}_{ij} \simeq \sum_{q=1}^{n_\eta}\sum_{s=1}^{n_{div}}\sum_{p=1}^{n_{\bar{\xi}}} \left(\nabla S_i^m \nabla S_j^l - k^2 S_i^m S_j^l \right) |\bar{J}|w(\bar{\xi}_p)w(\eta_q) - ik\sum_{q=1}^{n_\eta} S_i^m S_j^l \left(\frac{\partial y}{\partial \eta} - \frac{\partial x}{\partial \eta} \right) w(\eta_q) \tag{7.46}$$

The $\bar{\xi}$ derivatives of shape functions S_j^l are obtained by

$$\frac{\partial S_j^l}{\partial \bar{\xi}} = \frac{\partial S_j^l}{\partial \xi}\frac{\partial \xi}{\partial \bar{\xi}} \tag{7.47}$$

7.6 Effective Distance to the Outer Boundary

The convergence of the integral over an infinite element evaluated numerically by a Gauss-Legendre integration was observed by numerical tests. The actual element matrix of an mapped wave infinite element was integrated, and then compared to the element matrix obtained by the Zienkiewicz special integration [93]. The infinite element is coupled with the special wave finite elements to form the mesh model for the Hankel source problem, therefore the resultant potential obtained by using the infinite element matrix by Gauss-Legendre integration is compared to those obtained by the Zienkiewicz special integration.

The results show that the distance between the pole and the outer boundary of the element area for the numerical integration should be $50 - 250$ times of the wavelength or greater to obtain a sufficient accuracy.

7.6.1 Tested Infinite Element

The 6-node infinite element used for the numerical testing is shown in Figure 7.6. The element extends over $2 \leq r < \infty$ and $-15° \leq \theta \leq 15°$ where r, θ are the polar co-ordinates
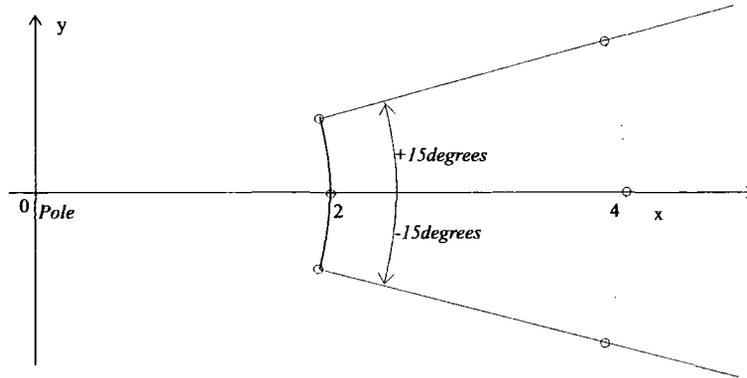
Figure 7.6: 6-node infinite element used for investigation of the use of Gauss-Legendre integration.
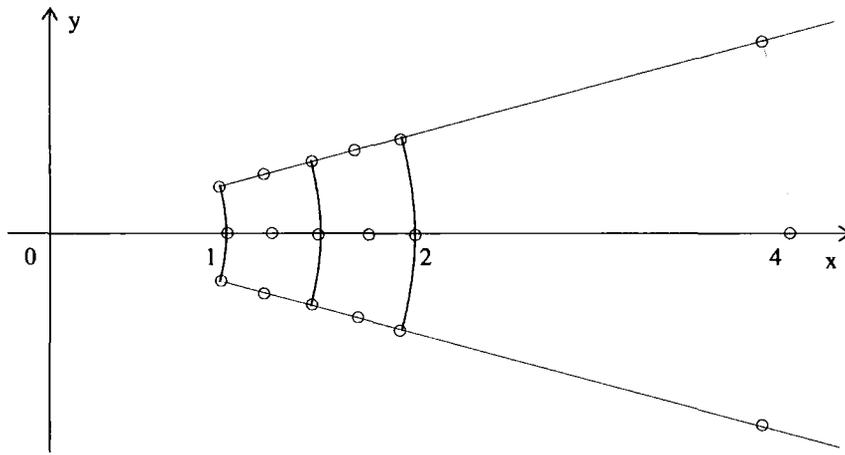
Figure 7.7: Mesh model for Hankel source problem.

in two dimensions.

The radius of the arc of the inner edge of the element is 2, i.e. $A(\eta) = 4$. The parent element of infinite element is quadratic in both ξ and η directions, therefore the element in the global co-ordinate is defined by six nodes as three nodes are at infinity. The length of each subelement in the r direction, r_{div}, was set to be $\lambda/2$ where λ is the wavelength. The number of the integration points, $n_{\bar{\xi}}$, applied to the $\bar{\xi}$ direction in each subelement was 10 to well satisfy the requirement of the ratio of the integration point interval to the wavelength, consequently the number of integration points in the $\bar{\xi}$ direction is 20 per wavelength. The number of subelements in the r direction, n_{div}, was varied from 10 to 10^3. The numerically evaluated value of the integral was compared to the value obtained by the Zienkiewicz special integration scheme. 24 Gauss-Legendre integration points were used for the angular direction of the infinite element.

7.6.2 Finite/Infinite Element Mesh Model

The infinite element was coupled to special wave finite elements to solve the Hankel source problem. The geometry of the problem is the same as that shown in Figure 6.5.

The problem is that of a circular cylinder of unit radius and infinite length in the domain filled with some medium. From the axisymmetric nature of the problem in the two dimensional plane, the domain around the cylinder was modelled by a sectorial mesh bounded by straight radii at $-15°$ and $15°$. The finite/infinite element mesh is shown in Figure 7.7. The sectorial domain over $1 \leq r \leq 2$ and $-15° \leq \theta \leq 15°$ is divided into two 9-node quadrilateral finite elements in the radial direction. On the inner boundary of the finite element domain $r = 1$ the normal derivatives of radiated potential were given as the Neumann boundary condition, and on the outer boundary at $r = 2$ the infinite element shown above is attached.

The problem was solved for the wavenumber $k = 4$. For the nodes in $1 \leq r < 2$, i.e., the nodes belonging only to finite elements, 8 equally spaced approximating plane waves are applied. The directions are $0°, 45°, \cdots, 315°$, where the reference direction $0°$ indicates the radial direction at each node. For the nodes at $r \geq 2$, i.e., the nodes belonging to infinite element, one plane wave in the radial direction at each node is applied. 24 Gauss-Legendre integration points are used for each direction of finite elements as well as the angular direction of the infinite element.

7.6.3 Errors in Element Matrix

Figure 7.8 shows the sum of square of the errors of the real and imaginary parts of the element matrix components given by

$$e = \sqrt{\left(\sum_{i=1}^{n_p}\sum_{j=1}^{n_p}\left|\mathcal{K}_{ij}^{gl} - \mathcal{K}_{ij}^{sp}\right|^2\right) \bigg/ \left(\sum_{i=1}^{n_p}\sum_{j=1}^{n_p}\left|\mathcal{K}_{ij}^{sp}\right|^2\right)} \tag{7.48}$$

where $\mathcal{K}_{ij}^{gl}$ and $\mathcal{K}_{ij}^{sp}$ are the element matrix components obtained by a Gauss-Legendre integration and the Zienkiewicz special integration scheme, respectively. n_p is the number of total degree of freedom of an element, which is 6 in this example.

The error almost converges by $n_{div} = 500$ for both of the real and imaginary parts of the element matrix.
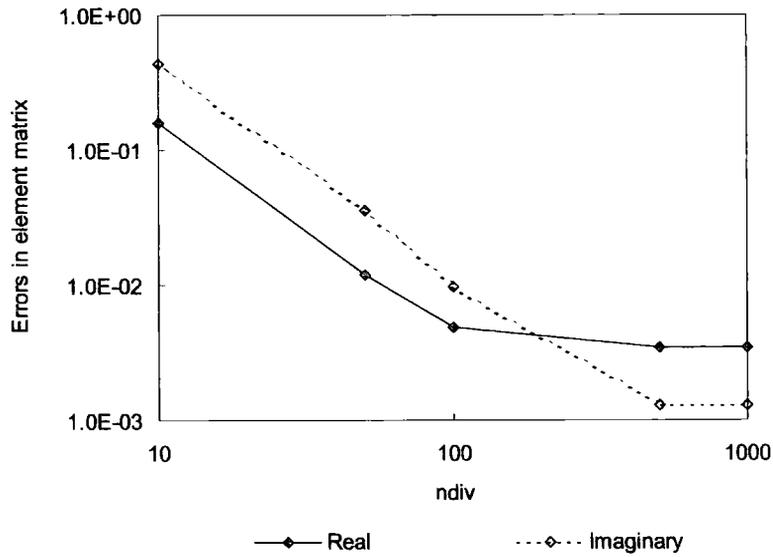
Figure 7.8: Error in infinite element matrix versus n_{div}, number of subelements considered.
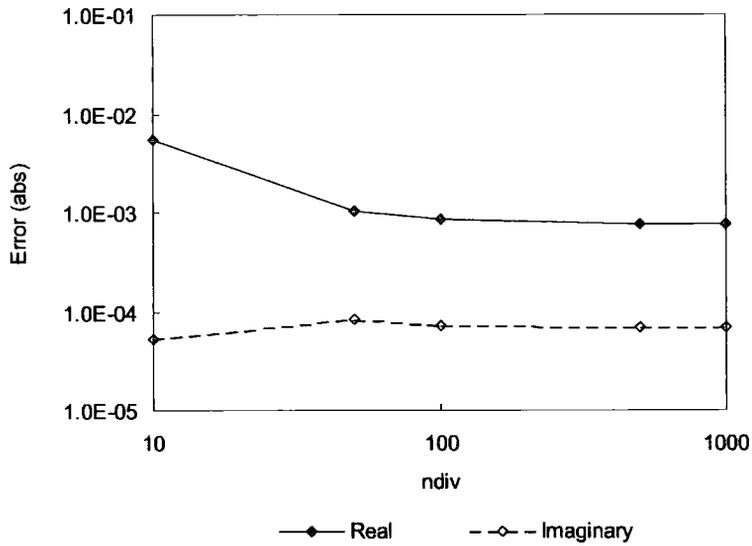
Figure 7.9: Error in potential at $r = 1.5$ for Hankel source problem versus n_{div}, number of subelements considered.

7.6.4 Errors in Calculated Potential

Figure 7.9 shows the absolute values of errors in the real and imaginary parts of calculated potential at $r = 1.5$.

$$e = \left| \frac{\phi^{gl} - \phi^{an}}{\phi^{an}} \right| \tag{7.49}$$

125

where ϕ^{gl} is the potential at $r = 1.5$ obtained by using element matrix by a Gauss-Legendre integration and ϕ^{an} is the analytical solution.

The error almost converges by $n_{div} = 100$ for both of the real and imaginary parts of the calculated potential.

These results show that the mapped wave infinite element matrix obtained by this method of applying a Gauss-Legendre integration scheme with respect to the infinite direction and the resultant calculated potential converge to the accurate values, and that this method can be useful. It is also shown n_{div} should be set to $100 - 500$ or greater for practical accuracy, i.e., the outer boundary of the element area for the numerical integration should be $50 - 250$ times of the wavelength or greater.

7.7   Accuracies due to Mappings and Integration Procedures

In Chapter 6, mappings of infinite element are presented for circular and non-circular cases. In the previous sections in this chapter, the application of Gauss-Legendre integration instead of the Zienkiewicz special integration scheme is discussed. In this section, the accuracies of calculated results obtained with computational models, which are slightly different with respect to mappings and integration procedures, by these methods are compared, for the examples of the Hankel source problem and a scattering problem, a problem of plane wave scattered by a circular cylinder.

To compare the accuracies between cases precisely, the numerical values of calculated potential are shown in tables and compared to the analytical solution at points $r = 1.0$, 1.5 and 2.0 on the x axis. The difference from the analytical solution and the error are defined for the evaluation of accuracy. The difference is given by

$$d = \phi^{num} - \phi^{an} \tag{7.50}$$

where ϕ^{num} and ϕ^{an} are the numerical results and the analytical solution of the potential, respectively. The error is given by

$$e = \frac{\phi^{num} - \phi^{an}}{\phi^{an}} \tag{7.51}$$

The results for the Hankel source problem show that quadratic mapping gives better accuracy than circular mapping because the compatibility between finite and infinite ele-

Table 7.1: Accuracy comparison test cases for Hankel source problem and scattering problem using curved edge models.

Cases	finite/infinite element interface	mapping	numerical integration
1	curved	circular	Zienkiewicz scheme
2	curved	quadratic	Zienkiewicz scheme
3	curved	circular	Gauss-Legendre
4	curved	quadratic	Gauss-Legendre

ments are well satisfied. For the scattering problem the accuracies of the results are almost the same and any significant difference due to the mappings or the integration procedures was not observed.

7.7.1 Test Cases

Table 7.1 shows test cases used for an accuracy comparison for the Hankel source problem and the scattering problem using curved edge model. Table 7.2 shows the additional test cases used for the Hankel source problem using straight edge model.

(a) Mappings

Two different mapping for infinite element were employed for check and comparison. The circular mapping is specialised for the current mesh model and uses the exact geometry of the circular arcs. The quadratic mapping uses the iso-parametric mapping by the general formulation using quadratic polynomials. In finite elements the shape function is given by quadratic polynomial.

(b) Integration Schemes

The use of the Zienkiewicz special integration scheme and a Gauss-Legendre integration as explained in the previous section are applied to integrate over the element area. In case of a Gauss-Legendre integration, the number of subelements in r direction n_{div} is equal to 500.

(c) Mesh Model

An additional mesh model was also applied to the Hankel source problem only. In the model the inner edge of the infinite element is straight instead of curved.

Table 7.2: Accuracy comparison test cases for Hankel source problem using straight edge model.

Cases	finite/infinite element interface	mapping	numerical integration
5	straight	quadratic	Zienkiewicz scheme
6	straight	quadratic	Gauss-Legendre

Table 7.3: Analytical solution and numerical results of potential for Hankel source problem obtained using curved edge model for the case of $k = 4$.

r	Analytical solution, k=4 Phi_r(An)	Phi_i(An)
1.0000	-3.97149807E-01	-1.69407446E-02
1.5000	1.50645259E-01	-2.88194691E-01
2.0000	1.71650807E-01	2.23521489E-01

	Numerical results		Difference from analytical solution		Error	
	Real	Imaginary	Real	Imaginary	Real	Imaginary
case1						
1.0000	-3.97653876E-01	-1.69930645E-02	-5.04068826E-04	-5.23199467E-05	1.26921584E-03	3.08840893E-03
1.5000	1.50696451E-01	-2.88153654E-01	5.11915081E-05	4.10370858E-05	3.39814929E-04	-1.42393621E-04
2.0000	1.70798444E-01	2.23946739E-01	-8.52363257E-04	4.25249750E-04	-4.96568161E-03	1.90250052E-03
case2						
1.0000	-3.97149821E-01	-1.69408517E-02	-1.38261459E-08	-1.07146679E-07	3.48134272E-08	6.32479161E-06
1.5000	1.50645356E-01	-2.88194220E-01	9.65081495E-08	4.71085750E-07	6.40631838E-07	-1.63460940E-06
2.0000	1.71656847E-01	2.23532645E-01	6.03974290E-06	1.11557503E-05	3.51862190E-05	4.99090730E-05
case3						
1.0000	-3.96833208E-01	-1.89628182E-02	3.16599174E-04	-2.02207365E-03	-7.97178214E-04	1.19361557E-01
1.5000	1.50919601E-01	-2.87717776E-01	2.74341508E-04	4.76915086E-04	1.82110947E-03	-1.65483647E-03
2.0000	1.76566079E-01	2.23964017E-01	4.91527174E-03	4.42527750E-04	2.86352964E-02	1.97979958E-03
case4						
1.0000	-3.96829358E-01	-1.92289553E-02	3.20449174E-04	-2.28821075E-03	-8.06872289E-04	1.35071439E-01
1.5000	1.50943079E-01	-2.87757656E-01	2.97819508E-04	4.37035086E-04	1.97695904E-03	-1.51645779E-03
2.0000	1.76913511E-01	2.22557125E-01	5.26270374E-03	-9.64364250E-04	3.06593591E-02	-4.31441403E-03

7.7.2   Hankel Source Problem using Curved Edge Model

The first problem is the Hankel source problem as it is almost the simplest possible example in two dimensions. The problem and the mesh model are exactly the same as that used in the previous section. The geometry and the finite/infinite element mesh model are shown in Figures 6.5 and 7.7, respectively.

Table 7.3 shows the analytical solution and the numerical results with the difference from the analytical solution and the error for the case of the wavenumber $k = 4$. Table 7.4 is for the case of the wavenumber $k = 8$.

From these results, it can be concluded that quadratic mapping gives better accuracy than circular mapping. This is because the compatibility between finite and infinite elements are satisfied when quadratic mapping is used as it is also used for finite elements. Circular mapping is more accurate for the geometry itself. However, it causes a small incompatibility between the two types of element. It can be also said that sufficient accuracy is obtained using Gauss-Legendre integration with $n_{div} = 500$

Table 7.4: Analytical solution and numerical results of potential for Hankel source problem obtained using curved edge model for the case of $k = 8$.

r	Analytical solution, k=8 Phi_r(An)	Phi_i(An)
1.0000	1.71650807E-01	2.23521489E-01
1.5000	4.76893108E-02	-2.25237313E-01
2.0000	-1.74899074E-01	9.58109971E-02

	Numerical results Real	Imaginary	Difference from analytical solution Real	Imaginary	Error Real	Imaginary
case1						
1.0000	1.71378638E-01	2.24027339E-01	-2.72169100E-04	5.05849600E-04	-1.58559755E-03	2.26309158E-03
1.5000	5.15656630E-02	-2.22883844E-01	3.87635220E-03	2.35346860E-03	8.12834603E-02	-1.04488398E-02
2.0000	-1.73209341E-01	9.69719815E-02	1.68973300E-03	1.16098442E-03	-9.66118894E-03	1.21174443E-02
case2						
1.0000	1.71650415E-01	2.23516318E-01	-3.92100000E-07	-5.17140000E-06	-2.28428871E-06	-2.31360305E-05
1.5000	4.77113414E-02	-2.25235292E-01	2.20306000E-05	2.02060000E-06	4.61960964E-04	-8.97098255E-06
2.0000	-1.74894139E-01	9.58127832E-02	4.93500000E-06	1.78612000E-06	-2.82162729E-05	1.86421189E-05
case3						
1.0000	1.71798922E-01	2.23282602E-01	1.48114900E-04	-2.38887400E-04	8.62884961E-04	-1.06874467E-03
1.5000	5.14971182E-02	-2.23409437E-01	3.80780740E-03	1.82787560E-03	7.98461403E-02	-8.11533213E-03
2.0000	-1.73159433E-01	9.65923481E-02	1.73964100E-03	7.81351020E-04	-9.94654208E-03	8.15512878E-03
case4						
1.0000	1.71446848E-01	2.23018684E-01	-2.03959100E-04	-5.02805400E-04	-1.18822104E-03	-2.24947231E-03
1.5000	4.80970721E-02	-2.25733473E-01	4.07761300E-04	-4.96160400E-04	8.55037100E-03	2.20283395E-03
2.0000	-1.74759021E-01	9.54929091E-02	1.40053000E-04	-3.18087980E-04	-8.00764674E-04	-3.31995272E-03
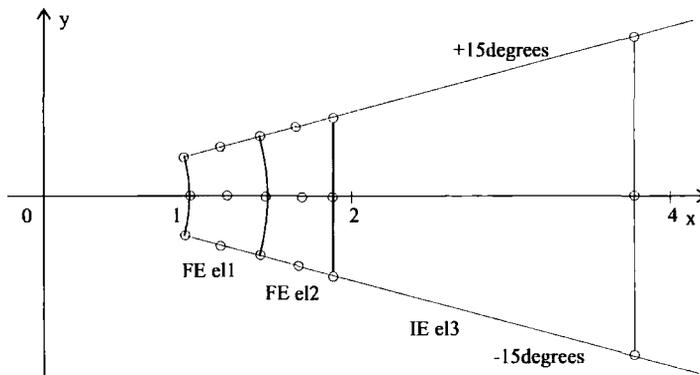
Figure 7.10: Straight edge mesh model for Hankel source problem.

7.7.3 Hankel Source Problem using Straight Edge Model

In the straight edge model, the curvature of finite element edges are therefore modified so as to change gradually from the circular arc with a radius of 1 to the chord connecting points at the angles $-15°$ and $15°$ on a circle with the radius of 2. The mesh model is shown in Figure 7.10.

Table 7.5 shows the analytical solution and the calculated potential with the difference from the analytical solution and the error for the case of the wavenumber $k = 4$. Table 7.6 is for the case of the wavenumber $k = 8$.

In both cases of $k = 4$ and 8, in Case 5 using the Zienkiewicz special integration scheme to integrate the infinite element the numerical results are quite accurate. However, in Case

Table 7.5: Analytical solution and numerical results of potential for Hankel source problem obtained by straight edge model for the case of $k = 4$.

r	Analytical solution, k=4	
	Phi_r(An)	Phi_i(An)
1.0000	-3.97149807E-01	-1.69407446E-02
1.5000	1.50645259E-01	-2.88194691E-01
1.9318	2.29526884E-01	1.71857472E-01

	Numerical results		Difference from analytical solution		Error	
	Real	Imaginary	Real	Imaginary	Real	Imaginary
case5						
1.0000	-3.97149647E-01	-1.69406832E-02	1.60173854E-07	6.13533209E-08	-4.03308402E-07	-3.62164253E-06
1.5000	1.50644094E-01	-2.88197034E-01	-1.16549185E-06	-2.34291425E-06	-7.73666463E-06	8.12962321E-06
1.9320	2.29506267E-01	1.71828041E-01	-2.06168695E-05	-2.94308237E-05	-8.98233319E-05	-1.71251348E-04
case6						
1.0000	-3.92167577E-01	-9.12844019E-03	4.98223017E-03	7.81230436E-03	-1.25449644E-02	-4.61154723E-01
1.5000	1.52081383E-01	-2.89588034E-01	1.43612351E-03	-1.39334291E-03	9.53314769E-03	4.83472790E-03
1.9320	2.58052109E-01	1.73101909E-01	2.85252251E-02	1.24443718E-03	1.24278362E-01	7.24110022E-03

Table 7.6: Analytical solution and numerical results of potential for Hankel source problem obtained by straight edge model for the case of $k = 8$.

r	Analytical solution, k=8	
	Phi_r(An)	Phi_i(An)
1.0000	1.71650807E-01	2.23521489E-01
1.5000	4.76893108E-02	-2.25237313E-01
1.9320	-1.01483481E-01	1.75707498E-01

	Numerical results		Difference from analytical solution		Error	
	Real	Imaginary	Real	Imaginary	Real	Imaginary
case5						
1.0000	1.71648264E-01	2.23519504E-01	-2.54310000E-06	-1.98540000E-06	-1.48155435E-05	-8.88236744E-06
1.5000	4.76705704E-02	-2.25243944E-01	-1.87404000E-05	-6.63140000E-06	-3.92968564E-04	2.94418359E-05
1.9320	-1.01533869E-01	1.75675016E-01	-5.03879000E-05	-3.24817000E-05	4.96513319E-04	-1.84862345E-04
case6						
1.0000	1.71202417E-01	2.23689292E-01	-4.48390100E-04	1.67802600E-04	-2.61222250E-03	7.50722449E-04
1.5000	5.16841547E-02	-2.22858776E-01	3.99484390E-03	2.37853660E-03	8.37681198E-02	-1.05601358E-02
1.9320	-9.89252222E-02	1.77255889E-01	2.55825890E-03	1.54839130E-03	-2.52086238E-02	8.81232344E-03

6 using a Gauss-Legendre integration instead the results are much less accurate. Although efforts have been made to try to find out the problem in the theory and the program code, it has not been discovered yet.

7.7.4 Scattering Problem

As a more realistic example than the Hankel source problem, the problem of plane wave scattered by a circular cylinder was considered. The geometry of the problem in two dimensions is the same as that shown in Figure 6.11.

The problem is that of a circular cylinder of unit radius and infinite length, and the plane wave of unit amplitude is incident perpendicular to the cylinder axis from the negative x direction. The wave field can be treated as a two dimensional problem.

The finite/infinite element model is shown in Figure 7.11. The cylindrical domain over $1 \leq r \leq 2$ is divided into 18 sectors of 20 degrees each, and each sector is divided into
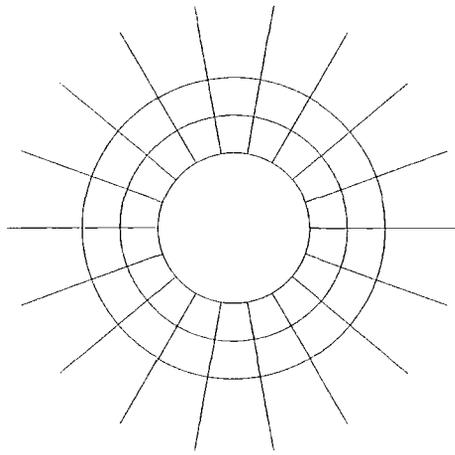
Figure 7.11: Finite and infinite element mesh model for scattering problem. Inner radius 1, radius of finite/infinite element interface 2.

two 9-node quadrilateral special wave finite elements in the radial direction. On the inner boundary $r = 1$ the normal derivatives of scattered potential were given as the Neumann boundary condition, and on the outer boundary at $r = 2$, 6-node special wave infinite elements are applied. The problem was solved for the wavenumber $k = 4$. The real and imaginary parts of the scattered potential are compared to the analytical solution.

Figures 7.12 and 7.13 show the real and imaginary parts of the numerical results of the scattered potential as a function of the angle around the cylinder, respectively, for the case of the wavenumber $k = 4$. Figures 7.14 and 7.15 show the difference of the between the numerical results and the analytical solution in real and imaginary parts, respectively.

To compare the accuracies of cases precisely, the numerical values of the analytical solution are shown every 10 degrees in Table 7.7, and the calculated scattered potential with the differences from the analytical solution and the error are also shown in Tables 7.8 - 7.11 for Cases 1 - 4, respectively.

The accuracies are almost the same in the four cases compared here. There are no clear trends in the accuracy displayed by the results obtained by different types of mappings and different integration procedures. However it can be said that all of the results have sufficient accuracy for engineering purposes. Also it has been confirmed again that Gauss-Legendre integration scheme can lead to the numerical results which are as accurate as those obtained by the Zienkiewicz special integration scheme.
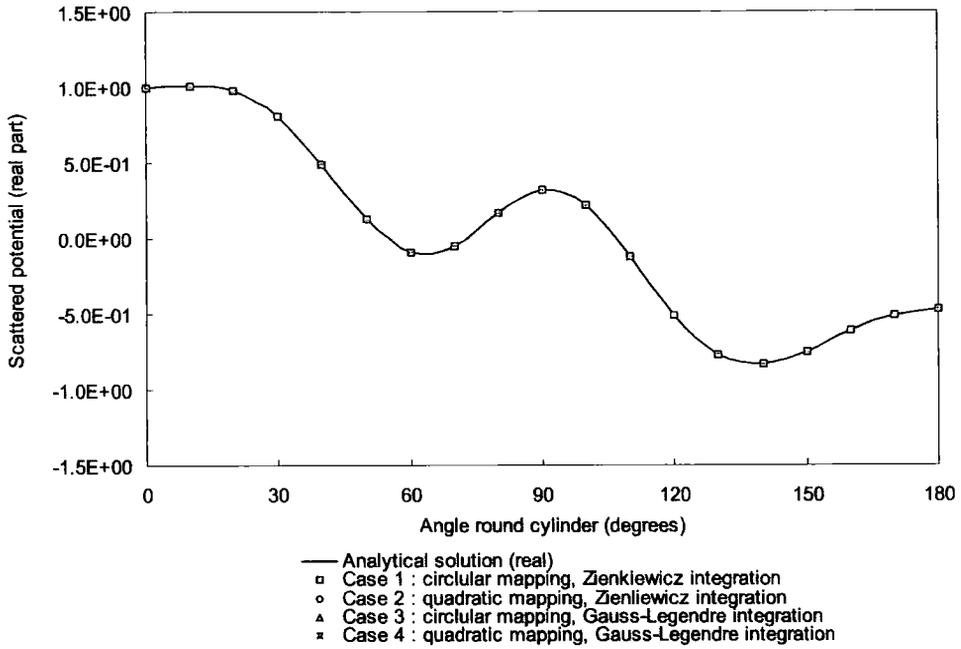
Figure 7.12: Real part of scattered potential along the circumference of the cylinder, for $k = 4$.
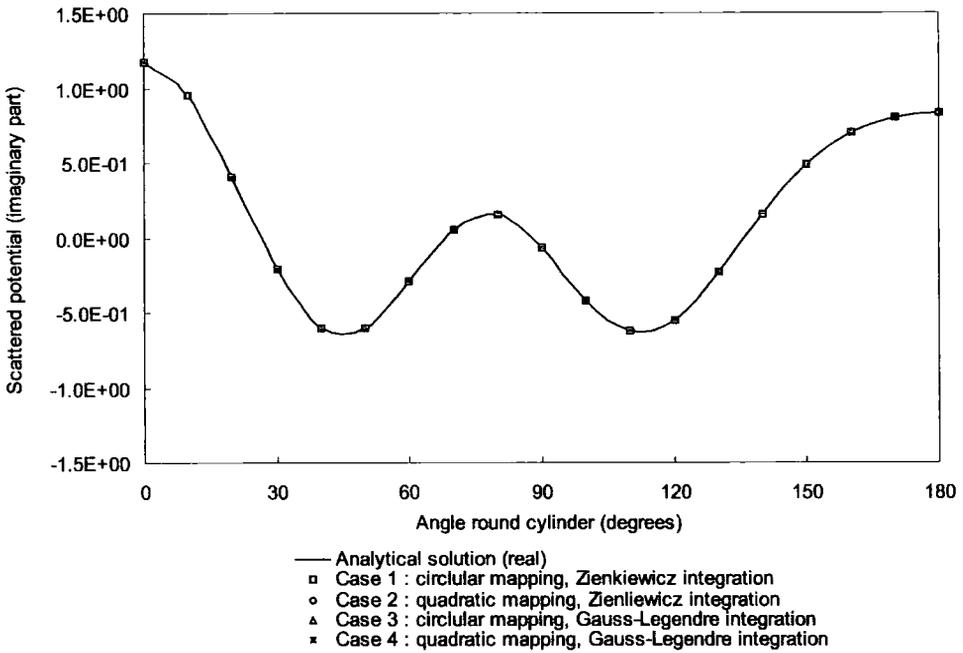
Figure 7.13: Imaginary part of scattered potential along the circumference of the cylinder, for $k = 4$.
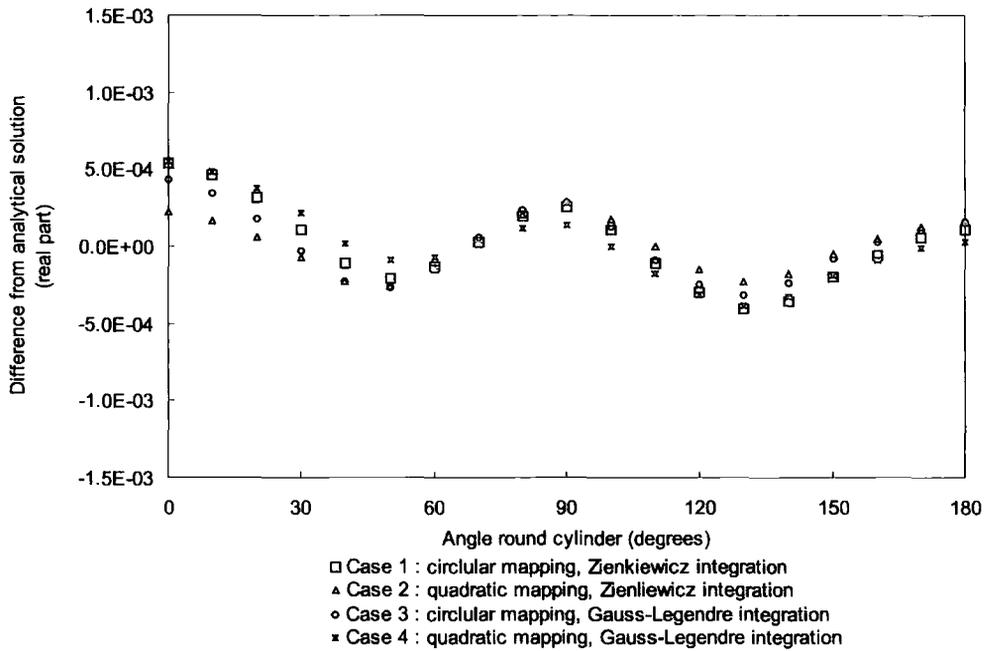
Figure 7.14: Difference from analytical solution in real part of scattered potential along the circumference of the cylinder, for $k = 4$.
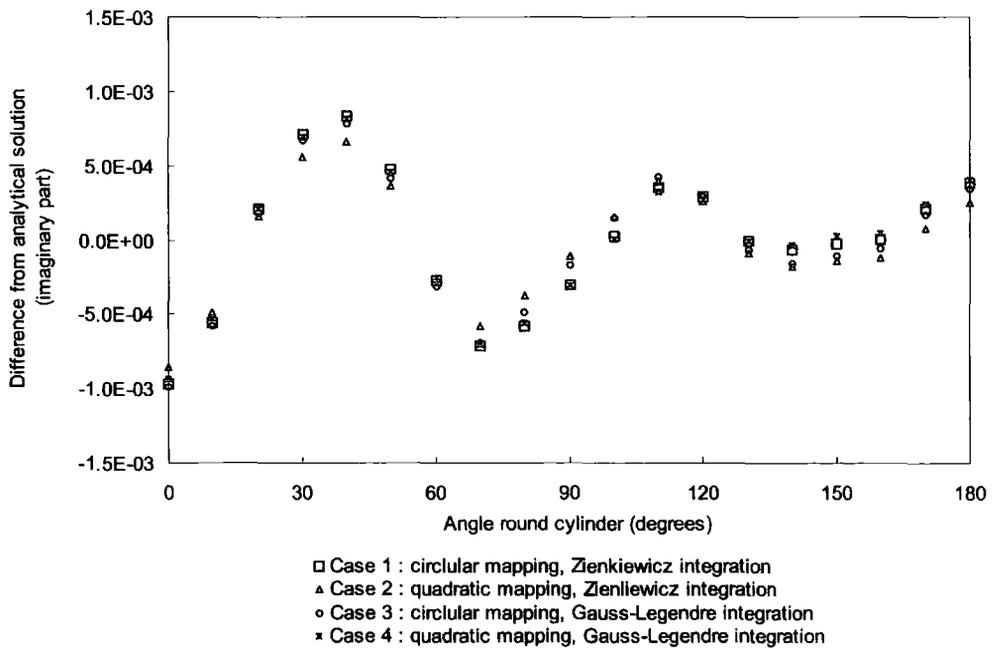
Figure 7.15: Difference from analytical solution in imaginary part of scattered potential along the circumference of the cylinder, for $k = 4$.

133

Table 7.7: Analytical solution of scattered potential along the circumference of the cylinder, for $k = 4$.

Angle	Analytical solution, k=4	
	Real	Imaginary
0	1.000058E+00	1.175352E+00
10	1.006232E+00	9.582543E-01
20	9.755316E-01	4.100076E-01
30	8.131896E-01	-2.073418E-01
40	4.925975E-01	-5.999055E-01
50	1.258151E-01	-6.030054E-01
60	-9.303400E-02	-2.913425E-01
70	-4.935015E-02	5.726446E-02
80	1.678317E-01	1.581820E-01
90	3.194760E-01	-6.133476E-02
100	2.177428E-01	-4.149224E-01
110	-1.203438E-01	-6.260900E-01
120	-5.111293E-01	-5.467983E-01
130	-7.699306E-01	-2.307995E-01
140	-8.318666E-01	1.602918E-01
150	-7.482925E-01	4.888000E-01
160	-6.137332E-01	7.002751E-01
170	-5.056034E-01	8.056680E-01
180	-4.655547E-01	8.359035E-01

Table 7.8: Numerical results of scattered potential along the circumference of the cylinder, for $k = 4$, Case1.

Case 1	Numerical results		Difference from analytical solution		Error	
	Real	Imaginary	Real	Imaginary	Real	Imaginary
0	1.000605E+00	1.174386E+00	5.465281E-04	-9.657787E-04	5.464964E-04	-8.216932E-04
10	1.006700E+00	9.576993E-01	4.681207E-04	-5.550283E-04	4.652215E-04	-5.792077E-04
20	9.758437E-01	4.102146E-01	3.121064E-04	2.070010E-04	3.199347E-04	5.048711E-04
30	8.133019E-01	-2.066344E-01	1.123473E-04	7.074507E-04	1.381564E-04	-3.412002E-03
40	4.924853E-01	-5.990675E-01	-1.122002E-04	8.380420E-04	-2.277726E-04	-1.396957E-03
50	1.256119E-01	-6.025266E-01	-2.032285E-04	4.788415E-04	-1.615295E-03	-7.940916E-04
60	-9.315764E-02	-2.916187E-01	-1.236442E-04	-2.761090E-04	1.329022E-03	9.477125E-04
70	-4.932154E-02	5.654879E-02	2.860704E-05	-7.156709E-04	-5.796749E-04	-1.249765E-02
80	1.680311E-01	1.576046E-01	1.994552E-04	-5.773897E-04	1.188424E-03	-3.650162E-03
90	3.197332E-01	-6.163754E-02	2.572401E-04	-3.027793E-04	8.051937E-04	4.936504E-03
100	2.178536E-01	-4.148998E-01	1.107697E-04	2.261932E-05	5.087183E-04	-5.451457E-05
110	-1.204555E-01	-6.257363E-01	-1.117516E-04	3.537077E-04	9.286035E-04	-5.649470E-04
120	-5.114283E-01	-5.465077E-01	-2.989335E-04	2.906025E-04	5.848490E-04	-5.314620E-04
130	-7.703351E-01	-2.308086E-01	-4.044197E-04	-9.046821E-06	5.252677E-04	3.919775E-05
140	-8.322176E-01	1.602204E-01	-3.510063E-04	-7.145673E-05	4.219503E-04	-4.457915E-04
150	-7.484850E-01	4.887767E-01	-1.924954E-04	-2.330355E-05	2.572462E-04	-4.767501E-05
160	-6.137895E-01	7.002792E-01	-5.632714E-05	4.073773E-06	9.177790E-05	5.817389E-06
170	-5.055473E-01	8.058800E-01	5.606251E-05	2.120256E-04	-1.108824E-04	2.631674E-04
180	-4.654422E-01	8.362874E-01	1.125252E-04	3.839271E-04	-2.417013E-04	4.592959E-04

134

Table 7.9: Numerical results of scattered potential along the circumference of the cylinder, for $k = 4$, Case2.

Case 2	Numerical results		Difference from analytical solution		Error	
	Real	Imaginary	Real	Imaginary	Real	Imaginary
0	1.000491E+00	1.174361E+00	4.332081E-04	-9.909887E-04	4.331830E-04	-8.431421E-04
10	1.006579E+00	9.576750E-01	3.470807E-04	-5.793053E-04	3.449311E-04	-6.045424E-04
20	9.757081E-01	4.101878E-01	1.764774E-04	1.802760E-04	1.809038E-04	4.396894E-04
30	8.131633E-01	-2.066743E-01	-2.632567E-05	6.675367E-04	-3.237335E-05	-3.219499E-03
40	4.923697E-01	-5.991264E-01	-2.278382E-04	7.791390E-04	-4.625241E-04	-1.298769E-03
50	1.255447E-01	-6.025904E-01	-2.703565E-04	4.150455E-04	-2.148840E-03	-6.882949E-04
60	-9.316908E-02	-2.916542E-01	-1.350838E-04	-3.116260E-04	1.451983E-03	1.069621E-03
70	-4.929357E-02	5.657383E-02	5.657684E-05	-6.906328E-04	-1.146437E-03	-1.206041E-02
80	1.680695E-01	1.576968E-01	2.378852E-04	-4.851607E-04	1.417404E-03	-3.067105E-03
90	3.197599E-01	-6.150600E-02	2.839361E-04	-1.712366E-04	8.887556E-04	2.791836E-03
100	2.178677E-01	-4.147772E-01	1.249467E-04	1.451633E-04	5.738272E-04	-3.498565E-04
110	-1.204349E-01	-6.256658E-01	-9.110764E-05	4.241847E-04	7.570616E-04	-6.775139E-04
120	-5.113779E-01	-5.465066E-01	-2.485345E-04	2.917475E-04	4.862458E-04	-5.335560E-04
130	-7.702461E-01	-2.308644E-01	-3.154647E-04	-6.491382E-05	4.097313E-04	2.812563E-04
140	-8.321037E-01	1.601368E-01	-2.371743E-04	-1.550217E-04	2.851110E-04	-9.671219E-04
150	-7.483738E-01	4.886946E-01	-8.126237E-05	-1.054235E-04	1.085971E-04	-2.156783E-04
160	-6.137045E-01	7.002155E-01	2.871886E-05	-5.963323E-05	-4.679372E-05	-8.515686E-05
170	-5.054928E-01	8.058354E-01	1.106125E-04	1.674006E-04	-2.187733E-04	2.077786E-04
180	-4.654009E-01	8.362505E-01	1.538772E-04	3.470301E-04	-3.305244E-04	4.151557E-04

Table 7.10: Numerical results of scattered potential along the circumference of the cylinder, for $k = 4$, Case3.

Case 3	Numerical results		Difference from analytical solution		Error	
	Real	Imaginary	Real	Imaginary	Real	Imaginary
0	1.000282E+00	1.174501E+00	2.237781E-04	-8.505887E-04	2.237652E-04	-7.236885E-04
10	1.006396E+00	9.577660E-01	1.640807E-04	-4.883513E-04	1.630645E-04	-5.096260E-04
20	9.755900E-01	4.101684E-01	5.839342E-05	1.608570E-04	5.985805E-05	3.923268E-04
30	8.131181E-01	-2.067861E-01	-7.154267E-05	5.557297E-04	-8.797785E-05	-2.680259E-03
40	4.923730E-01	-5.992491E-01	-2.245312E-04	6.564430E-04	-4.558107E-04	-1.094244E-03
50	1.255566E-01	-6.026420E-01	-2.585015E-04	3.633915E-04	-2.054615E-03	-6.026339E-04
60	-9.317798E-02	-2.916057E-01	-1.439843E-04	-2.631810E-04	1.547653E-03	9.033386E-04
70	-4.932555E-02	5.668759E-02	2.460214E-05	-5.768726E-04	-4.985221E-04	-1.007383E-02
80	1.680375E-01	1.578118E-01	2.058862E-04	-3.701807E-04	1.226742E-03	-2.340221E-03
90	3.197597E-01	-6.143889E-02	2.837401E-04	-1.041259E-04	8.881421E-04	1.697666E-03
100	2.179161E-01	-4.147679E-01	1.732757E-04	1.545243E-04	7.957817E-04	-3.724174E-04
110	-1.203452E-01	-6.256919E-01	-1.471641E-06	3.981067E-04	1.222864E-05	-6.358618E-04
120	-5.112731E-01	-5.465386E-01	-1.437725E-04	2.597635E-04	2.812840E-04	-4.750628E-04
130	-7.701549E-01	-2.308876E-01	-2.242447E-04	-8.804982E-05	2.912531E-04	3.814992E-04
140	-8.320403E-01	1.601164E-01	-1.737373E-04	-1.754677E-04	2.088524E-04	-1.094677E-03
150	-7.483370E-01	4.886603E-01	-4.447137E-05	-1.396835E-04	5.943047E-05	-2.857683E-04
160	-6.136822E-01	7.001536E-01	5.094086E-05	-1.215442E-04	-8.300164E-05	-1.735664E-04
170	-5.054752E-01	8.057472E-01	1.282385E-04	7.922958E-05	-2.536346E-04	9.834024E-05
180	-4.653833E-01	8.361515E-01	1.714052E-04	2.480501E-04	-3.681741E-04	2.967449E-04

135

Table 7.11: Numerical results of scattered potential along the circumference of the cylinder, for $k = 4$, Case4.

Case 4	Numerical results		Difference from analytical solution		Error	
	Real	Imaginary	Real	Imaginary	Real	Imaginary
0	1.000607E+00	1.174416E+00	5.492481E-04	-9.354787E-04	5.492163E-04	-7.959137E-04
10	1.006720E+00	9.577225E-01	4.879807E-04	-5.318463E-04	4.849585E-04	-5.550158E-04
20	9.759055E-01	4.102206E-01	3.738994E-04	2.130390E-04	3.832776E-04	5.195977E-04
30	8.134088E-01	-2.066487E-01	2.191823E-04	6.931247E-04	2.695341E-04	-3.342908E-03
40	4.926147E-01	-5.990932E-01	1.720377E-05	8.123060E-04	3.492460E-05	-1.354056E-03
50	1.257252E-01	-6.025475E-01	-8.984353E-05	4.578795E-04	-7.140919E-04	-7.593290E-04
60	-9.309826E-02	-2.916212E-01	-6.426382E-05	-2.786090E-04	6.907563E-04	9.562935E-04
70	-4.933667E-02	5.656413E-02	1.347974E-05	-7.003267E-04	-2.731449E-04	-1.222969E-02
80	1.679481E-01	1.576224E-01	1.164402E-04	-5.595847E-04	6.937917E-04	-3.537601E-03
90	3.196146E-01	-6.163640E-02	1.385711E-04	-3.016377E-04	4.337449E-04	4.917892E-03
100	2.177415E-01	-4.149220E-01	-1.272262E-06	4.163171E-07	-5.842960E-06	-1.003361E-06
110	-1.205262E-01	-6.257701E-01	-1.824656E-04	3.198407E-04	1.516204E-03	-5.108542E-04
120	-5.114456E-01	-5.465310E-01	-3.162335E-04	2.673665E-04	6.186956E-04	-4.889674E-04
130	-7.703134E-01	-2.308038E-01	-3.828087E-04	-4.283821E-06	4.971989E-04	1.856079E-05
140	-8.321874E-01	1.602526E-01	-3.207903E-04	-3.919773E-05	3.856271E-04	-2.445398E-04
150	-7.484779E-01	4.888210E-01	-1.854354E-04	2.103245E-05	2.478114E-04	4.302875E-05
160	-6.138221E-01	7.003169E-01	-8.895914E-05	4.176877E-05	1.449476E-04	5.964623E-05
170	-5.056163E-01	8.059036E-01	-1.286549E-05	2.356036E-04	2.544582E-05	2.924326E-04
180	-4.655252E-01	8.363038E-01	2.956020E-05	4.003231E-04	-6.349457E-05	4.789106E-04

136

7.8 Wave Directions in Infinite Elements

The special wave infinite elements can contain multiple number of the waves which propagate in the different directions. This is supposed to not only provide a straightforward extension to the special wave finite elements for the unbounded problems but also to make the element more accurate than using only a single wave in the radial direction. Therefore the effect of increasing the number of waves are investigated.

Also, there is another thing which needs to be considered about the wave directions in the infinite elements. In the conventional mapped wave infinite element and the special wave infinite element formulations, the shape functions contain the two-dimensional amplitude decay factor $1/\sqrt{r}$. The distance r is measured from the 'pole' and the exponential functions are multiplied by this factor to describe the wave-like oscillation $\exp(ikr)$ so that the shape functions will satisfy the radiation condition at infinity. This is suitable for the simulation of the radiated or scattered waves because the dominant component of them are the cylindrically outgoing waves in the far field in two dimensions. Because of this decay behaviour, these infinite elements must be applied to the radiated or scattered wave field instead of the total field. And also there may need to be a limitation of the choice of the wave directions in the special wave infinite elements due to this decay behaviour. It is natural to assume that the wave directions may need to be within the range between $-90°$ and $90°$ from the radial direction so that the wave propagates towards further field from the 'pole'. Waves outside this range would be incoming and hence excluded by the radiation condition.

In this section, using the Hankel source problem as the simplest example, the results of two series of numerical testing are shown. In the first test, the wave directions are restricted to be outward and the effect of the number of waves are investigated. In the second test, the effect of adding the inward wave directions are investigated.

The results show that the increase of wave directions generally leads to the better accuracy. However adding waves propagating inwards, which do not satisfy the radiation condition, to infinite elements clearly leads less accurate results.

7.8.1 Special Wave Finite and Infinite Element Model

The geometry of the Hankel source problem is the same as that shown in Figure 6.5.

The problem is that of a circular cylinder of unit radius and infinite length in the

domain filled with some medium. From the axisymmetric nature of the problem in the two dimensional plane, the domain around the cylinder was modelled by a sectorial mesh bounded by straight radii at $-15°$ and $15°$. The finite/infinite element mesh is the same as that shown in Figure 7.7. The sectorial domain over $1 \leq r \leq 2$ is divided into two 9-node quadrilateral finite elements in the radial direction. On the inner boundary of the finite element domain $r = 1$ the normal derivatives of radiated potential were given as the Neumann boundary condition, and on the outer boundary at $r = 2$ an infinite element extending over $2 \leq r < \infty$ and $-15° \leq \theta \leq 15°$ is attached. The problem was solved for the wavenumber $k = 4$ and 8.

7.8.2 Wave Directions

Let us deal with the nodes in groups as follow:

(1) Finite element only nodes:

Nodes in $1 \leq r < 2$ belonging only to the finite elements

(2) Finite/infinite element interface nodes:

Nodes at $r = 2$ on the finite/infinite element interface and belonging to both finite and infinite elements

(3) Infinite element only nodes:

Nodes at $r = 4$ belonging only to the infinite element

The wave directions associated with the finite element only nodes are kept globally constant. The wave directions associated with the finite/infinite element interface nodes and the infinite element only nodes vary within the element so that the relative angles from the radial direction are kept the same.

7.8.3 Number of Wave Directions

The wave directions are restricted to be outward and the effect of the number of waves are investigated.

(a) Test Cases

Cases 1 - 4c, the sets of number of waves and directions applied to the model are as shown in Table 7.12. Angle $0°$ indicates the radial direction. The other angles are measured from

138

Table 7.12: Test cases for investigation of increase of wave directions.

Cases	Nodes	Number	Angles
1 (1-1-1)	$1 \leq r < 2$	1	$0°$
	$r = 2$	1	$0°$
	$r > 2$	1	$0°$
2a (3-1-1)	$1 \leq r < 2$	3	$-30°, 0°, 30°$
	$r = 2$	1	$0°$
	$r > 2$	1	$0°$
2b (3-3-1)	$1 \leq r < 2$	3	$-30°, 0°, 30°$
	$r = 2$	3	$-30°, 0°, 30°$
	$r > 2$	1	$0°$
2c (3-3-3)	$1 \leq r < 2$	3	$-30°, 0°, 30°$
	$r = 2$	3	$-30°, 0°, 30°$
	$r > 2$	3	$-30°, 0°, 30°$
3a (5-1-1)	$1 \leq r < 2$	5	$-60°, -30°, 0°, 30°, 60°$
	$r = 2$	1	$0°$
	$r > 2$	1	$0°$
3b (5-5-1)	$1 \leq r < 2$	5	$-60°, -30°, 0°, 30°, 60°$
	$r = 2$	5	$-60°, -30°, 0°, 30°, 60°$
	$r > 2$	1	$0°$
3c (5-5-5)	$1 \leq r < 2$	5	$-60°, -30°, 0°, 30°, 60°$
	$r = 2$	5	$-60°, -30°, 0°, 30°, 60°$
	$r > 2$	5	$-60°, -30°, 0°, 30°, 60°$
4a (9-1-1)	$1 \leq r < 2$	9	$-80°, -60°, -40°, -20°, 0°, 20°, 40°, 60°, 80°$
	$r = 2$	1	$0°$
	$r > 2$	1	$0°$
4b (9-9-1)	$1 \leq r < 2$	9	$-80°, -60°, -40°, -20°, 0°, 20°, 40°, 60°, 80°$
	$r = 2$	9	$-80°, -60°, -40°, -20°, 0°, 20°, 40°, 60°, 80°$
	$r > 2$	1	$0°$
4c (9-9-9)	$1 \leq r < 2$	9	$-80°, -60°, -40°, -20°, 0°, 20°, 40°, 60°, 80°$
	$r = 2$	9	$-80°, -60°, -40°, -20°, 0°, 20°, 40°, 60°, 80°$
	$r > 2$	9	$-80°, -60°, -40°, -20°, 0°, 20°, 40°, 60°, 80°$

the radial direction anti-clockwise.

Case 1 is the most simple case possible. Through the cases from Case1 to Case 4, the number of the waves associated with the finite element only nodes from 1 to 9. Wave directions are distributed between $-90°$ and $90°$ so that no wave propagates inwards. The number of waves associated with the finite/infinite element interface nodes and the infinite element only nodes is chosen to be 1 or the same number as that for finite element only nodes. The numbers in brackets show the combination of number of waves associated with each types of nodes.

Table 7.13: Numerical results of test cases for investigation of increase of wave directions, for $k = 4$.

	Numerical results		Difference from analytical solution		Error	
	Real	Imaginary	Real	Imaginary	Real	Imaginary
Case1						
1.0000	-3.94240612E-01	-1.92371936E-02	2.90919517E-03	-2.29644905E-03	-7.32518340E-03	1.35557740E-01
1.5000	1.51230574E-01	-2.83138697E-01	5.85314508E-04	5.05599409E-03	3.88538285E-03	-1.75436753E-02
2.0000	1.74529553E-01	2.22208270E-01	2.87874574E-03	-1.31321925E-03	1.67709421E-02	-5.87513645E-03
Case2a						
1.0000	-3.96825891E-01	-1.92438206E-02	3.23916174E-04	-2.30307605E-03	-8.15601992E-04	1.35948927E-01
1.5000	1.50579194E-01	-2.87937611E-01	-6.60654919E-05	2.57080086E-04	-4.38550088E-04	-8.92036161E-04
2.0000	1.77023918E-01	2.22641126E-01	5.37311074E-03	-8.80363250E-04	3.13025661E-02	-3.93860676E-03
Case2b						
1.0000	-3.96235626E-01	-1.61589507E-02	9.14181174E-04	7.81793853E-04	-2.30185476E-03	-4.61487304E-02
1.5000	1.50348462E-01	-2.88419683E-01	-2.96797492E-04	-2.24991914E-04	-1.97017479E-03	7.80694167E-04
2.0000	1.68800903E-01	2.22868676E-01	-2.84990426E-03	-6.52813250E-04	-1.66029179E-02	-2.92058384E-03
Case2c						
1.0000	-3.97055938E-01	-1.92608684E-02	9.38691739E-05	-2.32012385E-03	-2.36357093E-04	1.36955247E-01
1.5000	1.50690346E-01	-2.88400702E-01	4.50865081E-05	-2.06010914E-04	2.99289259E-04	7.14832440E-04
2.0000	1.76760084E-01	2.22566185E-01	5.10927674E-03	-9.55304250E-04	2.97655270E-02	-4.27388102E-03
Case3a						
1.0000	-3.96781559E-01	-1.92572846E-02	3.68248174E-04	-2.31654005E-03	-9.27227377E-04	1.36743697E-01
1.5000	1.51136054E-01	-2.87691134E-01	4.90794508E-04	5.03557086E-04	3.25794857E-03	-1.74728092E-03
2.0000	1.76785811E-01	2.22606638E-01	5.13500374E-03	-9.14851250E-04	2.99154069E-02	-4.09290065E-03
Case3b						
1.0000	-3.97203364E-01	-1.70347180E-02	-5.35568261E-05	-9.39734467E-05	1.34852958E-04	5.54718515E-03
1.5000	1.50663372E-01	-2.88171097E-01	1.81125081E-05	2.35940858E-05	1.20232845E-04	-8.18685648E-05
2.0000	1.71751146E-01	2.23609867E-01	1.00338743E-04	8.83777503E-05	5.84551535E-04	3.95388160E-04
Case3c						
1.0000	-3.97151850E-01	-1.69420677E-02	-2.04282615E-06	-1.32314668E-06	5.14371683E-06	7.81043994E-05
1.5000	1.50649567E-01	-2.88193088E-01	4.30750815E-06	1.60308575E-06	2.85937185E-05	-5.56250965E-06
2.0000	1.71668442E-01	2.23559299E-01	1.76347429E-05	3.78097503E-05	1.02736149E-04	1.69154878E-04
Case4a						
1.0000	-3.96812487E-01	-1.92577512E-02	3.37320174E-04	-2.31700665E-03	-8.49352481E-04	1.36771240E-01
1.5000	1.51002883E-01	-2.87815556E-01	3.57623508E-04	3.79135086E-04	2.37394465E-03	-1.31555194E-03
2.0000	1.76918324E-01	2.22531707E-01	5.26751674E-03	-9.89782250E-04	3.06873986E-02	-4.42813017E-03
Case4b						
1.0000	-3.97157686E-01	-1.69233859E-02	-7.87882615E-06	1.73586533E-05	1.98384237E-05	-1.02466885E-03
1.5000	1.50646042E-01	-2.88195022E-01	7.82508150E-07	-3.30914250E-07	5.19437619E-06	1.14823160E-06
2.0000	1.71656003E-01	2.23545657E-01	5.19574290E-06	2.41677503E-05	3.02692599E-05	1.08122715E-04
Case4c						
1.0000	-3.97149837E-01	-1.69408267E-02	-2.98261459E-08	-8.21466791E-08	7.51004919E-08	4.84905955E-06
1.5000	1.50645793E-01	-2.88188136E-01	5.33508150E-07	6.55508575E-06	3.54148648E-06	-2.27453383E-05
2.0000	1.71666909E-01	2.23568501E-01	1.61017429E-05	4.70117503E-05	9.38052268E-05	2.10323180E-04

(b) Results

Tables 7.13 and 7.14 show the numerical results, the difference from the analytical solution and the error for the cases of $k = 4$ and $k = 8$, respectively.

Because the problem dealt with here is the Hankel source problem, even by a very simple model of Case 1 which uses only a single radial wave for all nodes, a reasonable accuracy is obtained. In the results for $k = 4$, there is a clear tendency that the increase of the number of waves leads to the better accuracy is clearly observed, although Case 2, where the maximum number of waves at a node is three, is a little exceptional. The same tendency can be seen also in the results for $k = 8$.

7.8.4 Incoming Waves

The effect of adding the inward wave directions are investigated.

Table 7.14: Numerical results of test cases for investigation of increase of wave directions, for $k = 8$.

	Numerical results		Difference from analytical solution		Error	
	Real	Imaginary	Real	Imaginary	Real	Imaginary
Case1						
1.0000	1.66898073E-01	2.15919611E-01	-4.75273410E-03	-7.60187840E-03	-2.76883877E-02	-3.40096087E-02
1.5000	5.00321065E-02	-2.19722793E-01	2.34279570E-03	5.51451960E-03	4.91262226E-02	-2.44831531E-02
2.0000	-1.79497515E-01	1.10045419E-01	-4.59844100E-03	1.42344219E-02	2.62919688E-02	1.48567726E-01
Case2a						
1.0000	1.70939945E-01	2.24006397E-01	-7.10862100E-04	4.84907600E-04	-4.14132687E-03	2.16940036E-03
1.5000	4.61611925E-02	-2.24167660E-01	-1.52811830E-03	1.06965260E-03	-3.20432037E-02	-4.74900267E-03
2.0000	-1.75791157E-01	9.18027897E-02	-8.92083000E-04	-4.00820738E-03	5.10055874E-03	-4.18345232E-02
Case2b						
1.0000	1.72158876E-01	2.24523624E-01	5.08068900E-04	1.00213460E-03	2.95989811E-03	4.48339264E-03
1.5000	4.75725329E-02	-2.32014378E-01	-1.16777900E-04	-6.77706540E-03	-2.44872274E-03	3.00885556E-02
2.0000	-1.78117832E-01	9.87510778E-02	-3.21875800E-03	2.94008072E-03	1.84035165E-02	3.06862553E-02
Case2c						
1.0000	1.71069018E-01	2.22007977E-01	-5.81789100E-04	-1.51351240E-03	-3.38937585E-03	-6.77121651E-03
1.5000	5.58637725E-02	-2.38422472E-01	8.17446170E-03	-1.31851594E-02	1.71410775E-01	5.85389661E-02
2.0000	-1.53557782E-01	1.01163243E-01	2.13412920E-02	5.35224592E-03	-1.22020612E-01	5.58625427E-02
Case3a						
1.0000	1.71439795E-01	2.23064557E-01	-2.11012100E-04	-4.56932400E-04	-1.22931027E-03	-2.04424372E-03
1.5000	4.80559040E-02	-2.25643929E-01	3.66593200E-04	-4.06616400E-04	7.68711466E-03	1.80527993E-03
2.0000	-1.75029184E-01	9.57801367E-02	-1.30110000E-04	-3.08603800E-05	7.43914745E-04	-3.22096429E-04
Case3b						
1.0000	1.71630059E-01	2.23414368E-01	-2.07481000E-05	-1.07121400E-04	-1.20873885E-04	-4.79244301E-04
1.5000	4.77341920E-02	-2.25375275E-01	4.48812000E-05	-1.37962400E-04	9.41116557E-04	6.12520183E-04
2.0000	-1.74861101E-01	9.61008673E-02	3.79730000E-05	2.89870220E-04	-2.17113785E-04	3.02543788E-03
Case3c						
1.0000	1.71895850E-01	2.23500300E-01	2.45042900E-04	-2.11894000E-05	1.42756626E-03	-9.47980441E-05
1.5000	4.84920347E-02	-2.25628504E-01	8.02723900E-04	-3.91191400E-04	1.68323653E-02	1.73679661E-03
2.0000	-1.75368923E-01	9.61807323E-02	-4.69849000E-04	3.69735220E-04	2.68640073E-03	3.85900608E-03
Case4a						
1.0000	1.71451200E-01	2.23023518E-01	-1.99607100E-04	-4.97971400E-04	-1.16286724E-03	-2.22784575E-03
1.5000	4.80815045E-02	-2.25722081E-01	3.92193700E-04	-4.84768400E-04	8.22393307E-03	2.15225619E-03
2.0000	-1.74760420E-01	9.54978098E-02	1.38654000E-04	-3.13187280E-04	-7.92765775E-04	-3.26880306E-03
Case4b						
1.0000	1.71643494E-01	2.23518971E-01	-7.31310000E-06	-2.51840000E-06	-4.26045186E-05	-1.12669256E-05
1.5000	4.76417067E-02	-2.25259610E-01	-4.76041000E-05	-2.22974000E-05	-9.98213210E-04	9.89951431E-05
2.0000	-1.74888433E-01	9.58088801E-02	1.06410000E-05	-2.11698000E-06	-6.08408024E-05	-2.20953759E-05
Case4c						
1.0000	1.71643911E-01	2.23517240E-01	-6.89610000E-06	-4.24940000E-06	-4.01751679E-05	-1.90111475E-05
1.5000	4.76394532E-02	-2.25256165E-01	-4.98576000E-05	-1.88524000E-05	-1.04546699E-03	8.37001640E-05
2.0000	-1.74886563E-01	9.58080815E-02	1.25110000E-05	-2.91558000E-06	-7.15326829E-05	-3.04305360E-05

(a) Test Cases

Cases 5a - 6c, the sets of number of waves and directions applied to the model are shown in Table 7.15. The wave directions are basically spaced every 30°. In the Cases 3a - 3c in Table 7.12, only the wave propagating outwards are applied. However, in Cases 5a - 5c, incoming waves are applied to the finite element only nodes, and in Cases 6a - 6c, incoming waves are applied also to the finite/infinite element interface nodes and the infinite element only nodes. The results are compared to those of Cases 3a - 3c.

Table 7.15: Test cases for investigation of inclusion of incoming waves.

Cases	Nodes	Number	Angles
5a (12-1-1)	$1 \leq r < 2$	12	$-150°, -120°, -90°, -60°, -30°, 0°, 30°, 60°, 90°,$ $120°, 150°, 180°$
	$r = 2$	1	$0°$
	$r > 2$	1	$0°$
5b (12-5-1)	$1 \leq r < 2$	12	$-150°, -120°, -90°, -60°, -30°, 0°, 30°, 60°, 90°,$ $120°, 150°, 180°$
	$r = 2$	5	$-60°, -30°, 0°, 30°, 60°$
	$r > 2$	1	$0°$
5c (12-5-5)	$1 \leq r < 2$	12	$-150°, -120°, -90°, -60°, -30°, 0°, 30°, 60°, 90°,$ $120°, 150°, 180°$
	$r = 2$	5	$-60°, -30°, 0°, 30°, 60°$
	$r > 2$	5	$-60°, -30°, 0°, 30°, 60°$
6a (12-1-1)	$1 \leq r < 2$	12	$-150°, -120°, -90°, -60°, -30°, 0°, 30°, 60°, 90°,$ $120°, 150°, 180°$
	$r = 2$	1	$0°$
	$r > 2$	1	$0°$
6b (12-12-1)	$1 \leq r < 2$	12	$-150°, -120°, -90°, -60°, -30°, 0°, 30°, 60°, 90°,$ $120°, 150°, 180°$
	$r = 2$	12	$-150°, -120°, -90°, -60°, -30°, 0°, 30°, 60°, 90°,$ $120°, 150°, 180°$
	$r > 2$	1	$0°$
6c (12-12-12)	$1 \leq r < 2$	12	$-150°, -120°, -90°, -60°, -30°, 0°, 30°, 60°, 90°,$ $120°, 150°, 180°$
	$r = 2$	12	$-150°, -120°, -90°, -60°, -30°, 0°, 30°, 60°, 90°,$ $120°, 150°, 180°$
	$r > 2$	12	$-150°, -120°, -90°, -60°, -30°, 0°, 30°, 60°, 90°,$ $120°, 150°, 180°$

Table 7.16: Numerical results of test cases for investigation of inclusion of incoming waves, for $k = 4$.

	Numerical results		Difference from analytical solution		Error	
	Real	Imaginary	Real	Imaginary	Real	Imaginary
Case5a						
1.0000	-3.96846905E-01	-1.92200460E-02	-3.02902174E-04	2.27930145E-03	-7.62689968E-04	1.34545530E-01
1.5000	1.50948625E-01	-2.87791034E-01	-3.03365508E-04	-4.03657086E-04	2.01377401E-03	-1.40064026E-03
2.0000	1.76922721E-01	2.22551658E-01	-5.27191374E-03	9.69831250E-04	3.07130146E-02	-4.33887253E-03
Case5b						
1.0000	-3.97202696E-01	-1.70347471E-02	5.28888261E-05	9.40025467E-05	1.33170973E-04	5.54890291E-03
1.5000	1.50660804E-01	-2.88173273E-01	-1.55445081E-05	-2.14180858E-05	1.03186175E-04	-7.43181135E-05
2.0000	1.71749301E-01	2.23610601E-01	-9.84937429E-05	-8.91117503E-05	5.73802969E-04	3.98671960E-04
Case5c						
1.0000	-3.97150312E-01	-1.69423631E-02	5.04826146E-07	1.61854668E-06	1.27112273E-06	9.55416495E-05
1.5000	1.50645932E-01	-2.88193704E-01	-6.72508150E-07	-9.87085750E-07	4.46418395E-06	-3.42506570E-06
2.0000	1.71666663E-01	2.23561785E-01	-1.58557429E-05	-4.02957503E-05	9.23720847E-05	1.80276851E-04
Case6a						
1.0000	-3.96846905E-01	-1.92200460E-02	-3.02902174E-04	2.27930145E-03	-7.62689968E-04	1.34545530E-01
1.5000	1.50948625E-01	-2.87791034E-01	-3.03365508E-04	-4.03657086E-04	2.01377401E-03	-1.40064026E-03
2.0000	1.76922721E-01	2.22551658E-01	-5.27191374E-03	9.69831250E-04	3.07130146E-02	-4.33887253E-03
Case6b						
1.0000	-4.02319458E-01	-1.93508726E-02	5.16965083E-03	2.41012805E-03	1.30168786E-02	1.42268130E-01
1.5000	1.53371922E-01	-2.88046751E-01	-2.72666251E-03	-1.47940086E-04	1.80998892E-02	-5.13333834E-04
2.0000	1.79901708E-01	2.22931279E-01	-8.25090074E-03	5.90210250E-04	4.80679402E-02	-2.64050786E-03
Case6c						
1.0000	-3.99637738E-01	-2.32775849E-02	2.48793083E-03	6.33684035E-03	6.26446439E-03	3.74059140E-01
1.5000	1.50742382E-01	-2.86621741E-01	-9.71225081E-05	-1.57295009E-03	6.44710019E-04	-5.45794261E-03
2.0000	1.70804276E-01	2.26597971E-01	8.46531257E-04	-3.07648175E-03	-4.93170566E-03	1.37636957E-02

(b) Results

Table 7.16 shows the numerical results, the difference from the analytical solution and the error for the case of $k = 4$. Firstly, comparing the results of Cases 5a - 5c to those of Cases 3a - 3c, the increase of the waves propagating inwards in *finite elements* improve the accuracy. However, comparing the results of Cases 6a - 6c to those of Cases 5a - 5c, it is confirmed that the increase of the waves propagating inwards for the *infinite element* make the results less accurate.

7.8.5 Wave Directions in Infinite Element

To see the effect of number and directions of waves in infinite element more clearly, the another sets of tests were carried out. The number and the directions of waves associated with the finite element only nodes were fixed to be 12 directions every 30°. The numbers of waves associated with the finite/infinte element interface nodes and the infinite element only nodes were kept to be the same, and varied from 1 to 12.

(a) Test Cases

Cases 7a - 7g, the sets of number of waves and directions applied to the model are shown in Table 7.17. The first and the reference direction denoted by 0° was the radial direction, and the waves were added by ±30° each until they filled 360° every 30°. Cases 7a - 7c include outward waves only, Case 7d includes the waves at ±90°, and Cases 7e - 7g include incoming waves.

(b) Results

Table 7.18 shows the numerical results, the difference from the analytical solution and the error for the case of $k = 4$. From Case 7a to 7c, the accuracy improves as waves propagating outwards are increased. However, the results of Case 7d are less accurate than 7c, which means that the waves at ±90° from the radial direction are not suitable to be used in the infinite element. From Case 7e to 7g, the accuracy clearly become worse as waves propagating inwards are increased. This result agrees with the results shown in Tables 7.13, 7.14 and 7.16 in the previous two subsections in this section.

143

Table 7.17: Test cases for investigation of effect of wave directions associated with infinite element nodes.

Cases	Nodes	Number	Angles
7a (12-1-1)	$1 \leq r < 2$	12	$-150°, -120°, -90°, -60°, -30°, 0°, 30°, 60°, 90°, 120°, 150°, 180°$
	$r = 2$	1	$0°$
	$r > 2$	1	$0°$
7b (12-3-3)	$1 \leq r < 2$	12	$-150°, -120°, -90°, -60°, -30°, 0°, 30°, 60°, 90°, 120°, 150°, 180°$
	$r = 2$	3	$-30°, 0°, 30°$
	$r > 2$	3	$-30°, 0°, 30°$
7c (12-5-5)	$1 \leq r < 2$	12	$-150°, -120°, -90°, -60°, -30°, 0°, 30°, 60°, 90°, 120°, 150°, 180°$
	$r = 2$	5	$-60°, -30°, 0°, 30°, 60°$
	$r > 2$	5	$-60°, -30°, 0°, 30°, 60°$
7d (12-7-7)	$1 \leq r < 2$	12	$-150°, -120°, -90°, -60°, -30°, 0°, 30°, 60°, 90°, 120°, 150°, 180°$
	$r = 2$	7	$-90°, -60°, -30°, 0°, 30°, 60°, 90°$
	$r > 2$	7	$-90°, -60°, -30°, 0°, 30°, 60°, 90°$
7e (12-9-9)	$1 \leq r < 2$	12	$-150°, -120°, -90°, -60°, -30°, 0°, 30°, 60°, 90°, 120°, 150°, 180°$
	$r = 2$	9	$-120°, -90°, -60°, -30°, 0°, 30°, 60°, 90°, 120°$
	$r > 2$	9	$-120°, -90°, -60°, -30°, 0°, 30°, 60°, 90°, 120°$
7f (12-11-11)	$1 \leq r < 2$	12	$-150°, -120°, -90°, -60°, -30°, 0°, 30°, 60°, 90°, 120°, 150°, 180°$
	$r = 2$	11	$-150°, -120°, -90°, -60°, -30°, 0°, 30°, 60°, 90°, 120°, 150°$
	$r > 2$	11	$-150°, -120°, -90°, -60°, -30°, 0°, 30°, 60°, 90°, 120°, 150°,$
7g (12-12-12)	$1 \leq r < 2$	12	$-150°, -120°, -90°, -60°, -30°, 0°, 30°, 60°, 90°, 120°, 150°, 180°$
	$r = 2$	12	$-150°, -120°, -90°, -60°, -30°, 0°, 30°, 60°, 90°, 120°, 150°, 180°$
	$r > 2$	12	$-150°, -120°, -90°, -60°, -30°, 0°, 30°, 60°, 90°, 120°, 150°, 180°$

144

Table 7.18: Numerical results of test cases for investigation of effect of wave directions associated with infinite element nodes, for $k = 4$.

	Numerical results		Difference from analytical solution		Error	
	Real	Imaginary	Real	Imaginary	Real	Imaginary
Case7a						
1.0000	-3.96846905E-01	-1.92200460E-02	-3.02902174E-04	2.27930145E-03	-7.62689968E-04	1.34545530E-01
1.5000	1.50948625E-01	-2.87791034E-01	-3.03365508E-04	-4.03657086E-04	2.01377401E-03	-1.40064026E-03
2.0000	1.76922721E-01	2.22551658E-01	-5.27191374E-03	9.69831250E-04	3.07130146E-02	-4.33887253E-03
Case7b						
1.0000	-3.97154759E-01	-1.69539302E-02	4.95182615E-06	1.31856467E-05	1.24684088E-05	7.78339266E-04
1.5000	1.50646407E-01	-2.88189194E-01	-1.14750815E-06	-5.49708575E-06	7.61728682E-06	-1.90742089E-05
2.0000	1.71668209E-01	2.23566748E-01	-1.74017429E-05	-4.52587503E-05	1.01378742E-04	2.02480533E-04
Case7c						
1.0000	-3.97150312E-01	-1.69423631E-02	5.04826146E-07	1.61854668E-06	1.27112273E-06	9.55416495E-05
1.5000	1.50645932E-01	-2.88193704E-01	-6.72508150E-07	-9.87085750E-07	4.46418395E-06	-3.42506570E-06
2.0000	1.71666663E-01	2.23561785E-01	-1.58557429E-05	-4.02957503E-05	9.23720847E-05	1.80276851E-04
Case7d						
1.0000	-3.97150567E-01	-1.69418463E-02	7.59826146E-07	1.10174668E-06	1.91319782E-06	6.50353162E-05
1.5000	1.50647049E-01	-2.88186439E-01	-1.78950815E-06	-8.25208575E-06	1.18789543E-05	-2.86337188E-05
2.0000	1.71666882E-01	2.23566719E-01	-1.60747429E-05	-4.52297503E-05	9.36479307E-05	2.02350792E-04
Case7e						
1.0000	-3.97158226E-01	-1.69460183E-02	8.41882615E-06	5.27374668E-06	2.11981121E-05	3.11305484E-04
1.5000	1.50647336E-01	-2.88186677E-01	-2.07650815E-06	-8.01408575E-06	1.37840922E-05	-2.78078882E-05
2.0000	1.71666311E-01	2.23566818E-01	-1.55037429E-05	-4.53287503E-05	9.03214098E-05	2.02793702E-04
Case7f						
1.0000	-3.98278260E-01	-1.71971059E-02	1.12845283E-03	2.56361347E-04	2.84137826E-03	1.51328264E-02
1.5000	1.48701206E-01	-2.87662424E-01	1.94405349E-03	-5.32267086E-04	-1.29048435E-02	-1.84690108E-03
2.0000	1.63653701E-01	2.25485576E-01	7.99710626E-03	-1.96408675E-03	-4.65893891E-02	8.78701532E-03
Case7g						
1.0000	-3.99637738E-01	-2.32775849E-02	2.48793083E-03	6.33684035E-03	6.26446439E-03	3.74059140E-01
1.5000	1.50742382E-01	-2.86621741E-01	-9.71225081E-05	-1.57295009E-03	6.44710019E-04	-5.45794261E-03
2.0000	1.70804276E-01	2.26597971E-01	8.46531257E-04	-3.07648175E-03	-4.93170566E-03	1.37636957E-02

7.9 Radiation Condition on Outer Boundary

As discussed in Section 7.4, the application of the radiation condition on the outer boundary should be unnecessary when the outer boundary is truly placed at infinity but necessary when it is at a finite distance. This is confirmed by numerical experiments by using the different expressions for the term regarding to the outer boundary.

The weak form is presented by Equation (7.21) for the special wave infinite elements. This expression already contains the application of the radiation condition over the outer boundary Γ_∞. If the radiation condition is not applied, the term over the outer boundary takes the form $\partial\phi/\partial n$ instead of $ik\phi$. Therefore in this case the last term in the left hand side of the weak form (7.21) becomes

$$-\int_{\Gamma_\infty} W \frac{\partial\phi}{\partial n} \phi d\Gamma \tag{7.52}$$

instead of

$$-\int_{\Gamma_\infty} ikW\phi d\Gamma \tag{7.53}$$

145

and the weak form becomes

$$\int_\Omega \left(\nabla W \nabla \phi - k^2 W \phi \right) d\Omega - \int_{\Gamma_\infty} W \frac{\partial \phi}{\partial n} \phi d\Gamma = 0 \tag{7.54}$$

then the element damping matrix component ikC_{ij} where C_{ij} is given by Equation (7.27) is replaced by

$$\int_{\Gamma_\infty} S_i^m \nabla S_j^l \cdot \mathbf{n} \, d\Gamma \tag{7.55}$$

In this section, using the Hankel source problem again, the results of three series of numerical testing are shown. In the first test, the effect of application of the radiation condition on the outer boundary is examined. In the second test, the radiation condition is applied only to non-radial waves. In the third test, the application of the cylindrical damper type radiation condition is considered.

The results show that the application of the radiation condition on the outer boundary improves the accuracy, but applying the radiation condition to the wave propagating in the radial direction has smaller effect than applying it to the waves propagating in non-radial directions. The difference of the form of the condition between a plane damper and a cylindrical damper is negligible for improvement of accuracy in the current test cases.

7.9.1 Special Wave Finite and Infinite Element Model

The geometry of the Hankel source problem and the finite/infinite mesh model are the same as those in Section 7.8.

7.9.2 Infinite Element Model Without Radiation Condition

(a) Test Cases

As concerns the details about wave directions, the model which is the same as Cases 5a - 5c in the previous section are used. However, because the modelling of the problem at the outer boundary is different these cases are named Cases 8a - 8c, respectively.

(b) Results

Table 7.19 shows the numerical results and the difference from the analytical solution and the error for the case of $k = 4$. Looking at the results of Cases 8a - 8c, the results become less accurate as the number of waves in infinite element is increased. This seems to be

146

Table 7.19: Numerical results for test cases without radiation condition applied on outer boundary, for $k = 4$.

	Numerical results		Difference from analytical solution		Error	
	Real	Imaginary	Real	Imaginary	Real	Imaginary
Case8a						
1.0000	-3.97151965E-01	-1.69408878E-02	2.15782615E-06	1.43246679E-07	5.43328010E-06	8.45574872E-06
1.5000	1.50645411E-01	-2.88194475E-01	-1.51508150E-07	-2.16085750E-07	1.00572796E-06	-7.49790876E-07
2.0000	1.71652266E-01	2.23528734E-01	-1.45874290E-06	-7.24475032E-06	8.49831659E-06	3.24118739E-05
Case8b						
1.0000	-3.95396617E-01	-1.70879817E-02	-1.75319017E-03	1.47237147E-04	-4.41443038E-03	8.69130316E-03
1.5000	1.49913938E-01	-2.87977905E-01	7.31321492E-04	-2.16786086E-04	-4.85459346E-03	-7.52220955E-04
2.0000	1.65590490E-01	2.19454489E-01	6.06031726E-03	4.06700025E-03	-3.53060807E-02	-1.81951197E-02
Case8c						
1.0000	-3.81268242E-01	-3.03138932E-02	-1.58815652E-02	1.33731486E-02	-3.99888528E-02	7.89407373E-01
1.5000	1.46719102E-01	-2.84692852E-01	3.92615749E-03	-3.50183909E-03	-2.60622704E-02	-1.21509493E-02
2.0000	1.63262490E-01	2.33921006E-01	8.38831726E-03	-1.03995168E-02	-4.88684987E-02	4.65258029E-02

unreasonable as the increase of waves has normally has improved the results. Compared to the results of Cases 5a - 5c, the results of Cases 8b and 8c are less accurate than those of Cases 5b and 5c, respectively. This means that using the term $ik\phi$ leads to the better accuracy than using the term $\partial\phi/\partial n$, and it proves that applying the radiation condition on the outer boundary leads to better accuracy. However, comparing the results of Case 8a to those of Case 5a, where these cases use only a single wave propagating in the radial direction in the infinite element, the former is closer to the analytical solution than the latter. This could mean that whether applying the radiation condition on the outer boundary or not has little effect on the accuracy regarding the wave propagating only in the radial direction like the conventional infinite elements. From these results, it can be concluded that the wave propagating in the radial direction satisfies the radiation condition with better accuracy than the non-radial waves do.

7.9.3 Infinite Element Model with Combined Radiation Condition

Because the application of the radiation condition on the outer boundary made the results less accurate for the infinite element in which only a single radial wave propagates, the attempt of a combined application of the radiation condition was made. In detail, the $ik\phi$ term is used only for non-radial waves and the $\partial\phi/\partial n$ term is used for the radial wave.

(a) Test Cases

As concerns the details about wave directions, the model which is the same as Cases 5a - 5c in the previous section are again used. However, because the modelling of the problem at the outer boundary is different these cases are named Cases 9a - 9c, respectively.

Table 7.20: Numerical results for test cases with combined radiation condition applied on outer boundary, for $k = 4$.

	Numerical results		Difference from analytical solution		Error	
	Real	Imaginary	Real	Imaginary	Real	Imaginary
Case9a						
1.0000	-3.97151965E-01	-1.69408878E-02	2.15782615E-06	1.43246679E-07	5.43328010E-06	8.45574872E-06
1.5000	1.50645411E-01	-2.88194475E-01	-1.51508150E-07	-2.16085750E-07	1.00572796E-06	-7.49790876E-07
2.0000	1.71652266E-01	2.23528734E-01	-1.45874290E-06	-7.24475032E-06	8.49831659E-06	3.24118739E-05
Case9b						
1.0000	-3.96131425E-01	-1.86096429E-02	-1.01838217E-03	1.66889835E-03	-2.56422679E-03	9.85138724E-02
1.5000	1.50041974E-01	-2.87994546E-01	6.03285492E-04	-2.00145086E-04	-4.00467624E-03	-6.94478739E-04
2.0000	1.73317351E-01	2.16514495E-01	-1.66654374E-03	7.00699425E-03	9.70891876E-03	-3.13481906E-02
Case9c						
1.0000	-3.90924729E-01	-1.10303659E-02	-6.22507817E-03	-5.91037865E-03	-1.56743830E-02	-3.48885413E-01
1.5000	1.49381346E-01	-2.90510486E-01	1.26391349E-03	2.31579491E-03	-8.38999844E-03	8.03552246E-03
2.0000	1.85593335E-01	2.21801958E-01	-1.39425277E-02	1.71953125E-03	8.12261123E-02	-7.69291246E-03

(b) Results

Table 7.20 shows the numerical results, the difference from the analytical solution, and the error for the case of $k = 4$. Case 9a is the exactly same as Case 8a and more accurate than Case 5a. Cases 9b and 9c, in which combined boundary condition is applied on the outer boundary, are more accurate than Cases 8b and 8c, however, less accurate than Cases 5b and 5c, respectively. And also, looking at Cases 9a - 9c, the results of Case 9b is the least accurate. This tendency of accuracy with respect to the increase of the wave directions does not seem to be reasonable.

7.9.4 Cylindrical Damper Condition on Outer Boundary

It has been presented that the application of the radiation condition on the outer boundary is necessary for better accuracy. This means that the radiation condition is not completely satisfied on the outer boundary, as it is at a finite distance from the 'pole' when a Gauss-Legendre integration scheme is used. Therefore another attempt to apply the cylindrical damper condition given by Equation (2.32) is considered. Because for the Hankel source problem in two dimensions, naturally cylindrical damper can be more accurate than plane damper condition given by the same form as the radiation condition applied above, the cylindrical damper could improve the accuracy of the results.

(a) Test Cases

As concerns the details about wave directions, the model which is the same as Cases 5a - 5c in the previous section are again used. However, because the modelling of the problem at the outer boundary is different these cases are named Cases 10a - 10c, respectively.

Table 7.21: Numerical results for test cases with cylindrical damper condition applied on outer boundary, for $k = 4$.

	Numerical results		Difference from analytical solution		Error	
	Real	Imaginary	Real	Imaginary	Real	Imaginary
Case10a						
1.0000	-3.96861330E-01	-1.91969340E-02	-2.88477174E-04	2.25618945E-03	-7.26368662E-04	1.33181245E-01
1.5000	1.50966348E-01	-2.87785729E-01	-3.21088508E-04	-4.08962086E-04	2.13142126E-03	-1.41904795E-03
2.0000	1.77049101E-01	2.22669653E-01	-5.39829374E-03	8.51836250E-04	3.14492768E-02	-3.81098145E-03
Case10b						
1.0000	-3.97202721E-01	-1.70345985E-02	5.29138261E-05	9.38539467E-05	1.33233921E-04	5.54013115E-03
1.5000	1.50661015E-01	-2.88173201E-01	-1.57555081E-05	-2.14900858E-05	1.04586817E-04	-7.45679446E-05
2.0000	1.71748425E-01	2.23615224E-01	-9.76177429E-05	-9.37347503E-05	5.68699585E-04	4.19354536E-04
Case10c						
1.0000	-3.97150362E-01	-1.69423202E-02	5.54826146E-07	1.57564668E-06	1.39701980E-06	9.30092933E-05
1.5000	1.50645954E-01	-2.88193752E-01	-6.94508150E-07	-9.39085750E-07	4.61022240E-06	-3.25851162E-06
2.0000	1.71666660E-01	2.23561785E-01	-1.58527429E-05	-4.02957503E-05	9.23546073E-05	1.80276851E-04

(b) Results

Table 7.21 shows the numerical results, the difference from the analytical solution, and the error for the case of $k = 4$.

Comparing the results of Cases 10a - 10c to those of Cases 5a - 5c, the differences between these numerical results are quite small, and the accuracies are almost the same. It can be said that the contribution of the additional term in the cylindrical damper condition compared to the plane damper condition is negligibly small. In these cases, application of the cylindrical damper does not improve the accuracy.

7.10 Scattering Problem

Table 7.22: Test cases for scattering problem using multiple waves in infinite elements.

Cases	Nodes	Number	Angles
11a (12-1-1)	$1 \leq r < 2$	12	$-150°, -120°, -90°, -60°, -30°, 0°, 30°, 60°, 90°, 120°, 150°, 180°$
	$r = 2$	1	$0°$
	$r > 2$	1	$0°$
11b (12-5-1)	$1 \leq r < 2$	12	$-150°, -120°, -90°, -60°, -30°, 0°, 30°, 60°, 90°, 120°, 150°, 180°$
	$r = 2$	5	$-60°, -30°, 0°, 30°, 60°$
	$r > 2$	1	$0°$
11c (12-5-5)	$1 \leq r < 2$	12	$-150°, -120°, -90°, -60°, -30°, 0°, 30°, 60°, 90°, 120°, 150°, 180°$
	$r = 2$	5	$-60°, -30°, 0°, 30°, 60°$
	$r > 2$	5	$-60°, -30°, 0°, 30°, 60°$

As a more realistic example than the Hankel source problem, the problem of plane wave scattered by a circular cylinder was considered. The problem is the same as dealt with in section 7.7. The geometry of the problem in two dimensions and the finite/infinite element mesh model are shown in Figures 6.11 and 7.11. The problem was solved for the wavenumbers $k = 4$ and 8.

7.10.1 Multiple Wave Infinite Element Model

(a) Test Cases

Cases 11a - 11c, the sets of number of waves and directions applied to the model are shown in Table 7.22. The wave directions are basically spaced every 30° so that 12 waves are applied to the finite element only nodes and 1 - 5 waves are applied to the finite/infinite element nodes and the infinite element only nodes. 0° indicates the radial direction. The other angles are measured from the radial direction anti-clockwise. The distribution of the wave directions as the function of the distance from the 'pole' is the same as Cases 5a - 5c for the Hankel source problem shown in Table 7.15 in Section 7.8.

(2) Results

Figure 7.16 shows the numerical results of the scattered potential with the analytical solution for the case of $k = 4$, and Figure 7.17 shows the difference from the analytical solution. Considering physically the wave field around the cylinder, it was anticipated that

150
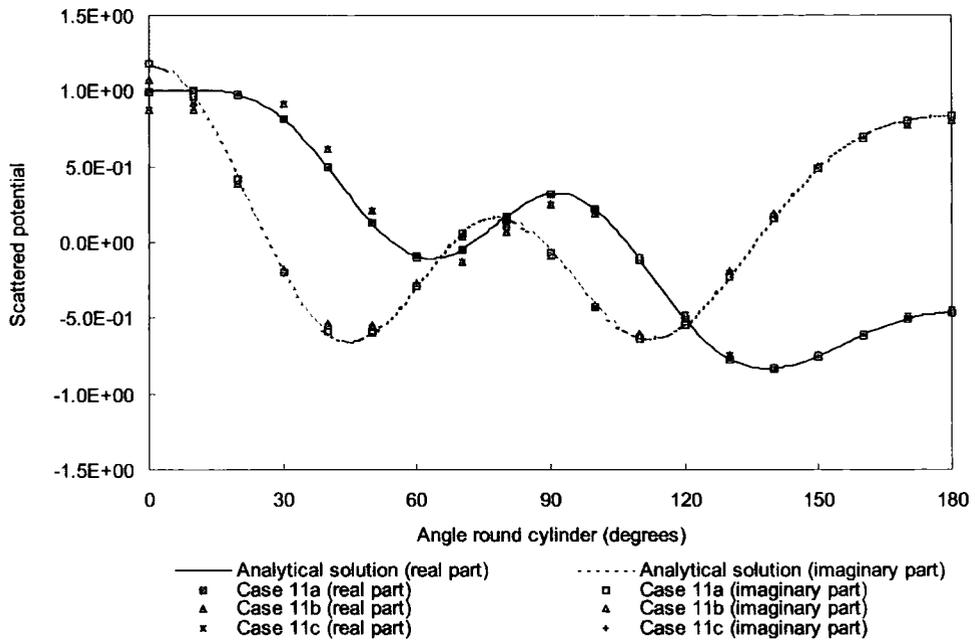
Figure 7.16: Real and imaginary parts of scattered potential obtained using multiple waves in infinite elements, along the circumference of the cylinder, for $k = 4$.

Figure 7.17: Difference from analytical solution in real and imaginary parts of scattered potential obtained using multiple waves in infinite elements, along the circumference of the cylinder, for $k = 4$.

the application of multiple waves is more suitable and effective for the scattering problem than the Hankel source problem in which the increase of the wave directions in infinite elements improved the accuracy of the results. However, the most accurate results are

151

Table 7.23: Test cases for scattering problem using single wave on finite/infinite element interface.

Cases	Nodes	Number	Angles
11d	$1 \leq r < 2$	12	$-150°, -120°, -90°, -60°, -30°, 0°, 30°, 60°, 90°, 120°, 150°, 180°$
	$r > 2$	1	$0°$
	$r = 2$	5	$-60°, -30°, 0°, (12\text{-}1\text{-}5) \ 30°, 60°$

obtained by Case 11a, which uses only a single wave propagating in the radial direction in infinite elements. The accuracies of the results of Cases 11b and 11c are roughly same and poorer than Case 11a although multiple waves are applied to the infinite elements in these cases. Although efforts have been made to try to discover the problem in the theory and the program code, the cause is not clear to date.

7.10.2 Single Wave on Finite/Infinite Element Interface Model

Although it is certain that the increase of the waves propagating outwards in infinite element improved accuracy of the results in case of the Hankel source problem, it made the results less accurate in case of the scattering problem as shown in Figure 7.16. The cause of this problem has not been discovered yet in spite of efforts to search for the cause of the problem in the code from the theory. However different way of applying multiple waves to the infinite element was tried, and the results has shown that the use of multiple waves in infinite element can improve the accuracy in case of the scattering problem.

(a) Test Cases

Case 11d, the new set of number of waves and directions applied to the model is shown in Table 7.23. The total number of waves applied to the whole problem is the same as Case 11b shown in Table 7.23, in which 5 waves were applied to the finite/infinite element interface nodes and a single radial wave was applied to the infinite element only nodes. However only a single radial wave was applied to the finite/infinite element interface nodes and 5 waves were applied to the infinite element only nodes in Case 11d. This model may look somewhat peculiar considering the scattered wave field. Normally it can be expected that the near field to the scattering object should contain components of waves propagating in many different directions, and that the further field should become simpler to become similar to the wave propagating only in the radial direction outwards.
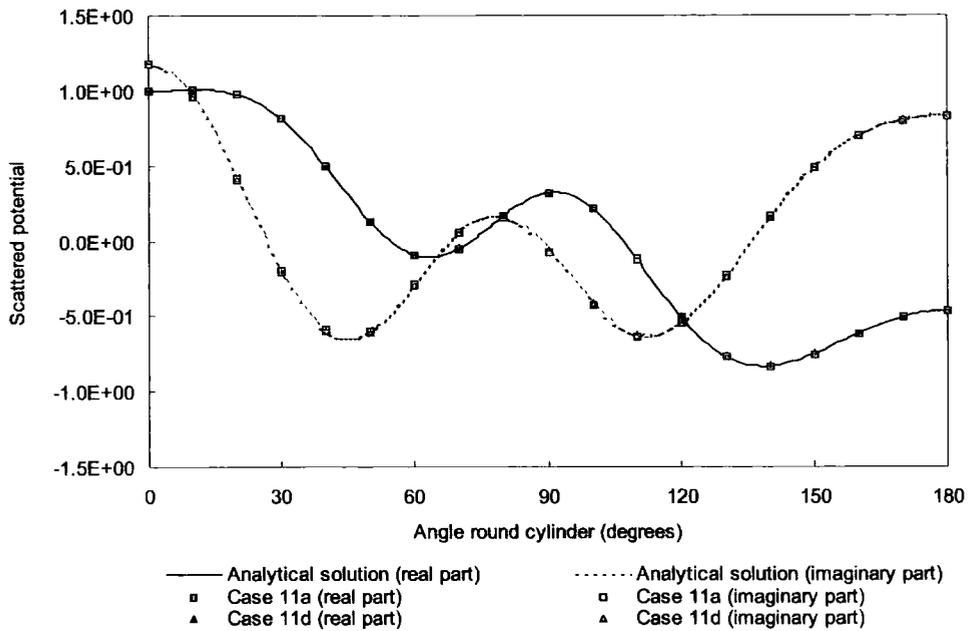
Figure 7.18: Real and imaginary parts of scattered potential obtained using single wave on finite/infinite element interface, along the circumference of the cylinder, for $k = 4$.
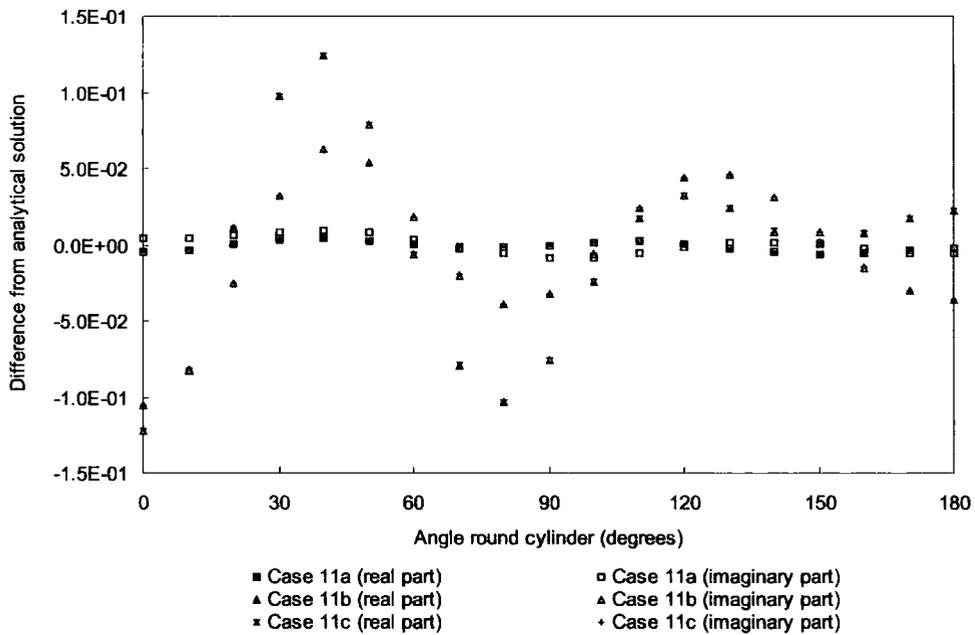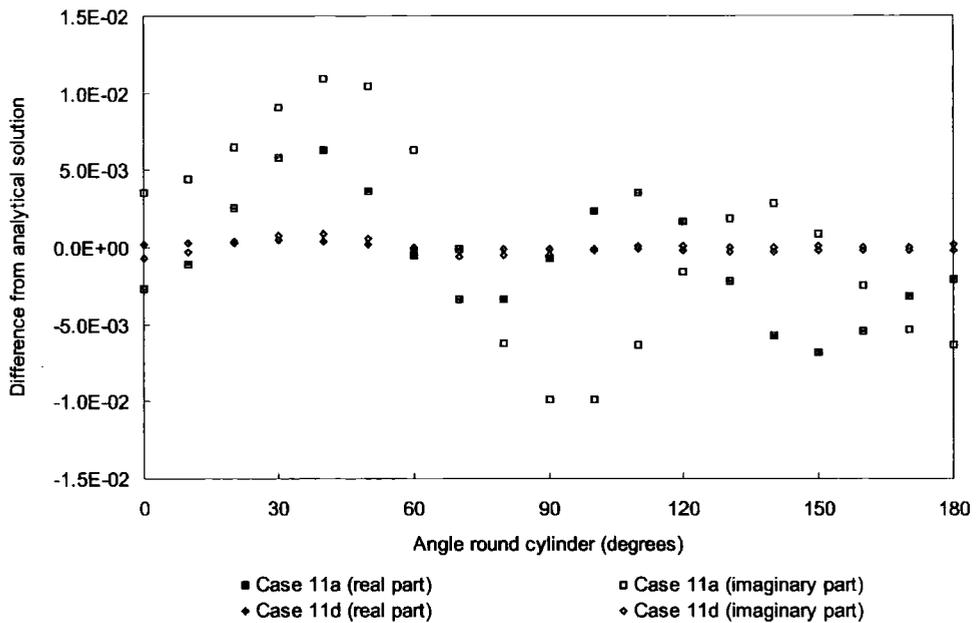

Figure 7.19: Difference from analytical solution in real and imaginary parts of scattered potential obtained using single wave on finite/infinite element interface, along the circumference of the cylinder, for $k = 4$.

(2) Results

Figure 7.18 shows the numerical results of the scattered potential with the analytical solution for the case of $k = 4$, and Figure 7.19 shows the difference from the analytical

solution. The accuracy is obviously better in the results of Case 11d than those in Case 11a. This means that the use of multiple waves at infinite element only nodes improved the accuracy. It may seem to be unusual to apply only a single wave to the node in the nearer field and multiple waves in the further field. However this shows that the increase of the waves in infinite elements improve the accuracy of the numerical results.

This result may indicate that there could be the cause of the inaccuracy in the results of Cases 11b and 11c in dealing with the wave directions on the finite/infinite element interface. However it has not been discovered yet.

7.11 Conclusions

The special wave infinite elements, which is the new concept of mapped wave infinite elements with multiple wave directions, have been developed. In the conventional mapped wave infinite elements only a single wave propagating in the radial direction is allowed. In contrast, the shape functions of the special wave infinite elements include trigonometric functions to describe multiple waves propagating in different directions. This is similar to the shape functions of the special wave finite elements discussed in Chapter 3, which include multiple plane waves propagating in different directions. The special wave infinite elements are therefore a more straightforward extension for use with the special wave finite elements for unbounded problems.

The special wave infinite elements have been coupled to the special wave finite elements and applied to the Hankel source problem and the problem of plane wave scattered by a circular cylinder. In similar way to the coupling of the conventional mapped wave infinite elements to the special wave finite elements, special attention is required to deal with wave directions to ensure compatibility on the finite/infinite element interface. All wave directions on the interface and within the special wave infinite elements are forced to vary so as to keep their angles relatively to the radial direction constant. Another point concerning the wave directions is that only angles within the range of $-90°$ and $90°$ should be chosen for the infinite elements where $0°$ is the radial direction. This is because waves outside this range would be incoming and hence excluded by the radiation condition.

The use of multiple waves in the infinite elements improves the accuracy of numerical results. The accuracy generally gets better as the number of waves increases. This trend is quite clear in the Hankel source problem. In the problem of plane wave scattered by a cylinder, however, the accuracy of the results exceptionally became worse when multiple waves are considered on the finite/infinite element interface. On the other hand the increase of number of waves associated with the infinite element only nodes clearly improved the accuracy, as well as for the Hankel source problem. Although efforts have been made to try to discover the cause of this exception about the finite/infinite element interface, it is not clear yet to date.

Gauss-Legendre integration scheme was successfully applied to obtain element matrices of the special wave infinite elements by dividing the element into subelements of the same length in the r direction in the global co-ordinate system, as one of general schemes which

do not restrict the wave directions. In the examples examined here, the effective area of an infinite element to be numerically integrated to achieve the sufficient accuracy was about 250 times of the wavelength from the inner edge of the element.

The cancellation of undefined oscillatory terms at infinity is taken into account in the Zienkiewicz special integration scheme for the conventional mapped wave infinite elements and the integration over the outer boundary at infinity does not appear in the formulation. However in the integration over a special wave infinite element by Gauss-Legendre scheme, the undefined terms are included in each stiffness, mass and damping term of the element matrix and they cancel out when these terms are summed up.

The area to be integrated in an infinite element is not infinite but finite when the Gauss-Legendre integration scheme is applied. The outer boundary of the infinite element is at a finite distance from the 'pole', which means that the radiation condition may not be automatically satisfied only by the decay factor of the shape functions. Therefore the application of the radiation condition on the outer boundary must be considered. The explicit inclusion of this boundary condition improves the accuracy of the results, especially regarding waves propagating in non-radial directions. The expression corresponding to a cylindrical damper condition was also applied but did not make big difference from the simplest expression of the form of the plane damper condition.

The cause of the inaccuracy caused by increasing the number of waves associated with the nodes on the finite/infinite element interface in the model of the scattered wave field is not yet known. However in the general trends the special wave infinite elements containing multiple waves lead to better accuracy in the results than the conventional mapped wave infinite elements. The coupling of the special wave infinite elements to the special wave finite elements should make possible efficient models of wave problems in unbounded domain.

Chapter 8

Conclusions and Implications for Further Research

In this thesis, the development of special wave finite elements and special wave infinite elements for the solution of the Helmholtz equation has been presented, and also related techniques have been discussed.

Details and discussions are given in each chapter. This chapter summarises the main points of these conclusions and gives some implications for further work.

8.1 Conclusions

8.1.1 Special Wave Finite Elements

The formulation of the special wave finite elements in which the multiple number of plane waves are included in the shape functions are described. Because of this choice of basis functions, a single finite element can contain many wavelengths, unlike standard finite elements. The shape functions contain oscillatory functions but the element matrix can be evaluated using high order Gauss-Legendre integration.

High accuracy can be obtained by the use of special wave finite elements, which is not limited by the ratio of the element size to the wavelength, unlike the standard finite elements. Therefore the mesh can remain the same for a wide range of wavenumbers. Generally the error decreases as the number of the approximating plane waves increases. About 10 integration points for a nodal spacing of one wavelength are required to obtain sufficient accuracy. One drawback of the method is the high order integration of the

element matrices.

8.1.2 Semi-analytical Integration Schemes for Special Wave Finite Elements

Methods for integrating semi-analytically the element matrices arising from the formulation of special wave finite elements for the solution of the Helmholtz equation have been presented. The element shapes dealt with are rectangular, triangular and quadrilateral. The new integration schemes for each element type have a number of special cases depending on the combination of constants in the exponent of the exponential functions included in the special shape functions. In the most general cases, the integration can be dealt with quite simply in an analytical way. In the other cases, the analytical expression of the integrals were obtained applying Taylor's expansion. Because of the presence of the term including the product of both co-ordinates in the exponent, it is most complicated to deal with quadrilateral elements. There are 12 special cases for quadrilateral elements, although there are only three and four special cases for rectangular and triangular elements, respectively.

The results show that the integration schemes give results which are hardly distinguishable from those obtained using very large numbers of conventional Gauss-Legendre integration points. The element matrix integrations appear to be independent of the wavenumber as expected. For larger wavenumbers the semi-analytical integrations lead to large savings in computational cost without any loss of accuracy. A timing test using square elements indicates that the break-even point between numerical and semi-analytical integrations is roughly for one wave length in each direction in the special wave finite elements, which corresponds to $kh = \pi$, although timing and efficiency can vary depending of coding.

8.1.3 Mapped Wave Infinite Elements

The formulation of the mapped wave infinite elements for the Helmholtz equation and the coupling of them to special wave finite elements was described. Their application to the Hankel source problem and the problem of plane wave scattered by a circular cylinder were presented. Mapped wave infinite elements can be applied to boundaries of arbitrary shape, although presently they can have only a single radial wave direction. The wave direction

158

on the finite/infinite element interface and within the mapped wave infinite elements were forced to be strictly radial from the 'pole' of the infinite elements to ensure compatibility between the two different types of elements.

The conventional mapped wave infinite elements enable us to deal with wave problems without truncation of the unbounded domain. Also they are easily implemented together with special wave finite elements as well as with standard finite elements and achieve solutions to wave problems in unbounded domain of high accuracy.

8.1.4   Special Wave Infinite Elements

The special wave infinite elements, which is the new concept of mapped wave infinite elements with multiple wave directions, have been developed. In the conventional mapped wave infinite elements only a single wave propagating in the radial direction is allowed. In contrast, the shape functions of the special wave infinite elements include trigonometric functions to describe multiple waves propagating in different directions.

The special wave infinite elements have been coupled to the special wave finite elements and applied to the Hankel source problem and the problem of plane wave scattered by a circular cylinder. Special attention is required to deal with wave directions to ensure compatibility on the finite/infinite element interface. All wave directions on the interface and within the special wave infinite elements are forced to vary so as to keep their angles relatively to the radial direction constant. Another point concerning the wave directions is that only angles within the range of $-90°$ and $90°$ should be chosen for the infinite elements where $0°$ is the radial direction. This is because waves outside this range would be incoming and hence excluded by the radiation condition.

The accuracy generally gets better as the number of waves increases, although some exceptional results were obtained for the problem of plane wave scattered by a circular cylinder when multiple waves are considered on the finite/infinite element interface.

Gauss-Legendre integration scheme has been successfully applied to obtain element matrices of the special wave infinite elements by dividing the element into subelements of the same length in the r direction in the global co-ordinate system. The effective area of an infinite element to be numerically integrated to achieve the sufficient accuracy was about 250 times of the wavelength from the inner edge of the element.

In the integration over a special wave infinite element by Gauss-Legendre scheme, the

undefined oscillatory terms are included in each stiffness, mass and damping term of the element matrix and they cancel out when summed up.

Because the outer boundary of the infinite element is at a finite distance from the 'pole' when Gauss-Legendre integration scheme is applied, the radiation condition may not be automatically satisfied by the decay factor of the shape functions. Therefore the application of the radiation condition on the outer boundary of the elements must be considered.

The general trend of the results obtained using the special wave infinite elements containing multiple waves is that there is better accuracy in the results than those from the conventional mapped wave infinite elements. The coupling of the special wave infinite elements to the special wave finite elements should make possible efficient models of wave problems in unbounded domain.

8.2 Implications for Further Research

The special wave infinite elements with multiple waves have been newly developed. The numerical results show, generally, that good accuracy can be achieved by the computational modelling using the coupling of the special wave infinite elements to the special wave finite elements with multiple plane waves. However there are still some problems. Therefore the discovery of the solutions to the currently remaining problems is crucial.

The most essential problem is the inaccuracy in the numerical results when multiple waves are considered on the finite/infinite element interface of the computational model for the problem of plane wave scattered by a circular cylinder. Considering physically the wave field around the cylinder, the application of the multiple waves should be more suitable and effective for the scattering problem than the Hankel source problem. Also, it should be reasonable to apply larger number of waves in the nearer field than in the further field to the scattering object. However, the results obtained to date do not follow these anticipations. Naturally it is supposed that there may be mistakes in the formulation or bugs in the code, although it has not been discovered yet despite strenuous efforts. It is the most crucial to sort out this problem for the further investigation of the special wave infinite elements.

It is also unknown why the accuracy of the numerical results of the Hankel source problem are poor when the straight edge model and the Gauss-Legendre integration scheme

160

are used. Because better accuracy was obtained by the same mesh model using the Zienkiewicz special integration scheme, the cause of the inaccuracy and the possibility of the improvement should be in the numerical integration procedure. This needs to be resolved, otherwise it may be hard to obtain a good accuracy in the computed results for the problems with more general and practical geometries.

In this thesis, only the cases where the same number and the same wave directions on the finite/infinite element interface are given for both finite and infinite elements were discussed. This is the most simple and the easiest choice to ensure compatibility of the waves on the interface. In this case the continuity of waves in each direction is ensured individually in the manner discussed in Chapters 6 and 7. However, it seems to be also possible to ensure continuity of the potential on the interface between two different element types rather than the continuity of each wave. For this purpose the additional equations to force the potentials in the finite and the infinite elements to be the same may be applied as the constraint. Some techniques such as the use of Lagrange multiplier can be used.

Also as concerns the special wave infinite elements, there remain some possible challenges. The special wave finite elements using multiple approximating plane waves lead to accurate solutions with fewer elements than standard finite elements. However the suitable number and wave directions are different for each problem. Using many number of waves distributed evenly for all nodes gives a good accuracy, but the computational cost could become unnecessarily high. Laghrouche *et al.* [69] investigated changing of the number of waves along the distance from the scattering object and gradually clustering the wave directions around the radial direction. The results showed that accurate numerical results can be obtained with a computational model using a reduced number of waves. If the number and directions of waves can be adaptively chosen to suit each node in each problem, some relatively small number of directions could be chosen. And consequently the suitable computational model for individual problems could be automatically obtained.

Regarding the special integration scheme, the semi-analytical integration codes for the special wave finite elements based on Chapter 4 and 5 are still experimental. It is likely that they could be improved upon. It may be also possible to develop a new special integration scheme for the special wave infinite elements. This would improve the efficiency and the accuracy in forming the element matrix.

The extension of the special wave finite elements to the three dimensions has been

investigated by Laghrouche *et al.* [70]. The similar tendency and the accuracy to those regarding the elements in two dimensions have been obtained, however, the numerical integration cost is extremely high. The extension of the special wave infinite elements to the three dimensions is also possible. However, because the Gauss-Legendre integration scheme applied to many sub-elements is used to obtain the element matrix at present, the element matrix formulation of a three-dimensional element would be very computationally expensive. Therefore the special integration scheme for three dimensional elements would be very important for both the special wave finite elements and the special wave infinite elements for practical applications.

Bibliography

[1] Astley, R. J. Wave envelope and infinite elements for acoustical radiation. *International Journal for Numerical Methods in Fluids*, 3, 1983, 507–526.

[2] Astley, R. J. Finite element, wave envelope formulation for acoustical radiation in moving flows. *Journal of Sound and Vibration*, 13, 1986, 471–485.

[3] Astley, R. J. A transient infinite element for multi-domain acoustic radiation. *DE Vol 84-2, Design Engineering Technical Conference*, 3, Part B, ASME, 1995, 97–111.

[4] Astley, R. J. Transient wave envelope elements for wave problems. *Journal of Sound and Vibration*, 192, 1, 1996, 245–261.

[5] Astley, R. J. Finite elements in acoustics. *Proceedings of Internoise98*, 1998, 13p.

[6] Astley, R. J. Mapped spheroidal wave-envelope elements for unbounded wave problems. *International Journal for Numerical Methods in Engineering*, 41, 1998, 1235–1254.

[7] Astley, R. J. Transient spheroidal elements for unbounded wave problems. *Computer Methods in Applied Mechanics and Engineering*, 164, 1998, 3–15.

[8] Astley, R. J. Infinite elements for wave problems: A review of current formulations and an assessment of accuracy. *International Journal for Numerical Methods in Engineering*, 49, 2000, 951–976.

[9] Astley, R. J., Bettess, P., and Clark, P. J. Letters to the editor: Mapped infinite elements for exterior wave problems. *International Journal for Numerical Methods in Engineering*, 32, 1991, 207–209.

[10] Astley, R. J., and Eversman, W. A note on the utility of a wave envelope approach in finite element duct transmission studies. *Journal of Sound and Vibration*, 76, 1981, 595–601.

[11] Astley, R. J., and Eversman, W. Finite element formulations for acoustical radiation. *Journal of Sound and Vibration*, 88, 1, 1983, 47–64.

[12] Astley, R. J., and Eversman, W. Wave envelope and infinite element schemes for fan noise radiation from turbofan inlets. *Journal of American Institute of Aeronautics and Astronautics*, 22, 12, 1984, 1719–1726.

[13] Astley, R. J., and Eversman, W. Wave envelope elements for acoustical radiation in inhomogeneous media. *Computers and Structures*, 30, 4, 1988, 801–810.

[14] Astley, R. J., Macaulay, G. J., and Coyette, J. P. Mapped wave envelope elements for acoustical radiation and scattering. *Journal of Sound and Vibration*, 170, 1, 1994, 97–118.

[15] Babuška, I., Ihlenburg, F., Strouboulis, T., and Gangaraj, S. K. A posteriori error estimation for finite element solutions of Helmholtz' equation. Part I: The quality of local indicators and estimators. *International Journal for Numerical Methods in Engineering*, 40, 1997, 3443–3462.

[16] Babuška, I., Ihlenburg, F., Strouboulis, T., and Gangaraj, S. K. A posteriori error estimation for finite element solutions of Helmholtz' equation. Part II: Estimation of pollution error. *International Journal for Numerical Methods in Engineering*, 40, 1997, 3883–3900.

[17] Babuška, I., and Melenk, J. M. The partition of unity method. *International Journal for Numerical Methods in Engineering*, 40, 1997, 727–758.

[18] Bando, K., Bettess, P., and Emson, C. The effectiveness of dampers for the analysis of exterior scalar wave diffraction by cylinders and ellipsoids. *International Journal for Numerical Methods in Engineering*, 4, 1984, 599–617.

[19] Bayliss, A., Gunzburger, M., and Turkel, E. Boundary conditions for the numerical solution of elliptic equations in exterior regions. *SIAM Journal on Applied Mathematics*, 42, 1982, 430–451.

[20] Beer, G., and Meek, J. L. 'infinite domain' elements. *International Journal for Numerical Methods in Engineering*, 17, 1, 1981, 43–52.

[21] Bettess, J. A., and Bettess, P. A new mapped infinite wave element for general wave diffraction problems and its validation on the ellipse diffraction problem. *Computer Methods in Applied Mechanics and Engineering*, 164, 1998, 17–48.

[22] Bettess, P. Operation counts for boundary integral and finite element methods. *International Journal for Numerical Methods in Engineering*, 17, 1981, 306–308.

[23] Bettess, P. A simple wave envelope element example. *Communications in Applied Numerical Methods*, 3, 1987, 77–80.

[24] Bettess, P. *Infinite Elements*. Penshaw Press, Sunderland, UK, 1992.

[25] Bettess, P., Emson, C. R. I., and Chiam, T. C. A new mapped infinite element for exterior wave problems. In *Numerical Methods in Coupled Systems*, R. W. Lewis, P. Bettess, and E. Hinton, Eds. John Wiley & Sons Ltd, Chichester, 1984, ch. 17, pp. 489–504.

[26] Bettess, P., Shirron, J., Laghrouche, O., Peseux, B., Sugimoto, R., and Trevelyan, J. A numerical integration scheme for special finite elements for Helmholtz equation. *International Journal for Numerical Methods in Engineering*, 56, 4, 2003, 531–552.

[27] Bettess, P., and Zienkiewicz, O. C. Diffraction and refraction of surface waves using finite and infinite elements. *International Journal for Numerical Methods in Engineering*, 11, 1977, 1271–1290.

[28] Bulirsch, R. Numerical calculation of the sine, cosine, and fresnel integrals. *Numerische Mathematik*, 9, 1967, 380–385.

[29] Burnett, D. S. A three-dimensional acoustic infinite element based on a prolate spheroidal multipole expansion. *The Journal of The Acoustical Society of America*, 96, 5, 1994, 2798–2816.

[30] Burnett, D. S., and Holford, R. L. An ellipsoidal acoustic infinite element. *Computer Methods in Applied Mechanics and Engineering*, 164, 1998, 49–76.

[31] Burnett, D. S., and Holford, R. L. Prolate and oblate spheroidal acoustic infinite elements. *Computer Methods in Applied Mechanics and Engineering*, 158, 1998, 117–141.

[32] Burton, A. J., and Miller, G. F. The application of integral equation methods to the numerical solution of some exterior boundary value problems. *Proceedings of the Royal Society of London*, A323, 1971, 201–210.

[33] Chadwick, E., Bettess, P., and Laghrouche, O. Diffraction of short waves modelled using new mapped wave envelope finite and infinite elements. *International Journal for Numerical Methods in Engineering*, 45, 1999, 335–354.

[34] Cipolla, J. L. Transient infinite elements for acoustics and shock. *DE Vol 84-2, Design Engineering Technical Conference*, Vol.3, Part B, ASME, 1995, 113–128.

[35] Cipolla, J. L., and Butler, M. J. Infinite elements in the time domain using a prolate spheroidal multipole expansion. *International Journal for Numerical Methods in Engineering*, 43, 1998, 889–908.

[36] Ciskowski, R. D., and Brebbia, C. A., Eds. *Boundary element methods in acoustics*. Computational Mechanics Publications, Boston, 1991.

[37] Clark, P. J. *The finite element method applied to Stokes wave diffraction*. PhD thesis, Department of Marine Technology, University of Newcastle upon Tyne, 1993.

[38] Craggs, A. The transient response of a coupled plate acoustic system using plate and acoustic finite elements. *Journal of Sound and Vibration*, 15, 1971, 509–528.

[39] Cremers, L., and Fyfe, K. R. On the use of variable order infinite wave envelope elements for acoustic radiation and scattering. *The Journal of The Acoustical Society of America*, 97, 4, 1995, 2028–2040.

[40] Cremers, L., Fyfe, K. R., and Coyette, J. P. A variable order infinite acoustic wave envelope element. *Journal of Sound and Vibration*, 171, 4, 1994, 483–508.

[41] Darve, E. The fast multipole method: Numerical implementation. *Journal of Computational Physics*, 160, 2000, 195–240.

[42] Davis, P. J., and Rabinowitz, P. *Numerical Integration*. Blaisdell, Woltham, 1967.

[43] de La Bourdonnaye, A. High frequency approximation of integral equations modeling scattering phenomena. *Mathematical Modelling and Numerical Analysis*, 28, 1994, 223–241.

[44] de La Bourdonnaye, A. Une méthode de discrétisation microlocale et son application à un problème de diffraction. *C. R. Acad. Sci. Paris, t.318, Série I*, 1994, 385–388.

[45] Farhat, C., Harari, I., and Franca, L. P. The discontinuous enrichment method. *Computer Methods in Applied Mechanics and Engineering*, 190, 2001, 6455–6479.

[46] F.J.Sánchez-Sesma, Herrera, I., and Avilés, J. A boundary method for elastic wave diffraction: application to scattering of *sh* waves by surface irregularities. *Bull. Seism. Soc. Am.*, 72, 1982, 491–506.

[47] Geers, T. L., Ed. *IUTAM Symposium on Computational Methods for Unbounded Domains*, vol. 49 of *Fluid Mechanics and its applications*. Kluwer Academic Publishers, 1998.

[48] Gerdes, K. The conjugated vs. the unconjugated infinite element method for the Helmholtz equation in exterior domains. *Computer Methods in Applied Mechanics and Engineering*, 152, 1998, 125–145.

[49] Gerdes, K. A review of infinite element methods. *Journal of Computational Acoustics*, 8, 1, 2000, 43–62.

[50] Givoli, D. Non-reflecting boundary conditions. *Journal of Computational Physics*, 94, 1991, 1–29.

[51] Givoli, D. *Numerical methods for problems in infinite domains*. Elsevier Science, Amsterdam, 1992.

[52] Gladwell, G. M. L. A variation model of damped acousto-structural vibration. *Journal of Sound and Vibration*, 4, 1965, 172–186.

[53] Hamming, R. W. *Numerical Methods for Scientists and Engineers*. McGraw Hill, New York, 1973.

[54] Harari, I., and Hughes, T. J. R. A cost comparison of boundary element and finite element methods for problems of time-harmonic acoustics. *Computer Methods in Applied Mechanics and Engineering*, 97, 1992, 77–102.

[55] Havelock, T. H. The pressure of water waves upon a fixed obstacle. *Proceedings of the Royal Society of London, Series A*, 175, 1940, 409–421.

[56] Herrera, I., and Sabena, F. J. Connectivity as an alternative to boundary integral equations. *Proc. Natl. Acad. Sci. USA*, 75, 1978, 2059–2063.

[57] Higdon, R. L. Absorbing boundary conditions for acoustic and elastic waves in stratified media. *Journal of Computational Physics*, 1992, 386–418.

[58] Hu, F. Q., Hussaini, M. Y., and Rasetarinera, P. An analysis of the discontinuous Galerkin method for wave propagation problems. *Journal of Computational Physics*, 151, 1999, 921–946.

[59] Ihlenburg, F. *Finite Element Analysis of Acoustic Scattering*, vol. 132 of *Applied Mathematical Sciences*. Springer, 1998.

[60] Ihlenburg, F., and Babuška, I. Dispersion analysis and error estimation of Galerkin finite element methodsfor the Helmholtz equation. *International Journal for Numerical Methods in Engineering*, 38, 1995, 3745–3774.

[61] Ihlenburg, F., and Babuška, I. Finite element solution to the Helmholtz equation with high wavenumber part I: the h-version of the FEM. *Computers and Mathematics with Applications*, 30, 1995, 9–37.

[62] Kumar, P. Letter to editor on ref. [97]. *International Journal for Numerical Methods in Engineering*, 20, 1984, 1173–1174.

[63] Laghrouche, O., and Bettess, P. Solving short wave problems using the partition of unity finite element method. *Proceedings of the 6th. ACME Conference, Exeter*, April 1998, 15–18.

[64] Laghrouche, O., and Bettess, P. Plane waves solution for the 2D-Helmholtz short wave equation. *Proceedings of the 7th. ACME Conference, Durham*, March 1999, 143–146.

[65] Laghrouche, O., and Bettess, P. Short wave modelling using special finite elements. *4th International Conference on Theoretical and Computational Acoustics, Trieste*, May 1999.

[66] Laghrouche, O., and Bettess, P. Solving short wave problems using special finite elements. *Proceedings of the 4th. International Congress on Industrial and Applied Mathematics, Edinburgh*, July 1999.

[67] Laghrouche, O., and Bettess, P. Short wave modelling using special finite elements. *Journal of Computational Acoustics*, 8, 1, 2000, 189–210.

[68] Laghrouche, O., and Bettess, P. Short wave modelling using special finite elements - Towards an adaptive approach. In *The Mathematics of Finite Elements and Applications X (MAFELAP 1999)*, J. R. Whiteman, Ed. Elsevier, 2000, ch. 10, pp. 181–194.

[69] Laghrouche, O., Bettess, P., and Astley, R. J. Modelling of short wave diffraction problems using approximating systems of plane waves. *International Journal for Numerical Methods in Engineering*, 54, 2002, 1501–1533.

[70] Laghrouche, O., Bettess, P., Perrey-Debain, E., and Trevelyan, J. Plane wave basis finite elements for wave scattering in three dimensions. *Communications in Numerical Methods in Engineering*, 2002.

[71] Laghrouche, O., Bettess, P., and Sugimoto, R. Short wave scattering by elliptical cylinder. *8th ACME Conference Extended Abstracts*, 2000, 70–73.

[72] MacCamy, R. C., and Fuchs, R. A. Wave forces on piles: A diffraction theory. Tech. rep., Technical memorandum No.69, Beach Erosion Board, Corps of Engineers, December 1954.

[73] Marques, J. M. M. C., and Owen, D. R. J. Infinite elements in quasi-static materially non-linear problems. *Computers and Structures*, 18, 4, 1984, 739–751.

[74] Mayer, P., and Mendel, J. *The Finite Ray Element Method for the Helmholtz equation of scattering: first numerical experiments*. Tech. Rep. Report Number CU-CAS-00-20, UCD/CCM Report 111, College of Engineering, University of Colorado, Boulder, Colorado, U.S.A., 1997.

[75] Melenk, J. M., and Babuška, I. The partition of unity finite element method: Basic theory and applications. *Computer Methods in Applied Mechanics and Engineering*, 139, 1996, 289–314.

[76] Morse, P. M. *Vibration and Sound.* McGraw-Hill, New York, 1936.

[77] Morse, P. M., and Feshbach, H. *Methods of Mathematical Physics*. McGraw-Hill, New York, 1953.

[78] Ortiz, P., and Sanchez, E. An improved partition of unity finite element method for diffraction problems. *International Journal for Numerical Methods in Engineering*, 50, 2001, 2727–2740.

[79] Perrey-Debain, E., Trevelyan, J., and Bettess, P. New special wave boundary elements for short wave problems. *Communications in Numerical Methods in Engineering*, 18, 4, 2002, 259–268.

[80] Perrey-Debain, E., Trevelyan, J., and Bettess, P. Plane wave interpolation in direct collocation boundary element method for radiation and wave scattering: Numerical aspects and applications. *Journal of Sound and Vibration*, 261, 5, 2003, 839–858.

[81] Press, W. H., Teukolsky, A. A., Vetterling, W. T., and Flannery, B. P. *Numerical Recipes in Fortran*. Cambridge University Press, 1992.

[82] Ralston, A. *A First Course in Numerical Analysis*. McGraw-Hill, New York, 1965.

[83] Rasetarinera, P., and Hussaini, M. Y. An efficient implicit discontinuous spectral Galerkin method. *Journal of Computational Physics*, 172, 2002, 718–738.

[84] Rayleigh, J. W. S. *Theory of Sound*. Macmillan Company, 1896.

[85] Rokhlin, V. Rapid solution of integral equations of classical potential theory. *Journal of Computational Physics*, 60, 1985, 187–207.

[86] Schenk, H. A. Improved integral formulation for acoustic radiation problems. *The Journal of The Acoustical Society of America*, 44, 1967, 41–58.

[87] Shirron, J. J., and Babuška, I. A comparison of approximate boundary conditions and infinite element methods for exterior Helmholtz problems. *Computer Methods in Applied Mechanics and Engineering*, 164, 1-2, 1998, 121–139.

[88] Sommerfeld, A. *Partial Differential Equations in Physics*. Academic Press, 1964.

[89] Sugimoto, R., and Bettess, P. Coupling of mapped wave infinite elements and plane wave basis finite elements for the Helmholtz equation in exterior domains. *Communications in Numerical Methods in Engineering*, 19, 10, 2003, 761–777.

[90] Sugimoto, R., Bettess, P., and Laghrouche, O. Special wave finite and infinite elements for Helmholtz equation. *Proceedings of 17th International Congress on Acoustics, Rome*, September 2001, 2p.

[91] Sugimoto, R., Bettess, P., and Laghrouche, O. Special wave finite and infinite elements for the Helmholtz equation. *Proceedings of The Spring Meeting of Acoustical Society of Japan, Tokyo*, March 2003, 2p.

[92] Sugimoto, R., Bettess, P., and Trevelyan, J. A numerical integration scheme for special quadrilateral finite elements for the Helmholtz equation. *Communications in Numerical Methods in Engineering*, 19, 3, 2003, 233–245.

[93] Zienkiewicz, O. C., Bando, K., Bettess, P., Emson, C., and Chiam, T. C. Mapped infinite elements for exterior wave problems. *International Journal for Numerical Methods in Engineering*, 21, 1985, 1229–1251.

[94] Zienkiewicz, O. C., and Bettess, P. Infinite elements in the study of fluid structure interaction problems. *Proceedings of 2nd International Symposium on Computing Methods in Applied Sciences, Versailles*, 1975.

[95] Zienkiewicz, O. C., and Bettess, P. Infinite elements in the study of fluid structure interaction problems. In *Computing Methods in Applied Sciences, Lecture Notes in Physics*, J. Ehlers, K. Hepp, H. A. Weidenmüller, and J. Zittarts, Eds., vol. 58. Springer-Verlag, Berlin, 1976, pp. 133–169.

[96] Zienkiewicz, O. C., Bettess, P., Chiam, T. C., and Emson, C. R. I. Numerical methods for unbounded field problems and a new infinite element formulation. *Proceedings of A.S.M.E. Winter Annual Meeting, Proceedings published by A.S.M.E. as AMD-vol.46*, 1981, 115–148.

[97] Zienkiewicz, O. C., Emson, C. R. I., and Bettess, P. A novel boundary infinite element. *International Journal for Numerical Methods in Engineering*, 19, 1983, 393–404.

[98] Zienkiewicz, O. C., and Newton, R. E. Coupled vibrations of a structure submerged in a compressible fluid. *Proceedings of International Symposium on Finite Element Techniques, Stuttgart, 1-15 May*, 1969, 360–378.

[99] Zienkiewicz, O. C., and Taylor, R. L. *The Finite Element Method, Fifth Edition,* vol. I-III. Butterworth Heinemann, Oxford, UK, 2000.